GABA and glutamate neurons in the VTA regulate sleep and wakefulness

Xiao Yu[1,8], Wen Li[2,8], Ying Ma[1], Kyoko Tossell[1], Julia J. Harris[1,3], Edward C. Harding[1], Wei Ba[1], Giulia Miracca[1], Dan Wang[2], Long Li[2], Juan Guo[2], Ming Chen[4], Yuqi Li[1], Raquel Yustos[1], Alexei L. Vyssotski[5], Denis Burdakov[3], Qianzi Yang[2], Hailong Dong[2*], Nicholas P. Franks[1,6, 7*], William Wisden[1,6, 7*].

[1]Department of Life Sciences, Imperial College London, London, U.K.

[2]Department of Anesthesiology & Perioperative Medicine, Xijing Hospital, Xi'an, Shanxi, China.

[3]The Francis Crick Institute, London, UK.

[4]iHuman Institute, ShanghaiTech University, Shanghai, China.

[5]Institute of Neuroinformatics, University of Zürich/ETH Zürich, Switzerland.

[6]Centre for Neurotechnology, Imperial College London, London, U.K

[7]UK Dementia Research Institute, Imperial College London, London, U.K.

[8]These authors contributed equally

[*]Correspondence: w.wisden@imperial.ac.uk, n.franks@imperial.ac.uk or hldong6@hotmail.com

Abstract

We screened for novel circuits in the mouse brain that promote wakefulness. Chemogenetic activation experiments and EEG recordings pointed to glutamatergic/nitrergic (NOS1) and GABAergic neurons in the VTA. Activating glutamatergic/NOS1 neurons, which were wake- and REM-sleep-active, produced wakefulness through projections to the nucleus accumbens and the lateral hypothalamus. Lesioning the glutamate cells impaired the consolidation of wakefulness. By contrast, activation of GABAergic VTA neurons elicited long-lasting NREM-like sleep resembling sedation. Lesioning these neurons produced an increase in wakefulness that persisted for at least 4 months. Surprisingly, these VTA GABAergic neurons were wake-and REM-sleep-active. We suggest that GABAergic VTA neurons may limit wakefulness by inhibiting the arousal-promoting VTA glutamatergic and/or dopaminergic neurons and through projections to the lateral hypothalamus. Thus, in addition to its contribution to goal- and reward-directed behaviours, the VTA has a role in regulating sleep and wakefulness.

We still do not know all the circuitry in mammals regulating wakefulness and sleep[1-4]. Broadly, wakefulness is promoted by ascending aminergic and peptidergic systems[1,5-8]. GABAergic and glutamatergic pathways can also induce wakefulness and physical activity[9-17]. On the other hand, sleep is promoted by GABAergic/peptidergic and glutamatergic/nitrergic neurons that inhibit the wake-promoting neurons[3,18-23].

Here, we describe a non-hypothesis driven chemogenetic search for further circuitry controlling vigilance states, and unexpectedly converge on the ventral tegmental area (VTA). The VTA is intensively investigated for its regulation of goal-, and reward-directed and social behaviors[24-28]. As well as dopamine neurons (VTA^{DA}), the VTA contains GABAergic and glutamatergic neurons, which independently project out of the VTA[24,29,30]. These GABA and glutamate neurons are believed to control reward-, goal-directed and social behaviour[31,32]. These behaviours require wakefulness, and indeed VTA^{DA} neurons are selectively wake and REM-sleep active, and actually promote wakefulness[5,8,33]. Complimenting this work, we find that VTA glutamate/NOS1 and GABA neurons increase and decrease wakefulness respectively. The VTA is, therefore, a node whose circuitry potently influences vigilance state.

Results

A chemogenetic search for glutamatergic circuitry enhancing wakefulness

We searched for glutamatergic neurons in the posterior hypothalamic/midbrain area (PH/MB) that could promote wakefulness (Fig. 1). By injecting AAV-DIO-hM3Dq-mCherry into *Vglut2-ires-Cre* mice, we expressed the excitatory hM3Dq DREADD receptor in *Vglut2* neurons in progressively more defined locations (Fig. 1). [note: for the following series of experiments, CNO (1 mg/kg) was injected *i.p.* at the start of ''lights on'', when the mice had their maximal sleep drive. Injecting CNO (1 mg/kg) *i.p.*

into AAV-naïve *Vglut2-ires-Cre* mice - *i.e.* mice not injected with AAV - did not produce any changes in the amounts of sleep or wakefulness (Supplementary Fig. 1a)].

We obtained dramatic results from large volume injections of AAV-DIO-hM3Dq-mCherry into the PH/MB of *Vglut2-ires-Cre* mice [$(PH/MB)_L^{Vglut2}$-hM3Dq mice] (Fig. 1a). Following CNO injections, 100% wakefulness was induced for 12 hours compared with saline-injected control mice (Fig. 1b, c). In these $(PH/MB)_L^{Vglut2}$-hM3Dq mice, hM3Dq-mCherry receptor expression (determined by mCherry staining) was found throughout the lateral hypothalamus (LH), dorsal medial hypothalamus (DMH), ventral medial hypothalamus (VMH), mammillary area (MM), tuberomammillary (TMN) area, supramammillary area (SuM), VTA and interpeduncular nucleus (IPN). A smaller AAV injection volume into the PH/MB of *Vglut2-ires-Cre* mice resulted in hM3Dq expression in the LH, MM and VTA $(PH/MB)_S^{Vglut2}$-hM3Dq mice, Fig. 1d). CNO *i.p.* injection into these $(PH/MB)_S^{Vglut2}$-hM3Dq mice produced continuous wakefulness for approximately 5 hours, followed by enhanced wakefulness for another 7 hours (Fig. 1e, f). Restricting hM3Dq expression to the LH and activating with systemic CNO also produced extended wakefulness (Fig. 1g, h, i).

By contrast, restricting hM3Dq expression to glutamatergic neurons in the mammillary area of *Vglut2-ires-Cre* mice (Fig. 1j, Supplementary Fig. 2a, M^{Vglut2}-hM3Dq mice), and giving CNO did not produce arousal above that resulting from baseline saline injections (Fig. 1k, l). Restricting hM3Dq receptor expression to the IPN of *Vglut2-ires-Cre* mice (Fig. 1m, Supplementary Fig. 2b, IPN^{Vglut2}-hM3Dq mice), and subsequent injection of CNO also did not elicit arousal compared with saline injection (Fig. 1n, o).

Glutamatergic neurons in the VTA produce wakefulness.

We next limited hM3Dq receptor expression to the VTA of *Vglut2-ires-Cre* mice to make VTA^{Vglut2}-hM3Dq mice (Fig. 1p, Supplementary Fig. 2c). Following 1 mg/kg CNO *i.p.* injection, there was 5 hours of 100% wakefulness; the extent of wakefulness remained elevated for nearly the entire “lights on” period (Fig. 1q, r). [note: as a further

control for the specificity of CNO's actions, we injected AAV-DIO-mCherry into the VTA of *Vglut2-ires-Cre* mice; CNO injection (*i.p.*) into these *VTA^{Vglut2}-mCherry* mice had no effect on the amounts of sleep or wakefulness (Supplementary Fig. 1c)].

Of the brain regions that we injected, the VTA^{Vglut2} population that promotes wakefulness had not previously been identified in this role, and so we decided to study these cells in detail. We first confirmed that these neurons were excited by CNO in VTA^{Vglut2}-hM3Dq mice. One hour after CNO *i.p.* injection into VTA^{Vglut2}-hM3Dq mice, cFOS protein was elevated in hM3Dq-expressing VTA^{Vglut2} neurons (saline: 41 ± 4, CNO: 378 ± 36 cFOS-positive cells), confirming excitation of VTA^{Vglut2} neurons (Supplementary Fig. 2d). Looking at the CNO-evoked EEG spectra of VTA^{Vglut2}-hM3Dq mice (Supplementary Fig. 2e), the excitation of VTA^{Vglut2} neurons produced higher theta (8 Hz) activity (Supplementary Fig. 2f) but the EMG signal did not change (Supplementary Fig. 2f). Activation of VTA^{Vglut2} neurons also strongly increased the latency to both NREM and REM sleep (Supplementary Fig. 2g). However, excitation of VTA^{Vglut2} neurons did not cause hyperactivity (Supplementary Fig. 2h). In an open field assay, the CNO-injected (*i.p.*) mice did not move further than saline-injected mice, but stayed awake for an extended period.

Confirming the behavioral effects of the chemogenetic activation of VTA^{Vglut2} neurons, optogenetic activation of VTA^{Vglut2} neurons with ChR2 also increased wakefulness (Supplementary Fig. 3a, 3b, c).

VTA^{Vglut2} neurons consolidate wakefulness during the sleep-wake cycle. To investigate how VTA^{Vglut2} neurons influence the sleep-wake cycle over 24 hours, we genetically ablated VTA^{Vglut2} neurons using AAV-DIO-CASP3 to produce VTA^{Vglut2}-CASP3 mice (Fig. 2a, Supplementary Fig. 3d). About 80% of the VTA^{Vglut2} neurons were destroyed (Supplementary Fig. 3d). Chronic lesioning of VTA^{Vglut2} cells reduced wakefulness, and increased NREM sleep, but only during the ''lights off'' phase (Fig. 2b). Looking at the sleep-wake microarchitecture, wake consolidation was impaired, with more episodes and shorter episode durations of wake (Fig. 2c), and with more

transitions between wake and NREM sleep (Fig. 2d), again with the phenotype appearing selectively during lights off".

VTA^{Vglut2} neurons are selectively wake- and REM sleep-active. To determine when during the natural sleep-wake cycle the VTA^{Vglut2} neurons were active, we made VTA^{Vglut2}-GCaMP6 mice (Fig. 2e), then recorded Ca^{2+} signals by fiber photometry (Fig. 2f; Supplementary Fig. 3e). (Note: we used GCaMP6s for all this and all subsequent photometry experiments). The Ca^{2+} signal increased selectively during wakefulness and REM sleep (Fig. 2f, g), and with novel objects and female scents (Supplementary Fig. 3e). During NREM sleep, the VTA^{Vglut2} neurons had lower Ca^{2+} signals (Fig. 2f, g). At the transitions between the vigilance states, the $\Delta F/F$ ratio increased from NREM to wake and from NREM to REM sleep (Fig. 2h), but decreased from wakefulness to NREM. The $\Delta F/F$ ratio changed little from REM sleep to wake transitions (Fig. 2h). [As controls, no changes in the $\Delta F/F$ ratio were found by photometry between vigilance states in VTA^{Vglut2}-GFP mice (Supplementary Fig. 3f, g); furthermore, there was no bleaching of the signal in VTA^{Vglut2}-GCaMP6s *mice*, as the $\Delta F/F$ ratios stayed constant over 6 hours (Supplementary Fig. 3h)].

VTA^{Vglut2} neurons promote wakefulness independently of dopamine.

Dopamine neurons in the VTA promote wakefulness[5,8], so we tested if the wake-promoting effect of VTA^{Vglut2} neurons depended on dopamine. We first verified that VTA^{Vglut2} neurons are largely distinct from VTA dopamine neurons. Immunohistochemistry confirmed that only 26 ± 1.6% of the *Vglut2* cells were TH-positive (Supplementary Fig. 4a, b), as shown previously[24]. Unlike dopamine neurons, VTA^{Vglut2} cells were mostly located in the midline VTA nuclei - the rostral linear nucleus (RLi) and the interfasicular nucleus (IF) (Supplementary Fig. 4b)[24,34]. Thus, the majority of VTA^{Vglut2} and VTA^{DA} neurons are distinct populations. We next chemogenetically activated the VTA^{Vglut2} neurons in VTA^{Vglut2}-hM3Dq mice with CNO in the presence of systemically administered dopamine antagonists SCH-23390 and raclopride for D1 and D2/D3 receptors respectively (Supplementary Fig. 4c, d) (note:

mice were injected *i.p.* with the dopamine receptor antagonists 30 mins before CNO *i.p.* injection – please see Methods for drug concentrations). Even when dopamine receptors were blocked, VTA^{Vglut2} neurons still promoted wakefulness (Supplementary Fig. 4d).

VTA^{Vglut2} neurons promote wakefulness via the nucleus accumbens and the lateral hypothalamus.

To identify the brain areas that participate in generating the VTA^{Vglut2}-mediated wakefulness, we mapped cFOS activity in VTA^{Vglut2}-hM3Dq mice. Following CNO *i.p.* injection, increased numbers of cFOS-positive cells were identified in multiple brain regions (Fig. 3a and Supplementary Fig. 5a, b). cFOS expression was particularly activated in the lateral hypothalamus (LH), nucleus accumbens (NAc) and ventral pallidum (VP) (Fig. 3a and Supplementary Fig. 5a, b). In the LH, 60% of cFOS-expressing cells that were activated by CNO *i.p.* injections were also orexin-positive compared with the low number of cFOS expressing cells following saline injection (Supplementary Fig. 5c).

We then undertook ChR2-based circuit mapping of the VTA^{Vglut2} neurons in VTA^{Vglut2}-ChR2-EYFP mice (Fig. 3b, Supplementary Fig. 5d). Consistent with the cFOS activation data, there was a dense projection of VTA^{Vglut2} neurons to the LH and NAc (Fig. 3b and Supplementary Fig. 5c), as described previously[29,30,35,36]. To test whether the VTA^{Vglut2}→LH or VTA^{Vglut2}→NAc projections can promote wakefulness, we placed optical fibers into the LH and NAc of VTA^{Vglut2}-ChR2-EYFP mice to stimulate the terminals (Fig. 3c, d, e, f). Optically stimulating VTA^{Vglut2} fibers in the LH strongly and consistently promoted waking from NREM sleep (Fig. 3c; Supplementary Fig. 6a); and chronic optical stimulation for 3 hours maintained wakefulness (Fig. 3d). Similarly, optogenetic stimulation of the VTA^{Vglut2} terminals in the NAc promoted waking from NREM sleep (Fig. 3e; Supplementary Fig. 6b) and chronic optogenetic stimulation for 3 hours increased wakefulness and reduced NREM and REM sleep (Fig. 3f). Thus the

LH and NAc are two areas contributing to wakefulness when excited by VTA^{Vglut2} neurons.

Nitric oxide synthase marks wake-promoting VTA^{Vglut2} neurons. To confirm the wake-promoting actions of the VTA^{Vglut2}→LH and VTA^{Vglut2}→NAc projections, we used retrograde-labeling by injecting AAV-Retro-DIO-Chronos-GFP into the LH and NAc of *Vglut2-ires-Cre* mice. We identified many GFP-positive soma in the VTA (Supplementary Fig. 7a, b). We optogenetically activated the Chronos-GFP retro-labeled cells by inserting optical fibers into the VTA (Supplementary Fig. 7b). Tonic opto-activation increased cFOS in these retro-labelled neurons (control: 31 ± 5, stimulation: 206 ± 41) (Supplementary Fig. 7c) Activation of the retro-labeled NAc→VTA^{Vglut2} neurons increased wakefulness (Supplementary Fig. 7d). To profile these retro-labeled VTA^{Vglut2} neurons, we stained VTA^{Vglut2} neurons with a panel of antibodies recognizing neurochemical markers (nitric oxide synthase NOS1, tyrosine hydroxylase TH, glutamic acid decarboxylase GAD67, parvalbumin PV, somatostatin SOM) (Fig. 4a, Supplementary Fig. 7e). Of these markers, double-labelling of retro-labeled NAc→VTA^{Vglut2} and LH→VTA^{Vglut2} neurons identified that about 68 ± 9 % of the GFP-positive cells were immuno-positive for NOS1 (Fig. 4a, Supplementary Fig. 7f), mostly in the midline VTA. This was confirmed by direct double-labelling with VTA^{Vglut2}-ChR2-EYFP neurons and VTA^{Nos1} neurons (Supplementary Fig. 8a, b). About 75 ± 3% of VTA^{Nos1} cells were VTA^{Vglut2}-positive (Supplementary Fig. 8b), as also seen independently[34].

To test if the VTA^{Nos1} neurons are functionally the same as the VTA^{Vglut2} neurons in producing wakefulness, we chemogenetically activated the VTA^{Nos1} neurons by delivering AAV-DIO-hM3Dq-mCherry into the VTA of *Nos1-ires-Cre* mice (Fig. 4b, c). As for the *VTA^{Vglut2}-hM3Dq* mice, giving 1 mg/kg CNO *i.p.* to the VTA^{Nos1}-hM3Dq mice produced sustained wakefulness (100%) for 4 hours (Fig. 4c, Supplementary Fig. 8c). Also similar to the VTA^{Vglut2}-hM3Dq mice, the wakefulness produced by *i.p.* administered CNO activation of VTA^{Nos1} neurons was not blocked by systemic *i.p.*

administered dopamine D1 and D2/D3 receptor antagonists (Supplementary Fig. 8d) (note: mice were injected *i.p.* with the dopamine receptor antagonists 30 mins before CNO *i.p.* injection – see Methods for drug concentrations). Thus, the wake-promoting VTA^{Nos1} neurons are a subset of VTA^{Vglut2} neurons. Chemogenetic inhibition of these VTA$^{Vglut2/Nos1}$ neurons, by delivering AAV-DIO-hM4D$_i$-mCherry into the VTA of *Nos1-ires-Cre* mice and giving CNO *i.p.,* decreased wakefulness and produced more NREM sleep (Fig. 4b, Fig. 4d, Supplementary Fig. 8e). Therefore, VTA$^{Vglut2/Nos1}$ neurons can bidirectionally regulate wakefulness. We next mapped projections of VTA^{Nos1} neurons by injecting AAV-DIO-ChR2-EYFP into the VTA of *Nos1-ires-Cre* mice. Similar to VTA^{Vglut2} neurons, VTA^{Nos1} neurons project to the NAc, VP and LH (Supplementary Fig. 8f), again implying that the NOS1-expressing neurons are a subset of the glutamatergic ones.

VTA^{Vgat} neurons limit wakefulness and induce NREM sleep. We next looked for neurons in the VTA that could potentially restrain the wake-promoting activity of the VTA$^{Vglut2/Nos1}$ neurons. The VTA contains many GABAergic neurons (Supplementary Fig. 9a, b)[24,30]. These can be detected by expression of the vesicular GABA transporter (VGAT). We first confirmed that *Vgat* gene-expressing neurons were mostly distinct from dopamine or glutamate neurons: only 0.3 ± 0.1% of these GABAergic neurons (as defined by VTA^{Vgat}-ChR2-EYFP staining) stained with TH (Supplementary Fig. 9a), and 12 ± 0.6% of these VTA^{Vgat} neurons were NOS1-positive; however, these cells were not in the midline but mostly in the lateral part of the VTA (PBP), which are distinct from VTA$^{Nos1/Vglut2}$ populations in the midline (Supplementary Fig. 9b)[34].

To examine if VTA^{Vgat} neurons contribute to sleep-wake regulation, AAV-DIO-hM3Dq-mCherry or AAV-DIO-hM4D$_i$-mCherry was injected into the VTA of *Vgat-ires-Cre* mice to generate VTA^{Vgat}-hM3Dq and VTA^{Vgat}-hM4D$_i$ mice respectively (Fig. 5a, Supplementary Fig. 9c, d). CNO injection *i.p.* into VTA^{Vgat}-hM3Dq mice produced sustained (80%) NREM sleep for 6 hours (Fig. 5b), with continuous δ power in the

EEG. Following CNO administration *i.p.*, the latency to NREM sleep was reduced to about 10 minutes compared with saline administration (Fig. 5c). However, latency to REM sleep was significantly increased - there was no REM sleep in the first 6 hours (Fig. 5c) [note: we did several further controls for the specificity of CNO's actions to ensure it was not acting as a sedative after conversion to clozapine[37]. We injected 1 mg/kg CNO *i.p.* into both AAV-naïve *Vgat-ires-Cre* mice - *i.e.* mice that had not received any AAV injections (Supplementary Fig. 1b), and into VTA^{Vgat}-mCherry mice (produced by injecting AAV-DIO-mCherry into the VTA of *Vgat-ires-Cre* mice). In neither of these types of mice did CNO alter the amounts of sleep or wakefulness compared with saline-injected controls, (Supplementary Fig. 1d). In a separate study[21], we similarly found that CNO systemically injected *i.p.* at the higher concentration of 5 mg/kg into AAV-naïve *Vgat-ires-Cre* mice also did not induce NREM sleep above the background of sleep occurring following saline injection[21]].

In converse experiments with chemogenetic inhibition of VTA^{Vgat} neurons, injecting CNO *i.p.* into VTA^{Vgat}-hM4D$_i$ mice produced 100% wakefulness for 6 hours with sustained theta frequencies in the EEG (Fig. 5d). There was an increased latency to the first NREM and REM sleep bouts to over 6 hours post-injection of CNO *i.p.* compared with saline *i.p.*-injected mice (Fig. 5e).

We next examined if subtypes of GABAergic neuron can induce NREM sleep. Subtypes of GABAergic neurons in the VTA include those expressing parvalbumin (*Pv*), somatostatin (*Som*), and in the PBP region, *Nos1*/*Vgat*[34] (see also Supplementary Fig. 9b). We chemogenetically activated VTA^{Pv}, VTA^{Som} and VTA-PBP$^{Nos1/Vgat}$ populations in the VTA (Supplementary Fig. 10) by expressing hM3Dq-mCherry in these cells. Activation of VTA^{Pv} and VTA^{Som} neurons each produced 3 hours of NREM sleep (Supplementary Fig. 10). However, activating VTA-PBP$^{Nos1/Vgat}$ neurons did not induce either sleep or wakefulness (Supplementary Fig. 10). Thus, several GABAergic subtypes in the VTA can contribute to induction of NREM sleep,

although each group activated individually does not give the full effect obtained with activating VTA^{Vgat} neurons.

Lesioning of VTA^{Vgat} neurons produces continuous wakefulness. To look at VTA^{Vgat} function in the sleep-wake cycle over 24 hours, we chronically lesioned VTA^{Vgat} neurons with AAV-DIO-CASP3 (Fig. 6a, Supplementary Fig. 11a). About 88% of the VTA^{Vgat} neurons were destroyed (Supplementary Fig. 11a). In these VTA^{Vgat}-CASP3 mice, there was an increase in wakefulness in both the "lights on" and "lights off" periods, but especially during the "lights off" period – the VTA^{Vgat}-CASP3 animals slept for only 40 minutes, whereas non-lesioned VTA^{Vgat}-GFP control mice slept 4 hours in the 12 hours of the "lights off" period (Fig. 6b). During "lights on", the least active period of the mice, the control mice slept for about 7 hours, and the VTA^{Vgat}-CASP3 mice slept for about 6 hours (Fig. 6b). During "lights-off" the average NREM episode duration of VTA^{Vgat}-CASP3 mice was much shorter, and transitions between vigilance states were dramatically decreased (Fig. 6c, d). The reduced sleep phenotype of *VTA^{Vgat}-CASP3* persisted unchanged for at least 4 months, resulting in the mice having a permanent and substantial sleep deficit (Supplementary Fig. 11b).

VTA^{Vgat} neurons are selectively wake- and REM-active. Based on the chemogenetic and lesioning results, we might have expected VTA^{Vgat} neurons to be NREM sleep-active. To test this, we made VTA^{Vgat}-GCaMP6 mice and measured the activity of VTA^{Vgat} neurons by fiber photometry during different vigilance states of freely moving mice (Fig. 6e). Surprisingly, as for the *Vglut2* neurons, we found that the Ca^{2+} signal for the VTA^{Vgat} neurons actually increased selectively during wakefulness and REM sleep (Fig. 6f). During NREM sleep the VTA^{Vgat} cells had a lower Ca^{2+} signal (Fig. 6f, g). At the transitions between the vigilance states (Fig. 6h), the $\Delta F/F$ ratio decreased from wakefulness to NREM sleep, and increased from NREM sleep to wake, and from NREM to REM sleep (Fig. 6h). Within an individual bout of wake or REM sleep, the Ca^{2+} signal of the VTA^{Vgat} cells did not differ between the earlier and later parts of the bouts (Supplementary Fig. 11c).

To search for NREM sleep-active VTA^{Vgat} neurons that might have been missed by fiber photometry, we used micro-endoscopic calcium imaging of these neurons in VTA^{Vgat}-GCaMP6f mice (Supplementary Fig. 12). We placed a gradient refractive index (GRIN) lens above the VTA, and recorded fluorescence of VTA^{Vgat} neurons during NREM sleep or wakefulness of freely moving mice (Supplementary Fig. 12a). For the single cells that were tracked (16 cells from 4 mice), Ca^{2+} levels in VTA^{Vgat} neurons increased during wake and decreased during NREM sleep (Supplementary Fig. 12b, c, d, e, f). This result further confirmed that VTA^{Vgat} neurons are selectively wake-active.

VTA^{Vgat} neurons reduce wakefulness and induce NREM sleep by both local inhibition and via projections to the LH. Because VTA^{Vgat} neurons are selectively wake- and REM-on, we hypothesized that they are not physiologically triggering NREM sleep, but they are instead limiting wakefulness. To explore how VTA^{Vgat} neurons do this**,** we conducted ChR2-based mapping of the projections of VTA^{Vgat} axons by delivering AAV-DIO-ChR2-EYFP into the VTA area of *Vgat-ires-Cre* mice. As published previously[38], dense VTA^{Vgat} ChR-positive fibers were found locally in the VTA (Fig. 7a), but also in the LH area (Fig. 7a), and to some extent in the lateral habenula and dentate granule cells of the hippocampus (Supplementary Fig. 13a); a few fibers were also in the PFC and lateral preoptic area (Supplementary Fig. 13a). The especially dense VTA^{Vgat} fibers in the VTA indicate strong local inhibition. To test these connections, we did cFOS activity-mapping by inhibiting VTA^{Vgat} neurons with 1 mg/kg CNO injected *i.p.* into VTA^{Vgat}-hM4D$_i$ mice to examine which areas of the brain expressed cFOS protein (by disinhibition). After CNO injection *i.p.*, which promoted wakefulness (Fig. 5d), cFOS was induced strongly in the VTA and LH (Fig. 7b, Supplementary Fig. 13b, c). Thus, based on cFOS expression as a readout of neuronal excitation, VTA^{Vgat} neurons cause inhibition by projecting to the LH, as well as local inhibition in the VTA.

We confirmed directly that VTA^{Vgat} neurons can mediate local inhibition. We prepared acute brain slices containing the midline VTA from *VTA^{Vgat}-ChR2-EYFP* mice, optogenetically activated the VTA^{Vgat} neurons (Fig. 7c), and observed the postsynaptic responses in non-*Vgat* cells. Whole cell patch-clamping confirmed that 87.5% of postsynaptic cells (14 out of 16 cells) received either optogentically-evoked (o) oIPSCs only, or both oIPSCs and oEPSCs (Fig. 7c); 12.5% of cells (2 out of 16 cells) had oEPSCs only (Fig. 7c). From the relative peak oIPSC and oEPSC ratios, most non-VGAT cells had significantly larger oIPSCs than oEPSCs (Fig. 7c). From single-cell PCR profiling, these non-*Vgat* neurons with oIPSCs were a mixture of VTA^{Vglut2}, VTA^{DA}, and VTA$^{Vglut2/DA}$ neurons (Fig. 7d); the two cells that responded with only oEPSCs were VTA^{Vglut2} and VTA^{DA} cells. Thus, the majority of non-*Vgat* cells in the midline VTA have a large density of inhibitory input from local VTA^{Vgat} neurons.

Because midline VTA^{Vgat} neurons inhibit midline dopamine neurons, we examined the effect of this local inhibition on wakefulness. We gave D1 and D2/3 receptor antagonists to CNO-injected VTA^{Vgat}-hM4D$_i$ mice (mice were injected *i.p.* with the dopamine receptor antagonists 30 mins before CNO *i.p.* injection – see Methods for drug concentrations). Without dopamine antagonists, CNO inhibition of VTA^{Vgat} neurons caused 6 hours of sustained wakefulness (as shown previously in Fig. 5d). With dopamine receptor antagonists, CNO-induced wakefulness was blocked by 20% (Fig. 7e), implying that the sustained wakefulness originating from the inhibited VTA^{Vgat} neurons could be partially due to the activation (disinhibition) of VTA dopamine neurons.

To test if VTA^{Vgat} neurons use local inhibition to restrict wakefulness, we infused the GABA$_A$ receptor antagonist Gabazine (SR95531) into the VTA of CNO *i.p.*-injected VTA^{Vgat}-hM3Dq mice (please see Methods for Gabazine concentration) (Fig. 7f). In

the CNO-injected VTA^{Vgat}-hM3Dq mice, Gabazine reduced CNO-induced NREM sleep by 40% (Fig. 7f). Thus, the sustained NREM sleep originating from the activated VTA^{Vgat} neurons was partially due to local inhibition of VTA^{Vglut2}, VTA^{DA}, and VTA$^{Vglut2/DA}$ neurons.

As blocking local GABA transmission with Gabazine did not completely abolish the ability of activated VTA^{Vgat} neurons to induce sustained NREM sleep, the projections of these VTA^{Vgat} neurons might also contribute. We found that following CNO inhibition of VTA^{Vgat} neurons in VTA^{Vgat}-hM4Di mice, the number of cFOS-expressing cells in the LH was strongly elevated compared with saline injections (Fig. 7b). About 50% of those FOS-positive LH cells were orexin neurons (Supplementary Fig. 13d). By injecting Retro-AAV-DIO-Chronos-GFP into the LH area of *Vgat-ires-Cre* mice, we also detected dense retro-labeled soma in the VTA (Supplementary Fig. 13e).

The results imply that the VTA^{Vgat}→LH projection participates in NREM sleep induction. We therefore placed optical fibers into the LH of VTA^{Vgat}-ChR2-EYFP mice to stimulate the terminals of VTA^{Vgat} neurons (Fig. 8a). Opto-activating VTA^{Vgat} fibers in the LH strongly and consistently initiated wake to NREM sleep transitions (Fig. 8a); Chronic opto-stimulation for 3 hours increased NREM sleep and reduced wakefulness and REM sleep (Fig. 8b). Moreover, activation could also maintain NREM sleep, with much longer episode duration but without affecting REM sleep duration (Fig. 8c), indicating that the VTA^{Vgat}→LH projection is sufficient to promote and maintain NREM sleep. However, the EEG power did not differ (Supplementary Fig. 14). Because cFOS expression is highly elevated in the DG when we inhibited VTA^{Vgat} neurons (Supplementary Fig. 13c), we also opto-stimulated the VTA^{Vgat}→DG projection, but we did not observe any effects on sleep or wakefulness (Supplementary Fig. 15a, b). The above results imply that VTA^{Vgat} neurons limit wakefulness by both inhibiting locally VTA glutamatergic and dopaminergic neurons, but also via projection targets (orexin neurons) in the lateral hypothalamus.

Discussion

Our search for novel circuits that promote wakefulness identified wake- and REM sleep-active glutamatergic/NOS1 neurons in the VTA (see Supplementary Fig. 16 for schematic summary). By contrast, we found that VTA GABAergic neurons, when artificially activated, produce a profound sedative state, but surprisingly these neurons, like VTA^{DA} and VTA^{Vglut2} cells, are selectively wake- and REM-active during normal sleep[5]. Because of this mismatch between physiological activity and the outcome of artificial activation, we speculate that VTA^{Vgat} neurons do not physiologically promote natural NREM sleep, but instead restrain wakefulness. This speculation is, in our view, supported by the results of lesioning the VTA^{Vgat} neurons (see below). Alternatively, there could be rare VTA GABAergic neurons, not detected by fiber photometry or *in vivo* Ca^{2+} imaging, that are NREM sleep-active. Such a cell type might actively induce NREM sleep. At the moment there is no direct evidence for either idea, limiting wakefulness or rare NREM-active GABA cells. There are certainly subtypes of GABA neuron in the VTA *e.g.* Pv- and Som-expressing cells, but we found that activating these also induced NREM sleep, although each subtype activated individually does not give the full effect obtained with activating the complete set of VTA^{Vgat} neurons. Future work needs to clarify how the subtypes of VTA^{Vgat} neurons interact to influence sleep and wakefulness.

When VTA^{Vgat} neurons are lesioned this causes permanent sleep loss that persists for months (Supplementary Fig. 11b). It will be interesting to identify metabolic changes produced by this long-term loss of sleep. The effects of the VTA^{Vgat} and VTA^{Vglut2} lesions, *i.e*. more and less wakefulness respectively, manifest selectively during the “lights-off”/active phase of the mice (Fig. 2b, Fig. 6a and Supplementary Fig. 11). This fits with multiunit recordings from mouse VTA neurons, where most cells are under circadian control and fire more during “lights off”[39].

Loss of VTA^{Vglut2} neurons doubles the number of NREM sleep episodes, and so fragments wakefulness. Nevertheless, the effects of the VTA^{Vgat} lesions on wakefulness (Fig. 6a) are greater than those of lesioning VTA^{Vglut2} cells (Fig. 2b). It is

difficult to predict the effects of ablations. For example, histamine neurons, cholinergic neurons and noradrenergic neurons can be triply lesioned without influencing the baseline amounts of sleep-wake[40], yet the acute activation or inhibition of these cell groups induces larges changes in vigilance state[1]. We speculate that VTA^{Vgat} neurons are strategically important as they influence diverse targets including VTA^{Vglut2}, VTA^{DA} and LH-orexin neurons. Hence the loss of VTA^{Vgat} neurons produces large effects. The persistence of this phenotype (chronic wakefulness) post-lesion, suggests no compensation is possible, and perhaps emphasizes the importance of VTA^{Vgat} neurons in regulating vigilance state.

We propose that VTA^{Vgat} neurons limit wakefulness both via projections to arousal-promoting orexin neurons in the LH (Supplementary Fig. 16), and by inhibiting glutamate and dopamine neurons locally in the VTA. As expected[41], we found some midline VTA^{Vgat} neurons co-release glutamate, although the ratio of optically-evoked IPSCs to EPSCs was about 5:1 in favor of inhibition. In the LH, many (60%) of the VTA^{Vgat} targets are orexinergic neurons, but VTA^{Vgat} terminals could also inhibit wake-promoting GABAergic projection neurons as well[11,15].

When VTA^{Vgat} neurons are chemogenetically excited the duration of the evoked NREM sleep is remarkable, lasting some 6 hours, similar to sedation. Thus, VTA^{Vgat} neurons could, in principle, be a target for novel sedatives that promote a sustained NREM-like sleep (Supplementary Fig. 16). It is surprising that this strong sedative effect arising from activating VTA^{Vgat} neurons has not been noticed. Previous work emphasized that activating VTA GABAergic neurons effects motivational states by inhibiting dopamine neurons in the VTA[42], or by inhibiting cholinergic neurons in the NAc[31]. But in none of these experiments was the EEG recorded, so it is unclear how to interpret the behaviors, especially when decreases in a particular behavior were reported, which could, in fact, be caused by sedation.

Inputs or modulators that physiologically excite VTA^{Vgat} neurons will tend to decrease wakefulness. The lateral habenula (LHb) is one such nucleus that sends

many excitatory glutamatergic projections to GABAergic neurons in the VTA[43]. Thus, strong activation of this LHb pathway would be predicted to induce NREM-like sleep. We have found that the anesthetic propofol requires activation of glutamatergic neurons of the lateral habenula to induce sedation *i.e.* slow wave (delta) power in the EEG and motor immobility[44]. Downstream of the LHb, this mechanism could include the activation of the VTA^{Vgat} neurons, including those GABAergic cells in the rostromedial tegmental nucleus at the posterior end of the VTA[45].

As with VTA^{Vgat} neurons, the extreme wakefulness produced by stimulating VTA$^{Vglut2/Nos1}$ neurons may not have been noticed before because no EEG analysis was performed. We found that the midline VTA$^{Vglut2/Nos1}$ neurons promote wakefulness, in part, through the NAc and in part through the LH. The VTA$^{Vglut2/Nos1}$ terminals in the LH could excite GABAergic projection neurons that in turn promote wakefulness[11,15], as well as exciting orexin neurons. On the other hand, because lesioning the NAc increases wakefulness[46,47], this implies NAc GABAergic projection neurons limit wakefulness, or are actively inducing NREM sleep. If terminals of VTA^{DA} neurons are stimulated in the NAc, wakefulness is produced[5]. This is similar to stimulating the VTA$^{Vglut2/Nos1}$ terminals. However, since the wake-promoting effect of VTA$^{Vglut2/Nos1}$ neurons is not blocked by dopamine receptor antagonists, it could be that the wake-promoting dopamine terminals do so by promoting glutamate release in the NAc. Similar to our findings, the paraventricular thalamus also promotes wakefulness by sending glutamatergic projections to the NAc[17]. It could be that glutamate inputs local GABA neurons in the NAc, which then inhibit the NREM sleep-promoting GABAergic projection neurons. In any case, the NAc is probably a core part of the wake-promoting circuitry.

Similar to GABA and glutamate, NOS1 associates with neurons regulating both wakefulness and sleep[21,48]. A recent report found *Vglut2*/*Nos1* projection neurons in the supramammillary nucleus promote wakefulness when chemogenetically activated[14]. Our CNO injections to activate mammillary *Vglut2* neurons did not

increase wakefulness (Fig. 1j). The reason for the difference is unclear, but in principle there could be a continuous population of *Vglut2*/*Nos1* cells from the VTA through to the supramammillary nucleus.

What is the significance of the VTA$^{Vglut2/Nos1}$ or the VTA^{Vgat} neurons being REM active? Activating the VTA$^{Vglut2/Nos1}$ or the VTA^{Vgat} neurons did not produce REM sleep, and activating VTA^{Vgat} neurons during NREM sleep did not alter REM sleep duration (Fig. 8c). Therefore, the VTA^{Vglut2} and VTA^{Vgat} neurons respond to the primary REM sleep-inducing circuitry, but do not induce or maintain REM sleep.

In summary, our findings on VTA$^{Vglut2/Nos1}$ and VTA^{Vgat} neurons, and other recent discoveries on dopamine VTA neurons[5] identify the VTA as a critical center regulating wakefulness. The VTA is exceptionally well-connected, receiving glutamate and GABA inputs from nearly all brain areas[42,43,49,50], making it well suited to serve as an integrator of vigilance state. This should be considered when designing experiments to look at the role of the VTA in reward, goal-directed and social behaviours.

Acknowledgements

We thank M. Ungless (Faculty of Medicine, Imperial College London) for comments on the manuscript. Our work was supported by the Wellcome Trust (107839/Z/15/Z, N.P.F. and 107841/Z/15/Z, W.W); the UK Dementia Research Institute (WW and NPF), and the Funds for International Cooperation and Exchange of the National Natural Science Foundation of China (Grant No. 81620108012, H.D. and N.P.F.); the China Scholarship Council (YM), a Rubicon Fellowship (019.161LW.010) from the Netherlands Organization for Scientific Research (WB), an Imperial College Schrödinger Scholarship (G.M.), and an Imperial College Junior Research Fellowship (JJH). DB and JJH were also supported by The Francis Crick Institute, which receives its core funding from Cancer Research UK (FC001055), the Medical Research Council (FC001055), and the Wellcome Trust (FC001055). The Facility for Imaging by Light

Microscopy (FILM) at Imperial College London is in part supported by funding from the Wellcome Trust (grant 104931/Z/14/Z) and BBSRC (grant BB/L015129/1).

Author contributions

N.P.F. and W.W. conceived, and with X.Y. and H.D. designed the experiments, X.Y., W.L., Y.M., K.T., J.J.H., E.C.H., W.B., G.M., D.W., L.L., J.G., M.C., Y.L., R.Y., D.B. and Q. Y. performed the experiments and/or data analysis, A.L.V. provided the Neurologgers, N.P.F. and W.W. contributed to the data analysis and with H.D. supervised the project. N.P.F., X.Y. and W.W. wrote the paper.

Competing interests

The authors declare no competing interests.

References

1 Scammell, T. E., Arrigoni, E. & Lipton, J. O. Neural Circuitry of Wakefulness and Sleep. *Neuron* **93**, 747-765, doi:10.1016/j.neuron.2017.01.014 (2017).

2 Weber, F. & Dan, Y. Circuit-based interrogation of sleep control. *Nature* **538**, 51-59, doi:10.1038/nature19773 (2016).

3 Saper, C. B. & Fuller, P. M. Wake-sleep circuitry: an overview. *Curr Opin Neurobiol* **44**, 186-192, doi:10.1016/j.conb.2017.03.021 (2017).

4 Gent, T. C., Bassetti, C. & Adamantidis, A. R. Sleep-wake control and the thalamus. *Curr Opin Neurobiol* **52**, 188-197, doi:10.1016/j.conb.2018.08.002 (2018).

5 Eban-Rothschild, A., Rothschild, G., Giardino, W. J., Jones, J. R. & de Lecea, L. VTA dopaminergic neurons regulate ethologically relevant sleep-wake behaviors. *Nat Neurosci* **19**, 1356-1366, doi:10.1038/nn.4377 (2016).

6 Yu, X. *et al.* Wakefulness Is Governed by GABA and Histamine Cotransmission. *Neuron* **87**, 164-178, doi:10.1016/j.neuron.2015.06.003 (2015).

7 Cho, J. R. *et al.* Dorsal Raphe Dopamine Neurons Modulate Arousal and Promote Wakefulness by Salient Stimuli. *Neuron* **94**, 1205-1219 e1208, doi:10.1016/j.neuron.2017.05.020 (2017).

8 Oishi, Y. *et al.* Activation of ventral tegmental area dopamine neurons produces wakefulness through dopamine D2-like receptors in mice. *Brain Struct Funct* **222**, 2907-2915, doi:10.1007/s00429-017-1365-7 (2017).

9 Kosse, C., Schone, C., Bracey, E. & Burdakov, D. Orexin-driven GAD65 network of the lateral hypothalamus sets physical activity in mice. *Proc Natl Acad Sci U S A* **114**, 4525-4530, doi:10.1073/pnas.1619700114 (2017).

10 Schone, C., Apergis-Schoute, J., Sakurai, T., Adamantidis, A. & Burdakov, D. Coreleased orexin and glutamate evoke nonredundant spike outputs and computations in histamine neurons. *Cell Rep* **7**, 697-704, doi:10.1016/j.celrep.2014.03.055 (2014).

11 Herrera, C. G. *et al.* Hypothalamic feedforward inhibition of thalamocortical network controls arousal and consciousness. *Nat Neurosci* **19**, 290-298, doi:10.1038/nn.4209 (2016).

12 Anaclet, C. *et al.* Basal forebrain control of wakefulness and cortical rhythms. *Nat Commun* **6**, 8744, doi:10.1038/ncomms9744 (2015).

13 Xu, M. *et al.* Basal forebrain circuit for sleep-wake control. *Nat Neurosci* **18**, 1641-1647, doi:10.1038/nn.4143 (2015).

14 Pedersen, N. P. *et al.* Supramammillary glutamate neurons are a key node of the arousal system. *Nat Commun* **8**, 1405, doi:10.1038/s41467-017-01004-6 (2017).

15 Venner, A., Anaclet, C., Broadhurst, R. Y., Saper, C. B. & Fuller, P. M. A Novel Population of Wake-Promoting GABAergic Neurons in the Ventral Lateral Hypothalamus. *Curr Biol* **26**, 2137-2143, doi:10.1016/j.cub.2016.05.078 (2016).

16 Gent, T. C., Bandarabadi, M., Herrera, C. G. & Adamantidis, A. R. Thalamic dual control of sleep and wakefulness. *Nat Neurosci* **21**, 974-984, doi:10.1038/s41593-018-0164-7 (2018).

17 Ren, S. *et al.* The paraventricular thalamus is a critical thalamic area for wakefulness. *Science* **362**, 429-434, doi:10.1126/science.aat2512 (2018).

18 Weber, F. *et al.* Regulation of REM and Non-REM Sleep by Periaqueductal GABAergic Neurons. *Nat Commun* **9**, 354, doi:10.1038/s41467-017-02765-w (2018).

19 Chung, S. *et al.* Identification of preoptic sleep neurons using retrograde labelling and gene profiling. *Nature* **545**, 477-481, doi:10.1038/nature22350 (2017).

20 Sherin, J. E., Shiromani, P. J., McCarley, R. W. & Saper, C. B. Activation of ventrolateral preoptic neurons during sleep. *Science* **271**, 216-219 (1996).

21 Harding, E. C. *et al.* A neuronal hub binding sleep initiation and body cooling in response to a warm external stimulus. *Current Biology* **28**, 2263-2273, doi:doi: 10.1016/j.cub.2018.05.054 (2018).

22 Anaclet, C. *et al.* The GABAergic parafacial zone is a medullary slow wave sleep-promoting center. *Nat Neurosci* **17**, 1217-1224, doi:10.1038/nn.3789 (2014).

23 Uygun, D. S. *et al.* Bottom-Up versus Top-Down Induction of Sleep by Zolpidem Acting on Histaminergic and Neocortex Neurons. *J Neurosci* **36**, 11171-11184, doi:10.1523/JNEUROSCI.3714-15.2016 (2016).

24 Morales, M. & Margolis, E. B. Ventral tegmental area: cellular heterogeneity, connectivity and behaviour. *Nat Rev Neurosci* **18**, 73-85, doi:10.1038/nrn.2016.165 (2017).

25 Russo, S. J. & Nestler, E. J. The brain reward circuitry in mood disorders. *Nat Rev Neurosci* **14**, 609-625, doi:10.1038/nrn3381 (2013).

26 Luscher, C. The Emergence of a Circuit Model for Addiction. *Annu Rev Neurosci* **39**, 257-276, doi:10.1146/annurev-neuro-070815-013920 (2016).

27 Gunaydin, L. A. *et al.* Natural neural projection dynamics underlying social behavior. *Cell* **157**, 1535-1551, doi:10.1016/j.cell.2014.05.017 (2014).

28 Hung, L. W. *et al.* Gating of social reward by oxytocin in the ventral tegmental area. *Science* **357**, 1406-1411, doi:10.1126/science.aan4994 (2017).

29 Hnasko, T. S., Hjelmstad, G. O., Fields, H. L. & Edwards, R. H. Ventral tegmental area glutamate neurons: electrophysiological properties and projections. *J Neurosci* **32**, 15076-15085, doi:10.1523/JNEUROSCI.3128-12.2012 (2012).

30 Taylor, S. R. *et al.* GABAergic and glutamatergic efferents of the mouse ventral tegmental area. *J Comp Neurol* **522**, 3308-3334, doi:10.1002/cne.23603 (2014).

31 Creed, M. C., Ntamati, N. R. & Tan, K. R. VTA GABA neurons modulate specific learning behaviors through the control of dopamine and cholinergic systems. *Front Behav Neurosci* **8**, 8, doi:10.3389/fnbeh.2014.00008 (2014).

32 Tan, K. R. *et al.* GABA neurons of the VTA drive conditioned place aversion. *Neuron* **73**, 1173-1183, doi:10.1016/j.neuron.2012.02.015 (2012).

33 Taylor, N. E. *et al.* Optogenetic activation of dopamine neurons in the ventral tegmental area induces reanimation from general anesthesia. *Proc Natl Acad Sci U S A*, doi:10.1073/pnas.1614340113 (2016).

34 Paul, E. J. *et al.* nNOS-expressing neurons in the ventral tegmental area and substantia nigra pars compacta. *eNeuro,* 0381-18, (2018).

35 Qi, J. *et al.* VTA glutamatergic inputs to nucleus accumbens drive aversion by acting on GABAergic interneurons. *Nat Neurosci* **19**, 725-733, doi:10.1038/nn.4281 (2016).

36 Yamaguchi, T., Wang, H. L., Li, X., Ng, T. H. & Morales, M. Mesocorticolimbic glutamatergic pathway. *J Neurosci* **31**, 8476-8490, doi:10.1523/JNEUROSCI.1598-11.2011 (2011).

37 Gomez, J. L. *et al.* Chemogenetics revealed: DREADD occupancy and activation via converted clozapine. *Science* **357**, 503-507, doi:10.1126/science.aan2475 (2017).

38 van Zessen, R., Phillips, J. L., Budygin, E. A. & Stuber, G. D. Activation of VTA GABA neurons disrupts reward consumption. *Neuron* **73**, 1184-1194, doi:10.1016/j.neuron.2012.02.016 (2012).

39 Fifel, K., Meijer, J. H. & Deboer, T. Circadian and Homeostatic Modulation of Multi-Unit Activity in Midbrain Dopaminergic Structures. *Sci Rep* **8**, 7765, doi:10.1038/s41598-018-25770-5 (2018).

40 Blanco-Centurion, C., Gerashchenko, D. & Shiromani, P. J. Effects of saporin-induced lesions of three arousal populations on daily levels of sleep and wake. *J Neurosci* **27**, 14041-14048, doi:10.1523/JNEUROSCI.3217-07.2007 (2007).

41 Root, D. H. *et al.* Single rodent mesohabenular axons release glutamate and GABA. *Nat Neurosci* **17**, 1543-1551, doi:10.1038/nn.3823 (2014).

42 Nieh, E. H. *et al.* Inhibitory Input from the Lateral Hypothalamus to the Ventral Tegmental Area Disinhibits Dopamine Neurons and Promotes Behavioral Activation. *Neuron* **90**, 1286-1298, doi:10.1016/j.neuron.2016.04.035 (2016).

43 Faget, L. *et al.* Afferent Inputs to Neurotransmitter-Defined Cell Types in the Ventral Tegmental Area. *Cell Rep* **15**, 2796-2808, doi:10.1016/j.celrep.2016.05.057 (2016).

44 Gelegen, C. *et al.* Excitatory Pathways from the Lateral Habenula Enable Propofol-Induced Sedation. *Curr Biol* **28**, 580-587 e585, doi:10.1016/j.cub.2017.12.050 (2018).

45 Jhou, T. C., Fields, H. L., Baxter, M. G., Saper, C. B. & Holland, P. C. The rostromedial tegmental nucleus (RMTg), a GABAergic afferent to midbrain dopamine neurons, encodes aversive stimuli and inhibits motor responses. *Neuron* **61**, 786-800, doi:10.1016/j.neuron.2009.02.001 (2009).

46 Qiu, M. H., Vetrivelan, R., Fuller, P. M. & Lu, J. Basal ganglia control of sleep-wake behavior and cortical activation. *Eur J Neurosci* **31**, 499-507, doi:10.1111/j.1460-9568.2009.07062.x (2010).

47 Qiu, M. H. *et al.* The role of nucleus accumbens core/shell in sleep-wake regulation and their involvement in modafinil-induced arousal. *PLoS One* **7**, e45471, doi:10.1371/journal.pone.0045471 (2012).

48 Morairty, S. R. *et al.* A role for cortical nNOS/NK1 neurons in coupling homeostatic sleep drive to EEG slow wave activity. *Proc Natl Acad Sci U S A* **110**, 20272-20277, doi:10.1073/pnas.1314762110 (2013).

49 Geisler, S., Derst, C., Veh, R. W. & Zahm, D. S. Glutamatergic afferents of the ventral tegmental area in the rat. *J Neurosci* **27**, 5730-5743, doi:10.1523/JNEUROSCI.0012-07.2007 (2007).

50 Beier, K. T. *et al.* Circuit Architecture of VTA Dopamine Neurons Revealed by Systematic Input-Output Mapping. *Cell* **162**, 622-634, doi:10.1016/j.cell.2015.07.015 (2015).

Fig. 1 Chemogenetic mapping for novel glutamatergic areas in the posterior hypothalamus and midbrain that promote wakefulness identifies the VTA

AAV-DIO-hM3Dq-mCherry was injected into different areas of the brain of *Vglut2-ires-Cre* mice. AAV expression was determined by immunocytochemistry for mCherry (red). The images show the actual mCherry staining.

(a, b and c) AAV injection into a large volume of posterior hypothalamus and midbrain $(PH/MB)_L$. The experiment in (a) was repeated independently 5 times. The graphs show percent of wake, NREM and REM sleep and how these states vary with saline (n=5 mice) or CNO (n=5 mice) *i.p.* injections.

(d, e and f) AAV injection into a smaller volume of posterior hypothalamus and midbrain, and sleep-wake states scored as above after saline (n=4 mice) or CNO (n=5 mice) *i.p.* injections. The experiment in (d) was repeated independently 5 times.

(g, h and i) AAV injection was restricted to the LH, and sleep wake states scored following saline and CNO injection after saline (n=6 mice) or CNO (n=6 mice) *i.p.* injections. The experiment in (g) was repeated independently 6 times.

(j, k and l) AAV injection was restricted to the mammillary area, and sleep wake states scored following saline (n=7 mice) and CNO (n=7 mice) *i.p.* injection. The experiment in (j) was repeated independently 5 times. See Supplementary Fig. 2a for examples of hM3Dq-mCherry expression in individual mice.

(m, n and o) AAV injection was restricted to the interpeduncular nucleus (IPN), and sleep wake states scored following saline (n=6 mice) and CNO (n=7 mice) *i.p.* injection. The experiment in (m) was repeated independently 6 times. See Supplementary Fig. 2b for examples of individual hM3Dq-mCherry expression.

(p, q and r) AAV injection was restricted to the VTA, and sleep wake states scored following saline (n=6) and CNO (n=6) *i.p.* injection. The experiment in (p) was repeated independently 6 times. See Supplementary Fig. 2c for examples of hM3Dq-mCherry expression in individual mice.

DMH, dorsomedial hypothalamus; LH, lateral hypothalamus; PH, posterior hypothalamus; IPN, interpeduncular nucleus; MM, medial mammillary area; TMN, tuberomammillary area; VMH, ventromedial hypothalamus; VTA ventral tegmental area. All error bars represent the SEM. **p<0.01, ***p<0.001, ****p<0.0001; two-sided unpaired t-test. For detailed statistics information, see Supplementary Table1.

Fig. 2 VTA^{Vglut2} neurons consolidate wakefulness and are selectively wake- and REM sleep-active

(a) Lesioning of VTA^{Vglut2} neurons. Injection of AAV-DIO-GFP (control) or AAV-DIO-GFP and AAV-DIO-taCASP3-TEV into the VTA area of *Vglut2-ires-Cre* mice. Pictures show GFP control expression in the VTA area of VTA^{Vglut2}-GFP mice and that this GFP expression has been greatly diminished in the VTA^{Vglut2}-CASP3 mice. The experiment was repeated independently 6 times. IF, interfasicular nucleus; IPN, interpeduncular nucleus; PBP, parabrachial pigmented nucleus; PN, paranigral nucleus; PBP, parabrachial pigmented nucleus; RLi, rostral linear nucleus.

(b) Lesioning of VTA^{Vglut2} neurons. Percentage of wake, NREM and REM sleep in control VTA^{Vglut2}-GFP mice (n=7 mice) and VTA^{Vglut2}-CASP3 mice (n=8 mice), and the total vigilance times in the “lights on” and “lights off” periods.

(c, d) Lesioning of VTA^{Vglut2} neurons. Episode number and duration for wake, NREM and REM sleep, and vigilance state transitions during the “lights off” periods in VTA^{Vglut2}-GFP control mice (n=7 mice) and VTA^{Vglut2}-CASP3 mice (n=8 mice).

(e) Fiber photometry for VTA^{Vglut2} neurons. Injection of AAV-DIO-GCaMP6 into the VTA of the *Vglut2-ires-Cre* mice. The experiment was repeated independently 7 times. GCaMP6 expression can be detected in the VTA area and the trace of where the optical fiber was placed is marked.

(f) Fiber photometry Ca^{2+}spectra (bottom trace) recorded in the VTA of VTA^{Vglut2}-GCaMP6 mice aligned with the EEG spectra (middle trace) and EMG (top trace) during wakefulness, NREM and REM sleep. “Epoch” indicates vigilance state: blue, wake; green, NREM sleep; magenta, REM sleep.

(g) Fiber photometry ΔF/F ratio of the Ca^{2+} signal in V*TA^{Vglut2}-GCaMP6* mice during wakefulness, NREM sleep and REM sleep (n=7 mice; 38 sessions).

(h) Detail of how the Ca^{2+} photometry signal in *Vglut2* neurons of VTA^{Vglut2}-GCaMP6 mice changes at the boundaries of the vigilance states (n=7 mice). Ca^{2+} photometry ΔF/F ratio (bottom trace) in the VTA^{Vglut2}-GCaMP6 mice aligned with the extracted δ power in the EEG, the EEG spectra itself and EMG during wakefulness, NREM and REM sleep. "Epoch" indicates vigilance state: blue, wake; green, NREM sleep; magenta, REM sleep. Grey shaded regions represent SEM.

*p<0.05, **p<0.01, ****p<0.0001; For b-d, two-sided unpaired t-test, for g, one-way ANOVA. All error bars represent the SEM. For detailed statistics information, see Supplementary Table1.

Fig. 3 VTA^{Vglut2} neurons promote wakefulness by their projections to the LH and NAc

(a) cFOS-based activity mapping of brain regions after exciting VTA^{Vglut2} neurons. In VTA^{Vglut2}-hM3Dq mice, labelled axons mainly project from the VTA to the LH and NAc. cFOS protein expression in neurons of the LH and NAc of VTA^{Vglut2}-hM3Dq mice 2 hours after saline or CNO *i.p.* injection at ZT0. The red in the histology figure is the primary fluorescence of the hM3Dq-mCherry-positive axons coming from the VTA area, the cFOS immunohistochemistry is shown in green. The experiment was repeated independently 6 times.

CPu, caudate-putamen; IF, interfasicular nucleus; LH, lateral hypothalamus; LHb, lateral habenula; MS, medial septum; NAc, nucleus accumbens; PeF, perifornical area; PBP, parabrachial pigmented nucleus; PN, paranigral nucleus; PBP, parabrachial pigmented nucleus; RLi, rostral linear nucleus; 3V, third ventricle; VP, ventral pallidum

(b) Axonal projections of VTA^{Vglut2} neurons. AAV-DIO-ChR2-EYFP was delivered into the VTA of *Vglut2-ires-Cre* mice, and axons projecting to the LH and NAc were strongly labelled. The experiment was repeated independently 4 times.

(c, d) To functionally investigate the VTA^{Vglut2}→LH projection, an optical fiber was placed into the LH area of VTA^{Vglut2}-ChR2-EYFP mice. (c) Mice were given 120 s of optostimulation (20 Hz) during NREM sleep ("lights on" period) and the percentage and time of wake and NREM were scored (control: n=6 mice; 23 trials; ChR2: n=6 mice; 21 trials). (d) *VTA^{Vglut2}-ChR2-EYFP* mice (control: n=8 mice; ChR2: n=8 mice) were given 3 hours of opto-stimulation at the start of the sleep period ("lights on" period) and the percentage and time of wake, NREM and REM sleep were scored.

(e, f) To functionally investigate the VTA^{Vglut2}→NAc projection, an optical fiber was placed into the NAc area of VTA^{Vglut2}-ChR2-EYFP mice. (e) Mice were given 120 s of opto-stimulation (20 Hz) during NREM sleep ("lights on" period) and the percentage and time of wake and NREM were scored (control: n=9 mice; 21 trials; ChR2: n=10 mice; 20 trials). (f) VTA^{Vglut2}-ChR2-EYFP mice (control: n=6 mice; ChR2: n=6 mice) were given 3 hours of opto-stimulation at the start of the sleep ("lights on" period) and the percentage and time of wake, NREM and REM sleep were scored.

**p<0.01, ***p<0.001, ****p<0.0001, for c and e, two-sided mann-whitney u test. For d and f, two-sided unpaired t-test. All error bars represent the SEM. For (c) and (e), the shaded region represents SEM. For detailed statistics information, see Supplementary Table1.

Fig. 4 VTA$^{Vglut2/Nos1}$ neurons promote wakefulness

(a) Retro-mapping of VTA^{Vglut2}→NAc connections. Retro-AAV-DIO-Chronos-GFP was injected into the NAc of *Vglut2-ires-Cre* mice. Chronos-GFP expression was detected in cells of the VTA and Chronos-GFP retro-labeled VTA midline soma (from the NAc injection) were doubled-labelled by immunocytochemistry with NOS1 antisera. The experiment was repeated independently 3 times.

(b) Testing how VTA^{Nos1} neurons influence vigilance state. AAV-DIO-hM3Dq-mCherry or AAV-DIO-hM4D$_i$-mCherry was injected into the VTA area of *Nos1-ires-Cre* mice. Images show the expression of hM3Dq-mCherry or hM4D$_i$-mCherry in the VTA. The experiment was repeated independently 6 times.

(c) Excitation of VTA^{Nos1} neurons induces wakefulness. Percentage and time of wake, NREM and REM sleep after saline (n=7 mice) or CNO (n=7 mice) *i.p.* injection at the start of sleep period (''lights on'' period) into VTA^{Nos1}-hM3Dq mice.

(d) Inhibition of VTA^{Nos1} neurons induces NREM sleep. Percentage and time of wake, NREM and REM sleep after saline (n=7 mice) or CNO (n=5 mice) *i.p.* injection during wake period (''lights off'' period) into VTA^{Nos1}-hM4D$_i$ mice.

IF, interfasicular nucleus; PBP, parabrachial pigmented nucleus; PN, paranigral nucleus; PBP, parabrachial pigmented nucleus; RLi, rostral linear nucleus; VTA, ventral tegmental area

**p<0.01, ****p<0.0001; two-sided unpaired t-test. All error bars represent the SEM. For detailed statistics information, see Supplementary Table1.

Fig. 5 Excitation of GABAergic neurons in the VTA induces sleep and their inhibition produces continuous wakefulness

(a) Excitation and inhibition of VTA^{Vgat} neurons. AAV-DIO-hM3Dq-mCherry or AAV-DIO-hM4D$_i$-mCherry was injected into the VTA of *Vgat-ires-Cre* mice. Images show the expression of hM3Dq-mCherry or hM4D$_i$-mCherry in the VTA. The experiment was repeated independently 6 times. IF, interfasicular nucleus; PBP, parabrachial pigmented nucleus; PN, paranigral nucleus; PBP, parabrachial pigmented nucleus; RLi, rostral linear nucleus;

(b) Excitation of VTA^{Vgat} neurons induces NREM sleep and suppresses REM sleep. Two individual EEG/EMG spectra and extracted delta power from the EEG are shown for VTA^{Vgat}-hM3Dq mice that received saline (n=7 mice) or CNO (n=7 mice) *i.p.* injection during wake period (''lights off'' period). The percentage and time in wake,

NREM and REM sleep after saline (n=7 mice) or CNO (n=7 mice) injection are shown. “Epoch” indicates vigilance state: blue, wake; green, NREM sleep; magenta, REM sleep.

(c) Excitation of VTA^{Vgat} neurons reduces latency to NREM sleep. Latencies to NREM and REM sleep after saline (n=7 mice) or CNO (n=7 mice) *i.p.* injection into VTA^{Vgat}-hM3Dq mice.

(d) Inhibition of VTA^{Vgat} neurons induces wakefulness. Two individual EEG/EMG spectra and extracted delta power from the EEG are shown for VTA^{Vgat}-hM4D$_i$ mice that received saline (n=7 mice) or CNO (n=7 mice) *i.p.* injection at the start of sleep period (‘‘lights on’’ period). The percentage and time in wake, NREM and REM sleep after saline (n=7 mice) or CNO (n=7 mice) *i.p.* injection are shown. “Epoch” indicates vigilance state: blue, wake; green, NREM sleep; magenta, REM sleep.

(e) Inhibition of VTA^{Vgat} neurons increases latency to sleep. Latencies to NREM (n=7 mice) and REM sleep (n=7 mice) after CNO or saline *i.p.* injection into VTA^{Vgat}-hM4D$_i$ mice.

*p<0.05, **p<0.01, ****p<0.0001; two-sided unpaired t-test. All error bars represent the SEM. For detailed statistics information, see Supplementary Table1.

Fig. 6 VTA^{Vgat} neurons inhibit wakefulness. Lesioning of VTA^{Vgat} neurons produces extended wakefulness, but VTA^{Vgat} neurons are selectively wake- and REM-active.

(a) Lesioning of VTA^{Vgat} neurons. Injection of AAV-DIO-GFP (control) or AAV-DIO-taCASP3-TEV into the VTA area of Vgat-ires-Cre mice. Pictures show GFP control expression in the VTA area of VTA^{Vgat}-GFP mice and that this GFP expression has been greatly diminished in the caspase treated mice. The experiment was repeated independently 5 times. IF, interfasicular nucleus; PBP, parabrachial pigmented nucleus; PN, paranigral nucleus; PBP, parabrachial pigmented nucleus; RLi, rostral linear nucleus

(b) Lesioning of VTA^{Vgat} neurons increases wakefulness. Percentage of wake, NREM and REM sleep in control VTA^{Vgat}-GFP mice (n=7 mice) and VTA^{Vgat}-CASP3 mice (n=5 mice), and the total vigilance times in the “lights on” and “lights off” periods.

(c, d) Lesioning of VTA^{Vgat} neurons reduces the transitions between vigilance states and stabilizes wakefulness. Episode number and duration for wake, NREM and REM sleep, and vigilance state transitions during the “lights off” periods in VTA^{Vgat}-GFP control mice (n=7 mice) and VTA^{Vgat}-CASP3 mice (n=5 mice).

(e) Fiber photometry for Ca^{2+} levels in VTA^{Vgat} neurons. Injection of AAV-DIO-GCaMP6 into the VTA of *Vgat-ires-Cre* mice. GCaMP6 expression can be detected in the VTA area and was co-stained with GABA. The trace of where the optical fiber was placed is illustrated. The experiment was repeated independently 7 times.

(f) Fiber photometry for VTA^{Vgat} neurons. Neurons are more active in wake and REM sleep. Ca^{2+} photometry spectra (bottom trace) recorded in the VTA of VTA^{Vgat}-GCaMP6 mice aligned with the EEG spectra (middle trace) and EMG (top trace) during wakefulness, NREM and REM sleep. “Epoch” indicates vigilance state: blue: wake; green: NREM sleep; magenta, REM sleep.

(g) Fiber photometry for VTA^{Vgat} neurons. $\Delta F/F$ ratio of the Ca^{2+} photometry signal in *VTA^{Vgat}-GCaMP6f* mice during wakefulness, NREM sleep and REM sleep (n=7 mice; 41 trials).

(h) Fiber photometry for VTA^{Vgat} neurons. Detail of how the Ca^{2+} signal in *Vgat* neurons of VTA^{Vgat}-GCaMP6 mice changes at the boundaries of the vigilance states (n=7 mice). “Epoch” indicates vigilance state: blue, wake; green, NREM sleep; magenta: REM sleep. Grey shaded regions represent SEM.

*p<0.05, **p<0.01, ****p<0.0001; For b-d, two-sided unpaired t-test, for g, one-way ANOVA. All error bars represent the SEM. For detailed statistics information, see Supplementary Table1.

Fig. 7 VTA^{Vgat} neurons limit wakefulness in part by locally inhibiting dopamine and *Vglut2* neurons in the VTA

(a) Mapping axonal projections of VTA^{Vgat} neurons. AAV-DIO-ChR2-EYFP was delivered into the VTA of *Vgat-ires-Cre* mice, and axons in the local VTA and projecting to the LH were strongly labelled. The experiment was repeated independently 4 times. DG: detent granule cells; IF, interfasicular nucleus; LH, lateral hypothalamus; LHb: lateral habenula; LPO: lateral preoptic area; MCLH, magnocellular nucleus, lateral hypothalamus; MTu, medial tuberomammillary nucleus; PBP, parabrachial pigmented nucleus; PN, paranigral nucleus; RLi, rostral linear nucleus; VTA: ventral tegmental area.

(b) cFOS-based activity mapping of brain regions after inhibiting VTA^{Vgat} neurons. In VTA^{Vgat}-hM4D$_i$ mice, cFOS protein expression is found in neurons of the VTA and LH 2 hours after saline or CNO *i.p.* injection at ZT0. The red in the histology figure is the primary fluorescence of the hM4D$_i$-mCherry-positive axons, the cFOS immunohistochemistry is shown in green. The experiment was repeated independently 6 times.

(c, d) (c) Investigating the local transmitter properties of VTA^{Vgat} neurons in the midline VTA. Acute brain slice electrophysiology was performed on non-Vgat neurons in the midline VTA area in *VTA^{Vgat}-ChR2-EYFP* mice. Non-Vgat cells were visually selected by YFP negative signals, and after whole-cell status was successfully achieved, a 5ms single blue LED light pulse was given to the local VTA area. The percentages of recorded non-Vgat cells which had either oIPSCs only, or oEPSCs only, or both oIPSCs and oEPSCs were: oIPSC only: 6.25% (n=1); oIPSC and oEPSC (oIPSC: oEPSC), 81.25% (n=13); oEPSC only, 12.5% (n=2). The relative amplitude ratio of the oIPSC peaks versus the oEPSC peaks of non-Vgat cells was 5.71±1.8 (n=16). (d) Heat map for the single-cell PCR of patched cells. The genes tested for were: *Slc17a6 (vglut2); Slc6a3 (dat), Slc32a1 (vgat), th, and gad1*.

(e) VTA^{Vgat} neurons inhibit wakefulness in part by inhibiting dopamine neurons. Dopamine receptor D1 and D2/3 antagonists (SCH23390 and raclopride respectively) were injected into VTA^{Vgat}-hM4D$_i$ mice 30 min before saline or CNO injection. Percentage and time of wake was scored after saline or CNO injection (saline: n=4 mice; antagonists: n=5 mice; CNO: n=4 mice; CNO+antagonists: n=4 mice).

(f) Local inhibition from VTA^{Vgat} neurons limits wakefulness. A cannula was placed into the VTA of VTA^{Vgat}-hM3Dq mice and mice were given gabazine 10 min before saline or CNO *i.p.* injection. Percentage and time of wake was scored (saline: n=6 mice; gabazine: n=7 mice; CNO: n=8 mice; CNO+gabazine: n=6 mice).

*p<0.05, for e and f, repeated measures two-way ANOVA and Bonferroni-Holm *post hoc* test. All error bars represent the SEM. For detailed statistics information, see Supplementary Table1.

Fig. 8 VTA^{Vgat} neurons inhibit wakefulness in part via projections to the lateral hypothalamus

(a, b) To functionally test the VTA^{Vgat}→LH projections, an optical fiber was placed into the LH area of VTA^{Vgat}-ChR2-EYFP mice. (a) Mice were given 120 s of opto-stimulation (20 Hz) during their active period (during the ‘‘lights off’’ period) and the percentage and time of wake and NREM sleep were scored (control: n=7 mice; 16 trials; ChR2: n=7 mice; 16 trials). The envelopes in the graph indicate the sem; (b) VTA^{Vgat}-ChR2-EYFP mice (control: n=6 mice; ChR2: n=5 mice) were given 3 hours of opto-stimulation during the active period (“lights-off” period) and the percentage and time of wake, NREM and REM sleep were scored.

(c) Mice were given 5 min of opto-stimulation when NREM sleep occurred (control: n=5 mice; 5 trials; ChR2: n=5 mice; 5 trials). The duration of NREM and REM sleep was scored.

**p<0.01, ***p<0.001, ****p<0.0001, for a, two-sided mann-whitney u test. For b and c, two-sided unpaired t-test. All error bars represent the SEM. Shaded regions represent SEM. For detailed statistics information, see Supplementary Table1.

Methods

Mice

All experiments were performed in accordance with the UK Home Office Animal Procedures Act (1986); all procedures were approved by the Imperial College Ethical Review Committee and the Ethics Committee for Animal Experimentation of Xijing Hospital, Xi'an, and was conducted according to the Guidelines for Animal Experimentation of Chinese Council institutes. The following strains of mice were used: *Vglut2-ires-Cre: Slc17a6$^{tm2(cre)Lowl}$/J*, kindly provided by B.B. Lowell, JAX stock 016963[51]; *Vgat-ires-Cre: Slc32a1$^{tm2(cre)Lowl}$/J* kindly provided by B.B. Lowell, JAX stock 016962[51]; *Nos1-ires-Cre$^{tm1(cre)Mgmj}$/J,* JAX stock 017526[52]; *Som-ires-Cre*: *Sst$^{tm2.1(cre)Zjh/J}$*, JAX stock 013044[53]; and *Pv-Cre* B6;*129P2-Pvalb$^{tm1(cre)Arbr/J}$*, JAX stock 008069[54]. All mice used in the experiments were male and aged 8 weeks at the start of the stereotaxic injections and experiments. Mice were maintained on a 12 hr:12 hr light:dark cycle at constant temp and humidity with ad libitum food and water.

AAV transgene plasmids

pAAV-hSyn-DIO-hM3Dq-mCherry and pAAV-hSyn-DIO-hM4Di-mCherry were gifts from Bryan L. Roth (Addgene plasmids 44361 and 44362)[55]; pAAV-CBA-DIO-GFP was a gift from Edward Boyden (Addgene plasmid 28304); pAAV-EF1α-DIO-taCASP3-TEV was a gift from Nirao Shah (Addgene plasmid 45580)[56]. pAAV-EF1α-DIO-hChR2(H314R)-EYFP was a gift from Karl Deisseroth (Addgene plasmid 20298). AAV2/9-CAG-DIO-GCaMP6f was a gift from HanBio Co., Ltd (Shanghai, China), and packaged by BrainVTA (Wuhan, China).

To create pAAV-hSyn-DIO-GCaMP6s, we used the GCaMP6s reading frame from pGP-CMV-GCaMP6s-EGFP (gift of Douglas Kim[57], Addgene plasmid 40753). The plasmid pAAV-hSyn-DIO-hM3D$_q$-mCherry (see above) was digested with AscI and NheI, to remove the hM3D$_q$-mCherry reading frame but keeping both sets of loxP sites to give the pAAV-DIO backbone. The modified GCaMP6s reading frame (in-frame-mutated to remove AscI and NheI sites) was amplified by PCR from pAAV-hsyn-GCaMP6s, digested with AscI and NheI, and then ligated into the pAAV-DIO backbone to give pAAV-hSyn-DIO-GCaMP6s.

Adeno-associated virus (AAV) preparation and stereotaxic injections

To produce AAV (capsid serotype 1/2), the adenovirus helper plasmid *pFΔ6*, capsid-plasmids pH21 (AAV1) and pRVI (AAV2), and the relevant pAAV transgene plasmid (see section "AAV transgene plasmids") were co-transfected into HEK293 cells and the subsequent AAV particles were harvested on heparin columns, as described previously[58,59].

To produce retro-AAV-DIO-rc(Chronos-GFP), we used the rAAV2 packaging plasmid, a gift from Alla Karpova and David Schaffer[60] (Addgene plasmid 81070), and the helper plasmid pFΔ6, together with pAAV-EF1α-DIO-rc[Chronos-GFP]**,** a gift from Edward Boyden[61] (Addgene plasmid 62725). These plasmids were co-transfected into HEK293 cells. To purify the retro-AAV we used the AAVpro Purification Kit (all Serotypes) (Takara-Clontech, Cat#: 6666).

Surgery. Mice were anesthetized 2% isoflurane in oxygen by inhalation and received buprenorphine injection and placed on a stereotaxic frame (Angle Two, Leica Microsystems, Milton Keynes, Buckinghamshire, UK). The AAV was injected through a stainless steel 33-gauge/15mm/PST3 internal cannula (Hamilton) attached to a 10

μl Hamilton syringe, at a rate of 0.1 μl min^{-1}.

The injection co-ordinates and volume were $(PH/MB)_L$: ML (±0.85 mm), AP (-2.7 mm), DV (-5.05 mm), 1.5 ul + 1.5 ul;

$(PH/MB)_S$: ML (±0.85 mm), AP (-2.7 mm), DV (-5.05 mm), 1 ul + 1 ul;

LH: ML (±1.00 mm), AP (-1.56 mm), DV (-5.20 mm), 100 nl + 100 nl;

M: ML (±0.86 mm), AP (-2.7 mm), DV (-5.04 mm), 100 nl + 100 nl;

IPN: ML (-0.02mm), AP (-3.52 mm), DV (-4.67 mm), 20 nl + 20 nl;

VTA: ML (±0.35 mm), AP (-3.3 mm), DV (-4.25 mm), 50 nl + 50 nl;

PBP of the VTA: ML (±0.54 mm), AP (-3.52 mm), DV (-4.29 mm), 20 nl + 20 nl

After injection, the cannula was left at the injection site for at 5 min and then slowly pulled out. After injections, mice were implanted with 3 gold-plated miniature screw electrodes (–1.5 mm Bregma, +1.5 mm midline; +1.5 mm Bregma, –1.5 mm midline; –1 mm Lambda, 0 mm midline – reference electrode) with two EMG wire (AS634, Cooner Wire, CA). The EMG electrodes were inserted between the neck musculature. The EEG-EMG device was affixed to the skull with Orthodontic Resin power and Orthodontic resin liquid (Tocdental, UK).

For the telemetry EEG and EMG surgery, a TL11M2-F20-EET device (Data Science International, USA) was implanted in the abdominal cavity in mice, and four wires of which were subcutaneously lead to mouse's neck by a guiding cannula. Mice were then fixed onto the stereotaxic apparatus in a prone position. A pair of wires was imbedded into the bilateral parietal skulls (AP 0.2 mm, ML 1.5 mm, DV -0.1 mm; AP -1.7 mm, ML -0.2 mm, DV -0.1 mm) by the dental cement to record EEG. The other pair of wires was implanted in the neck muscles to monitor the EMG.

For fiber optogenetic experiments, mice received surgical implantation of a monofiberoptic cannula (200 µm; Doric Lenses, Inc., Quebec, Canada) after virus injection, above the VTA (AP −3.3 mm; ML 0.13 mm; DV −3.93 mm), NAc (AP 1.1 mm; ML 0.6 mm; DV −4.2 mm), DG (AP -1.94 mm; ML 1 mm; DV -2 mm) and LH (AP -1.4 mm; ML 1.0 mm; DV -5.16 mm). For fiber photometry experiments, mice received surgical implantation of a monofiberoptic cannula (200 µm, respectively; Doric Lenses, Inc., Quebec, Canada), after virus injection above the VTA (AP −3.3 mm; ML 0.13 mm; DV −3.93 mm) to target VTA^{Vglut2} neurons and (AP −3.3 mm; ML 0.35 mm; DV −4.15 mm) to target VTA^{Vgat} neurons and EEG/EMG implants.

The placements of the fibers from all the experiments are shown in Supplementary Fig. 17.

For the microendoscopic calcium imaging, *Vgat-ires-Cre* mice, which had already been injected with AAV2/9-CAG-DIO-GCaMP6f into the VTA were allowed to recovery from surgery for three weeks. They were then re-anesthetized with isoflurane and had TL11M2-F20-EET telemetry devices fitted (see other protocols in the Methods section). The skull was coated with UV curable resin. After 20 s of exposure to ultraviolet light, a protective coating was formed on the skull. A small hole (1 mm diameter) was drilled on the skull (AP -3.45 mm, ML 1.25 mm). To avoid bleeding or drying of the meninges and brain tissue, saline (0.9% NaCl) was superfused constantly. The tissue drill with a PCB bit (500 µm diameter) was fixed on the stereotaxic frame carefully to remove the brain tissue over the target area. By using a micromanipulator (MP285, Sutter, USA), a GRIN lens (diameter 500 µm, long 7.6 mm) was slowly implanted into the VTA (AP -3.3 mm, ML 0.35 mm, DV -4.15 mm). During

the insertion process, the lens stayed still for 10 minutes for every 1 mm insertion. The lens was then secured by dental cement and the part left outside the skull was covered by tissue glue (Kwik-Sil). One week later, the tissue glue was removed. The camera (nVista, Inscopix) was connected with the lens to check the fluorescence signals, and then the camera base (baseplate) was secured to the skull with dental cement. After surgery, mice were allowed to recover for at least 2 weeks before experiments. The positions of the GRIN lens placements for all mice are shown in Supplementary Fig. 17f.

Behavioural protocols and drug treatments

For chemogenetic experiments, clozapine-N-oxide (C0832, Sigma-Aldrich, dissolved in saline, 1 mg/kg) or saline was injected *i.p*. and the vigilance states recorded. Mice were split into random groups that received either saline or CNO injection. To test for sleep promoting effects, we injected saline or CNO during the “lights off” period when the mice were likely to be most active; and to test for wake-promoting effects, we injected saline or CNO at the start of the “lights on” period when the mice had their maximum sleep drive. For the PH/MB^{Vglut2}-hM3Dq mice, LH^{Vglut2}-hM3Dq mice, M^{Vglut2}-hM3Dq mice, IPN^{Vglut2}-hM3Dq mice, VTA^{Vglut2}-hM3Dq mice, VTA^{Nos1}-hM3Dq mice, VTA^{Vgat}-hM4Di mice, CNO or saline were injected at the start of the “lights on” sleep phase. For the VTA^{Nos1}-hM4Di mice, VTA^{Vgat}-hM3Dq mice, VTA^{Pv}-hM3Dq mice, VTA^{Som}-hM3Dq mice, VTA-PBP$^{Nos1/Vgat}$-hM3Dq mice, CNO or saline were injected i.p. during the “lights off” active phase. For the optogenetic experiments, VTA^{Vglut2}-ChR2-EYFP mice or VTA^{Vglut2}-GFP were opto-stimulated (20 Hz, 1 min) during the “lights on” phase; VTA^{Vglut2}-ChR2-EYFP→LH or VTA^{Vglut2}-ChR2-EYFP→NAc mice were opto-stimulated (20 Hz, 2 min or 5 Hz, 1 min) during the “lights on” sleep phase. For chronic

optogenetic stimulation: VTA^{Vglut2}-ChR2-EYFP→LH or VTA^{Vglut2}-ChR2-EYFP→NAc mice or NAc^{Vglut2}-Chronos-GFP→VTA mice were opto-stimulated (20 Hz, 2 s with 58 s interval) at the start of “lights on” sleep phase for 3 hours;

VTA^{Vgat}-ChR2-EYFP→LH mice were stimulated (20 Hz, 2 min) during “lights off” active phase. For chronic optogenetic stimulation: VTA^{Vgat}-ChR2-EYFP→LH mice were opto-stimulated (20 Hz, 2 s with 58 s interval) at the start of “lights on” sleep phase for 3 hours;

To examine the maintenance of NREM sleep, stimulation were performed during “lights on” sleep phase and EEG/EMG tracing were observed in a real-time window. Laser was turned on for 5 min when NREM sleep occurred.

Note: in all the Ca^{2+} photometry experiments we used GCaMP6s, and for the *in vivo* microscopy experiments for Ca^{2+} imaging we used GCaMP6f. For the photometry experiments, the Ca^{2+} signal of VTA^{Vglut2}-GCaMP6 or VTA^{Vgat}-GCaMP6 mice were measured for 2 to 6 hours during both the “lights off” wake phase and “lights on” sleep phase. To challenge the mice with novel objects or female, novel objects or female mice were put in the home cage during the “lights off” wake phase and the Ca^{2+} signal of the VTA^{Vglut2}-GCaMP6 mice was measured.

For the chemogenetic pharmacological experiments, VTA^{Vglut2}-hM3Dq, VTA^{Nos1}-hM3Dq or VTA^{Vgat}-hM4Di mice were injected (*i.p.*) with dopamine receptor D1 (SCH23390 0.03 mg/kg) and D2/3 receptor antagonists (raclopride 2 mg/kg) injection and 30 min after the antagonists’ injection, the mice were received a saline or CNO (1 mg/kg) *i.p.* injection, as previously reported[8]. VTA^{Vgat}-hM3Dq mice, gabazine (0.001 μg) or saline (300 nl) was infused through a gilded cannula according to a previous

study[62]. 10 min after infusion, the mice were received saline or CNO (1 mg/kg) by *i.p.* injection.

Locomotor activity: The locomotor activity was detected in an activity test chamber (Med Associates, Inc) with ANY-maze video tracking system. We injected saline or CNO (1 mg/kg) *i.p.* at the start of the ‘‘lights on’’ period when the mice had their maximum sleep drive, and we performed the locomotion experiment 30 min after injection. The behavior was recorded by a video tracking system (ANY-maze) using a camera (FUJIFILM co.) and measured by ANY-maze software (Stoelting Co. US.).

EEG analysis, fiber photometry, microendoscopic calcium imaging, and sleep-wake behavior

EEG and EMG: EEG and EMG signals were recorded using Neurologger 2A devices[63] or using TL11M2-F20-EET telemetry devices and dataquest ART (version 4.33). NREM sleep, REM sleep and wake states were first automatically classified using a sleep analysis software Spike2 or NeuroScore and then manually scored.

For the fiber photometry[27], a Grass SD9 stimulator was used to control a 473-nm Diode-pumped solid state (DPSS) blue laser with fiber coupler (Shanghai Laser & Optics century Co., Shanghai, China). The laser light was passed through a single source fluorescence cube (FMC_GFP_FC, Doric Lenses, Quebec, Canada) through an optical fiber patch cord (Ø 200 μm, 0.22 NA, Doric Lenses). From the filter cube, a multimodal optical patch cord (Ø 200 μm, 0.37 NA, Doric Lenses) was connected to the mouse chronically implanted fiber (Ø 200 μm, 0.37 NA) with a ceramic split mating sleeves ferrules (Thorlabs, Newton, New Jersey). The GCaMP6 output was then

filtered at 500-550 nm using a second dichroic in the fluorescence cube and converted to voltage by an amplified photodiode (APD-FC, Doric Lenses). The photodiode output was amplified by a lock-in amplifier (SR810, Stanford Research Systems, California, USA), also used to drive the laser at 125 Hz with an average power of 80 µW at the fiber tip. The signal was then digitized using a CED 1401 Micro box (Cambridge Electronic Design, Cambridge, UK) and recorded at 1 kHz using Spike2 software (Cambridge Electronic Design, Cambridge, UK).

Photometry: The photometry signal was matched with the EEG and EMG recordings. For each experiment, the photometry signal F was converted to ΔF/F by ΔF/F(t)=(F(t)-median (F))/median (F)[5]. In some recordings, we observed a decay of photometry signal at the beginning of the recordings. All the sessions were selected after the photometry signal became stable. For the sleep–wake analysis, we performed the recording 3-4 sessions per mouse, each 1-6 hours long and 1 session for 8 hours. To analyze vigilance states for wake, NREM and REM sleep, we selected the all the sessions that mice had all three states[5], and we calculated the ΔF/F photometry ratio during the contiguous three vigilance states. To analyse the transitions for vigilance states, we selected one randomly chosen session per mouse.

For the micorendoscopic Ca^{2+} imaging[64], the signal was recorded with the nVista HD system (Inscopix). We analyzed the Ca^{2+} imaging data using ImageJ plug-ins and custom MATLAB script. Video acquisitions were corrected for movement artifacts using TurboReg. Mosaic (Inscopix) was used to analyse the data using independent component analyses (PCA-ICA) as described in previous studies[65,66]. The ΔF/F ratio was calculated as ΔF/F(t)=(F(t)-median (F))/median (F). Ca^{2+} traces and ΔF/F were

matched to the EEG/EMG, which was simultaneously recorded with the Ca^{2+} imaging data.

Immunohistochemistry

Mice were transcardially perfused with 4% paraformaldehyde (Thermo scientific) in phosphate buffered saline (Sigma). Brains were removed and left in 30% sucrose/PBS. 40 or 60-µm-thick coronal sections were cut using a Leica VT1000S vibratome. Free-floating sections were washed in PBS three times for 5 min, permeabilized in PBS plus 0.4% Triton X-100 for 30 min, blocked by incubation in PBS plus 5% normal goat serum (NGS) (Vector), 0.2% Triton X-100 for 1 hour.

Sections were incubated with primary antibody diluted in PBS plus 2% NGS overnight at 4°C in a shaker. Incubated slices were washed three times in PBS for 10 min, and incubated for 2 hours with secondary antibody (Molecular Probes) in PBS and subsequently washed 4 times in PBS for 10 min (all at room temperature).

Primary antibodies used: rabbit polyclonal cFOS (1:4000, Santa Cruz Biotechnology, UK); rat monoclonal mCherry (1:2000, ThermoFisher); rabbit polyclonal GFP (1:1000, ThermoFisher); mouse monoclonal TH (1:2000, Sigma); mouse monoclonal NOS1 (1:200, Santa Cruz, UK); mouse monoclonal NOS1 (1:200, Sigma); rat monoclonal somatostatin (1:1000, Merck); mouse monoclonal parvalbumin (1:1000, Merck); mouse monoclonal Orexin-A (1:200, Santa Cruz, UK). Secondary antibodies were Alexa Fluor 488 goat anti-rabbit, Alexa Fluor 488 goat anti-mouse, Alexa Fluor 594 goat anti-rabbit, Alexa Fluor 594 goat anti-mouse, Alexa Fluor 594 goat anti-rat (1:1000, Invitrogen Molecular Probes, UK).

Slices were mounted on slides, embedded in Mowiol (with DAPI), cover-slipped, and analyzed using an upright fluorescent microscope (Nikon Eclipse 80i, Nikon Corporation, JAPAN) or a Zeiss LSM 510 inverted confocal microscope or a Leica SP5 MP confocal microscope (Facility for Imaging by Light Microscopy, FILM, Imperial College London). Images were acquired using Z-scan.

Acute brain slice electrophysiology and single-cell RT-PCR from the midline VTA area of VTA^{Vgat}-ChR2-EYFP mice

Slice preparation

VTA^{Vgat}-ChR2-EYFP mice were killed by cervical dislocation. Following decapitation, the brains were quickly removed and placed into cold oxygenated N-Methyl-D-glucamine (NMDG) solution (in mM: NMDG 93, HCl 93, KCl 2.5, NaH_2PO_4 1.2, $NaHCO_3$ 30, HEPES 20, glucose 25, sodium ascorbate 5, Thiourea 2, sodium pyruvate 3, $MgSO_4$ 10, $CaCl_2$ 0.5). Coronal brain slices (220-µm thickness) encompassing the midline VTA were obtained using a vibratome (Vibrating Microtome 7000smz-2; Campden Instruments LTD, UK). Slices were kept in NMDG solution at 33^{o}C for 15min with constant oxygenation, and transferred to fully oxygenated standard aCSF (in mM: NaCl 120, KCl 3.5, NaH_2PO_4 1.25, $NaHCO_3$ 25, glucose 10, $MgCl_2$ 1, $CaCl_2$ 2) and were maintained in a chamber that was gently and continuously aerated with carbogen gas for at least 90 min at room temperature (20–22 ^{o}C) before use for electrophysiology.

Electrophysiological recording from midline VTA neurons innervated by VTA^{Vgat} neurons in VTA^{Vgat}-ChR2-EYFP mice

Slices were transferred to a submersion recording chamber and were continuously perfused at a rate of 4-5 ml/ min with fully oxygenated aCSF at room temperature. For whole-cell recording, patching pipettes at 4-6 MΩ were pulled from autoclaved borosilicate glass capillaries (1.5mm OD, 0.86mm ID, Harvard Apparatus, #GC150F-10) and filled with RNase-free intracellular solution containing (in mM): 140 K-gluconate, 5 NaCl, 10 HEPES, 0.1 EGTA, 2 $MgCl_2$, 2 Mg-ATP, and 0.3 Na-GTP (pH 7.35, osmolality 285 mOsm) or 125 KCl, 20 NaCl, 10 HEPES, 1 EGTA, 1 $CaCl_2$, 1 $MgCl_2$, 2 Mg-ATP and 0.5 Na-GTP (pH 7.35, osmolality 285 mOsm). 0.1% Neurobiotin was included in the intracellular solutions to identify the cell position and morphology following recording. Recordings were performed in current clamp or voltage clamp mode using a Multiclamp 700B amplifier (Molecular Devices, CA). Access and input resistances were monitored throughout the experiments using a 5-mV voltage step. The access resistance was typically <20 MΩ, and results were discarded if resistance changed by more than 20%. Membrane capacitance (C_m) was measured under voltage clamp at -50 mV using a hyperpolarizing 10 mV, 250 ms step. C_m was measured from the change in membrane charge taken from the integrated capacity transients (pClamp, Molecular Devices).

Non YPF+ neurons (presumed non VTA^{Vgat} neurons) were visually identified and randomly selected. To maximize RNA recovery, the internal solution in the patch pipette was limited up to 1 µl. A blue light (470 nM) was delivered by TTL-control LED to the entire field through the objective. After the stable voltage clamp was achieved, a single 5 ms or 25 Hz (5 ms) were given at the 30 s and 60 s inter-sweep interval, subsequently. The light intensity was adjusted according to the magnitude of its response.

At the end of each recording, cytoplasm was aspirated into the patch pipette, and expelled into a PCR tube contained lysate buffer. The single cell RT-PCR assays were performed using the Single-Cell to-CT Kit (Ambion). The content of the neuron was aspirated into the recording pipette and expelled into cell lysis/DNase I solution. Reverse transcription and cDNA pre-amplification were performed according to the kit protocol. qPCR was performed using the TaqMan Gene Expression Assay system (Applied Biosystems machine, Foster City, USA). The mouse TaqMan assay probes were designed by, and purchased from Invitrogen (Thermofisher): m18srRNA, Mm03928990_g1; mSlc17a6 (*Vglut2*) Mm00499876_m1; mSlc6a3 (*dat*) Mm00438388_m1; mTh Mm00447557_m1; mGad1: Mm04207432_g1; mSlc32a1 (*Vgat*) Mm00494138_m1; The single cell gene expression matrix was made in Origin.

Quantification and statistics. All statistical tests were run in "Origin 2015" (Origin Lab). The individual tests we used are given in the figure legends and the details are supplied in Supplementary Table 1. All data are given as mean ± SEM unless otherwise stated in the figure legends. No statistical methods were used to pre-determine sample sizes but our sample sizes are similar to those reported in previous publications[21,44]. The data met the assumptions of the statistical tests used. Before using any given statistical test we formally tested for normality and equal variances. When we found the data were non-normal we used non-parametric tests (details in the relevant figure legends and in in Supplementary Table 1). All t-tests were two-sided.

We excluded mice where it was subsequently found that the placement of the opto-fibers was misplaced or that there was no AAV transgene expression or when this

expression was in the wrong place. Mice were assigned randomly to the experimental and control groups. When possible, experimental treatments were also randomized. When mice were given drugs verses saline, for example, they received the drug or saline in random order. All experimental data analysis was blinded, including cFOS counting, the analysis of EEG data and animal behaviour that was scored from videos.

Reporting Summary. Further information on research design is available in the Life Sciences Reporting Summary linked to this article.

Data availability statement

The datasets generated during and/or analyzed during the current study are available from the corresponding authors on reasonable request.

References

51 Vong, L. *et al.* Leptin action on GABAergic neurons prevents obesity and reduces inhibitory tone to POMC neurons. *Neuron* **71**, 142-154, doi:10.1016/j.neuron.2011.05.028 (2011).

52 Leshan, R. L., Greenwald-Yarnell, M., Patterson, C. M., Gonzalez, I. E. & Myers, M. G., Jr. Leptin action through hypothalamic nitric oxide synthase-1-expressing neurons controls energy balance. *Nat Med* **18**, 820-823, doi:10.1038/nm.2724 (2012).

53 Taniguchi, H. *et al.* A resource of Cre driver lines for genetic targeting of GABAergic neurons in cerebral cortex. *Neuron* **71**, 995-1013, doi:10.1016/j.neuron.2011.07.026 (2011).

54 Hippenmeyer, S. *et al.* A developmental switch in the response of DRG neurons to ETS transcription factor signaling. *PLoS Biol* **3**, e159, doi:10.1371/journal.pbio.0030159 (2005).

55 Krashes, M. J. *et al.* Rapid, reversible activation of AgRP neurons drives feeding behavior in mice. *J Clin Invest* **121**, 1424-1428, doi:10.1172/JCI46229 (2011).

56 Yang, C. F. *et al.* Sexually dimorphic neurons in the ventromedial hypothalamus govern mating in both sexes and aggression in males. *Cell* **153**, 896-909, doi:10.1016/j.cell.2013.04.017 (2013).

57 Chen, T. W. *et al.* Ultrasensitive fluorescent proteins for imaging neuronal activity. *Nature* **499**, 295-300, doi:10.1038/nature12354 (2013).

58 Klugmann, M. *et al.* AAV-mediated hippocampal expression of short and long Homer 1 proteins differentially affect cognition and seizure activity in adult rats. *Mol Cell Neurosci* **28**, 347-360, doi:10.1016/j.mcn.2004.10.002 (2005).

59 Murray, A. J. *et al.* Parvalbumin-positive CA1 interneurons are required for spatial working but not for reference memory. *Nat Neurosci* **14**, 297-299, doi:10.1038/nn.2751 (2011).

60 Tervo, D. G. *et al.* A Designer AAV Variant Permits Efficient Retrograde Access to Projection Neurons. *Neuron* **92**, 372-382, doi:10.1016/j.neuron.2016.09.021 (2016).

61 Klapoetke, N. C. *et al.* Independent optical excitation of distinct neural populations. *Nat Methods* **11**, 338-346, doi:10.1038/nmeth.2836 (2014).

62 Jennings, J. H. *et al.* Distinct extended amygdala circuits for divergent motivational states. *Nature* **496**, 224-228, doi:10.1038/nature12041 (2013).

63 Anisimov, V. N. *et al.* Reconstruction of vocal interactions in a group of small songbirds. *Nat Methods* **11**, 1135-1137, doi:10.1038/nmeth.3114 (2014).

64 Flusberg, B. A. *et al.* High-speed, miniaturized fluorescence microscopy in freely moving mice. *Nat Methods* **5**, 935-938, doi:10.1038/nmeth.1256 (2008).

65 Groessl, F. *et al.* Dorsal tegmental dopamine neurons gate associative learning of fear. *Nat Neurosci* **21**, 952-962, doi:10.1038/s41593-018-0174-5 (2018).

66 Chen, K. S. *et al.* A Hypothalamic Switch for REM and Non-REM Sleep. *Neuron* **97**, 1168-1176 e1164, doi:10.1016/j.neuron.2018.02.005 (2018).

Figure 1

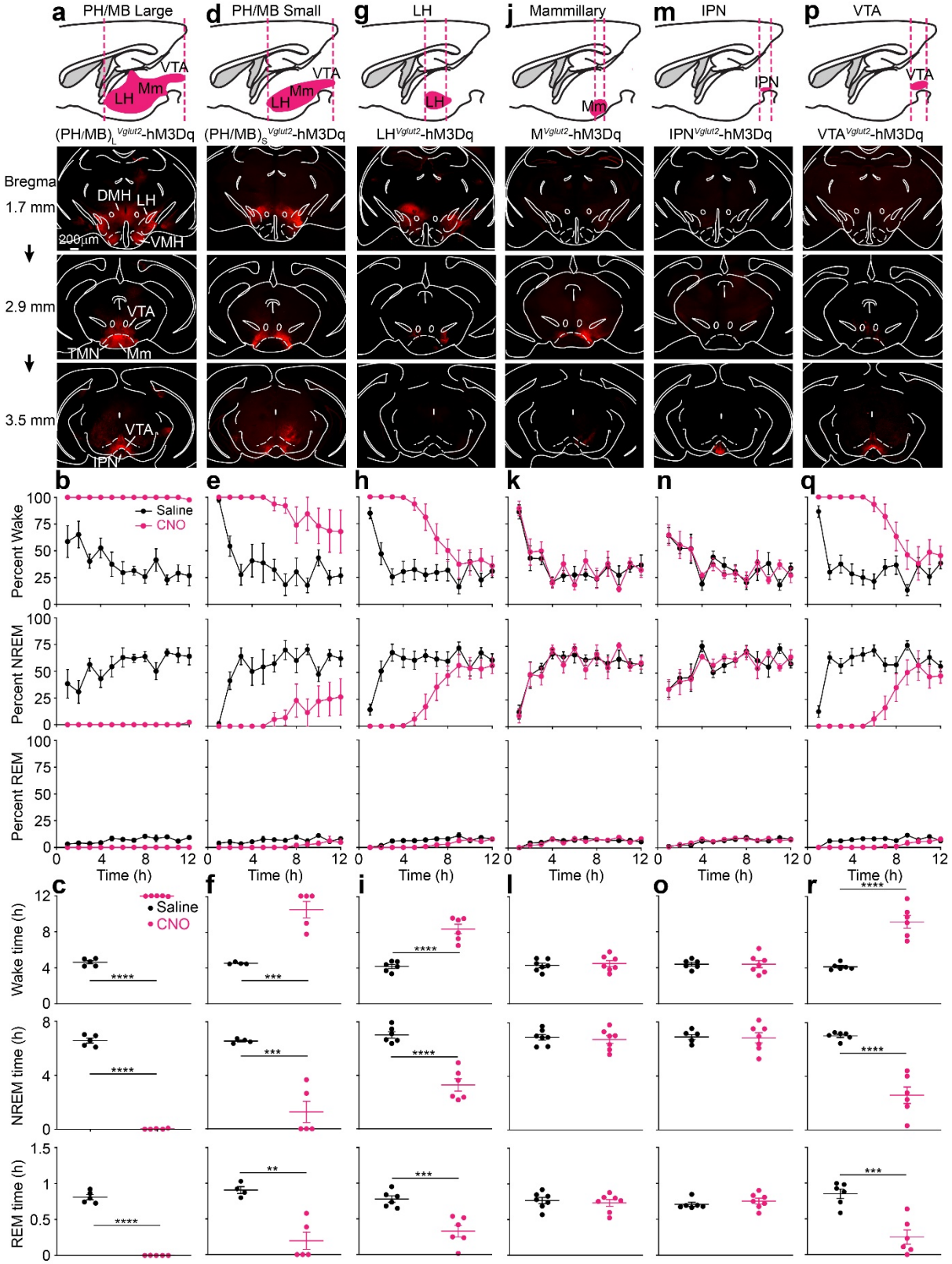

a PH/MB Large
d PH/MB Small
g LH
j Mammillary
m IPN
p VTA
(PH/MB)L Vglut2-hM3Dq
(PH/MB)S Vglut2-hM3Dq
LH Vglut2-hM3Dq
M Vglut2-hM3Dq
IPN Vglut2-hM3Dq
VTA Vglut2-hM3Dq
Bregma
1.7 mm
2.9 mm
3.5 mm
DMH
LH
VMH
VTA
TMN
Mm
IPN
200 µm
b
e
h
k
n
q
Saline
CNO
Percent Wake
Percent NREM
Percent REM
Time (h)
c
f
i
l
o
r
Wake time (h)
NREM time (h)
REM time (h)

Figure 2

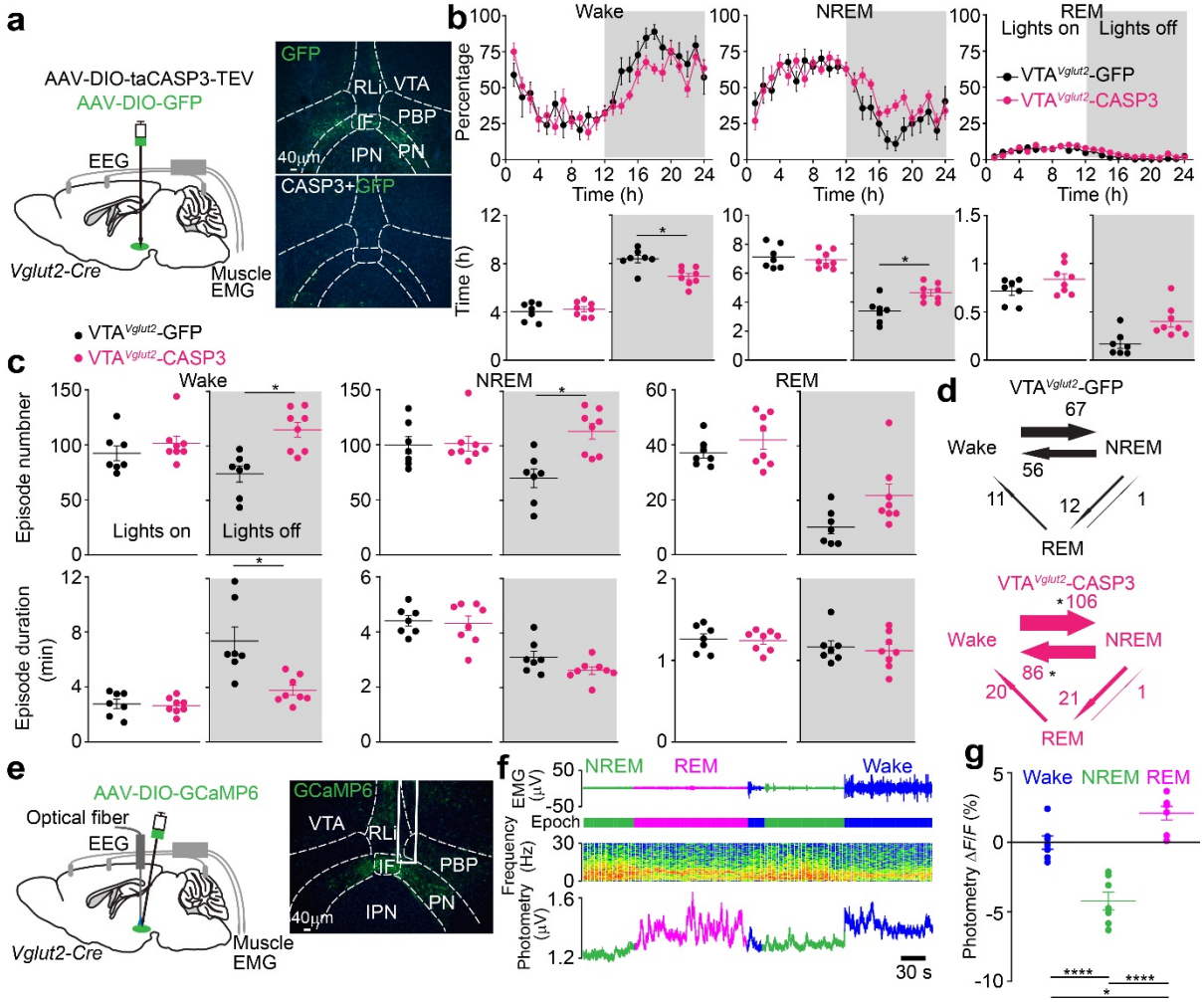

a
AAV-DIO-taCASP3-TEV
AAV-DIO-GFP
EEG
Vglut2-Cre
Muscle EMG
GFP
RLi
VTA
IF
PBP
IPN
PN
40μm
CASP3+GFP
b
Wake
NREM
REM
Lights on
Lights off
Percentage
Time (h)
VTA Vglut2-GFP
VTA Vglut2-CASP3
c
Episode number
Episode duration (min)
Lights on
Lights off
d
67
56
11
12
1
106
86
20
21
e
AAV-DIO-GCaMP6
Optical fiber
GCaMP6
f
EMG (μV)
Epoch
Frequency (Hz)
Photometry (μV)
30 s
g
Photometry ΔF/F (%)
****
h
Wake to NREM
NREM to Wake
NREM to REM
REM to Wake
Delta (μV²)
Photometry ΔF/F (%)
Time (s)

Figure 3

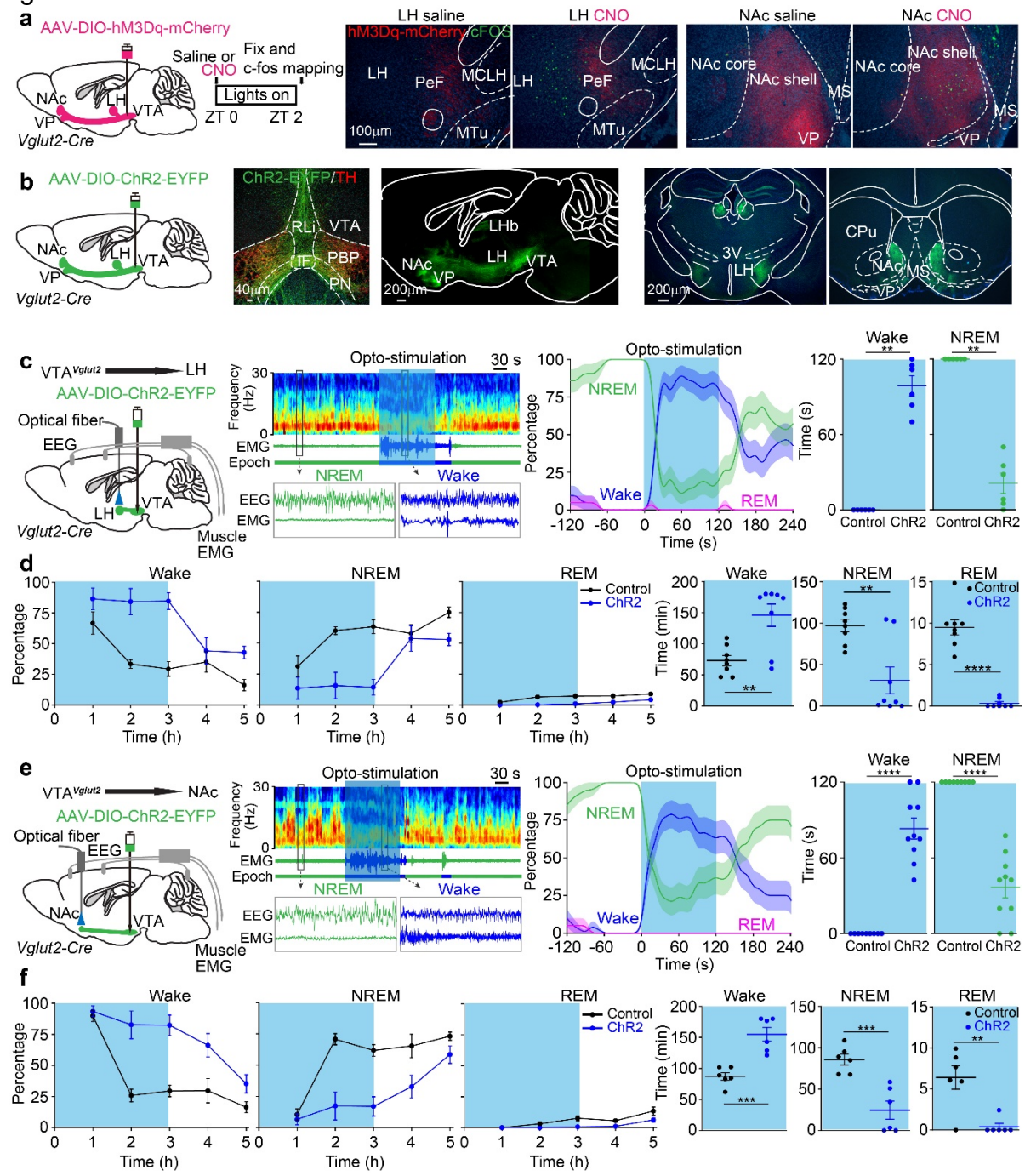

a
AAV-DIO-hM3Dq-mCherry
Saline or CNO
Fix and c-fos mapping
Lights on
ZT 0
ZT 2
NAc
LH
VTA
VP
Vglut2-Cre
LH saline
LH CNO
NAc saline
NAc CNO
hM3Dq-mCherry/cFOS
PeF
MCLH
MTu
NAc core
NAc shell
MS
100μm
b
AAV-DIO-ChR2-EYFP
ChR2-EYFP/TH
RLi
PBP
IF
PN
40μm
LHb
3V
CPu
200μm
c
VTA Vglut2 LH
AAV-DIO-ChR2-EYFP
Optical fiber
EEG
Muscle EMG
Opto-stimulation
30 s
Frequency (Hz)
EMG
Epoch
NREM
Wake
REM
Percentage
Time (s)
Control
ChR2
d
Time (h)
Time (min)
e
VTA Vglut2 NAc
f

Figure 4

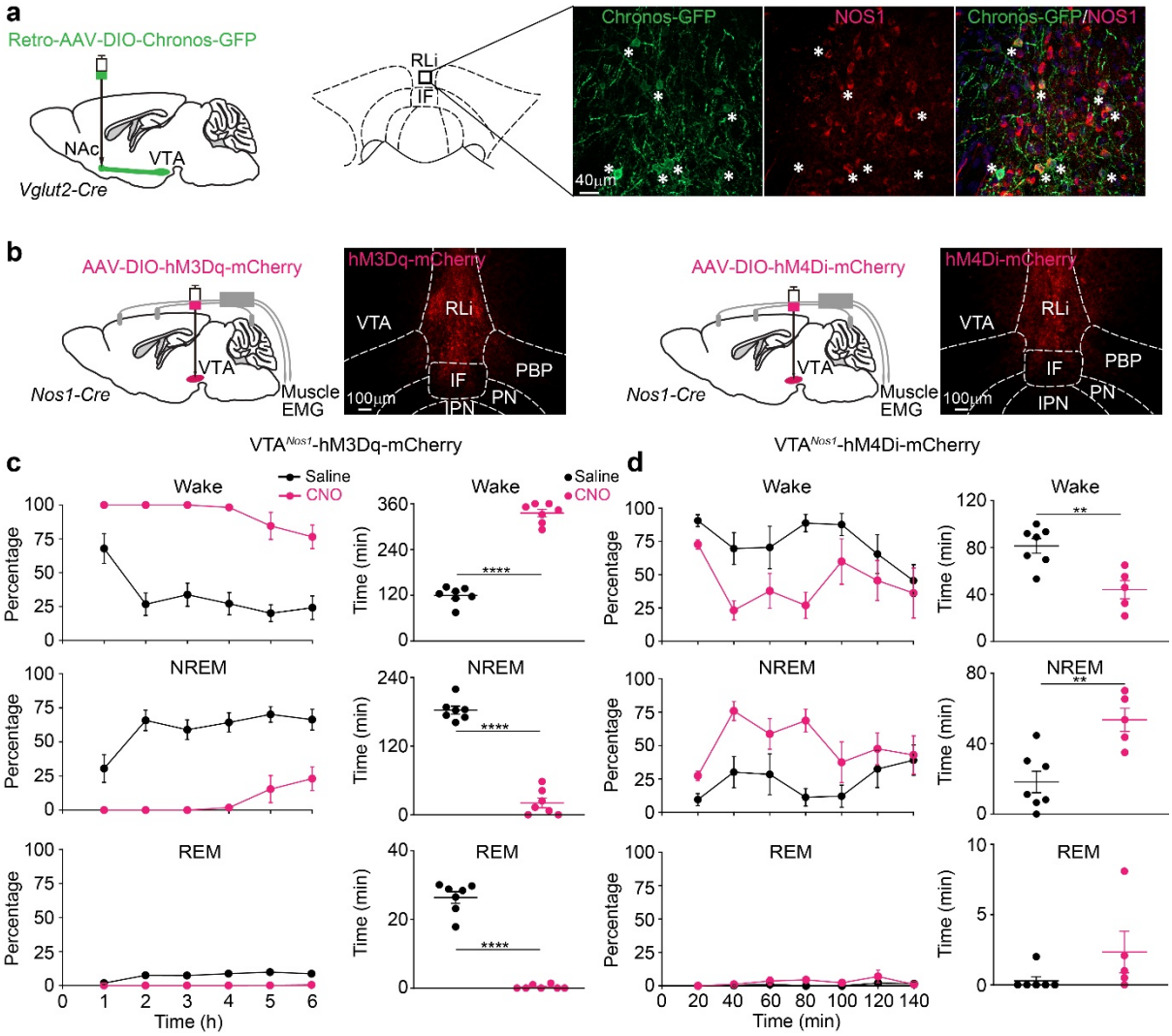

a
Retro-AAV-DIO-Chronos-GFP
NAc
VTA
Vglut2-Cre
RLi
IF
Chronos-GFP
NOS1
Chronos-GFP/NOS1
40μm
b
AAV-DIO-hM3Dq-mCherry
Nos1-Cre
VTA
Muscle EMG
hM3Dq-mCherry
RLi
PBP
IF
PN
IPN
100μm
AAV-DIO-hM4Di-mCherry
hM4Di-mCherry
c
VTANos1-hM3Dq-mCherry
Saline
CNO
Wake
NREM
REM
Percentage
Time (min)
Time (h)
****
d
VTANos1-hM4Di-mCherry
**
Time (min)

Figure 5

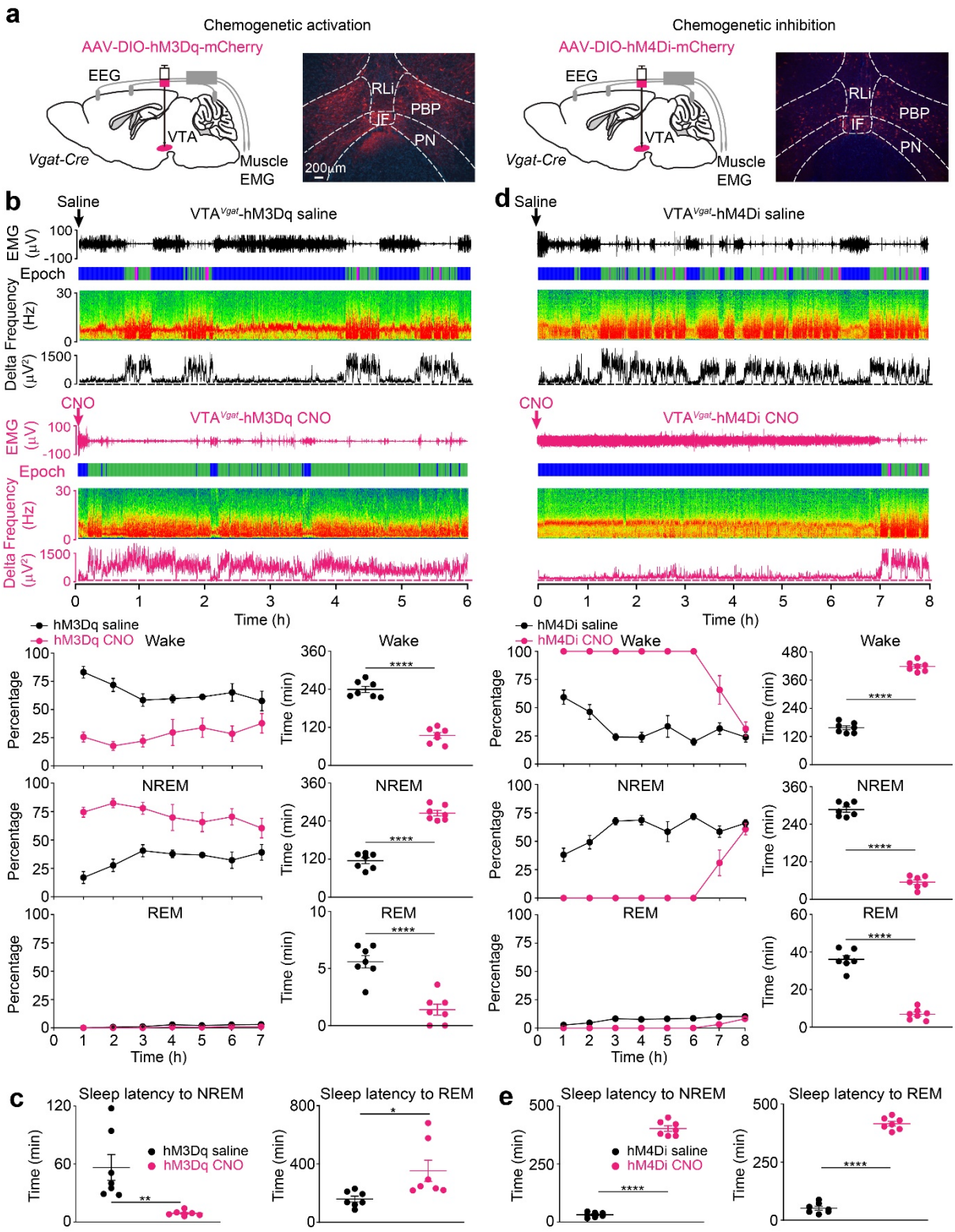

a
Chemogenetic activation
AAV-DIO-hM3Dq-mCherry
EEG
VTA
Vgat-Cre
Muscle EMG
RLi
PBP
IF
PN
200μm
Chemogenetic inhibition
AAV-DIO-hM4Di-mCherry
b
Saline
VTA Vgat-hM3Dq saline
EMG (μV)
Epoch
Delta Frequency (Hz)
Delta (μV²)
CNO
VTA Vgat-hM3Dq CNO
Time (h)
hM3Dq saline
hM3Dq CNO
Wake
NREM
REM
Percentage
Time (min)
d
VTA Vgat-hM4Di saline
VTA Vgat-hM4Di CNO
hM4Di saline
hM4Di CNO
c
Sleep latency to NREM
Sleep latency to REM
e

Figure 6

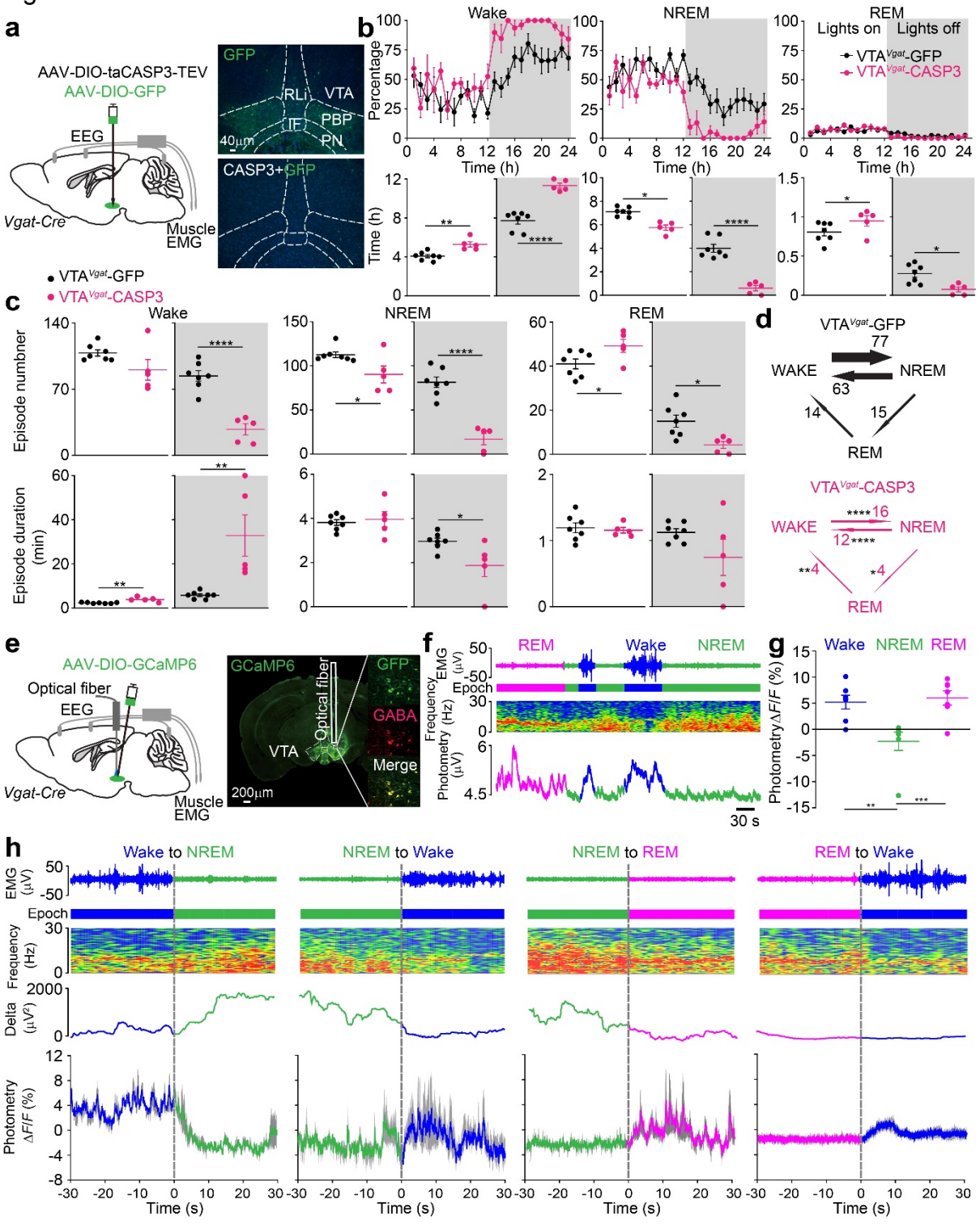

a
AAV-DIO-taCASP3-TEV
AAV-DIO-GFP
EEG
Vgat-Cre
Muscle EMG
GFP
RLi
VTA
IF
PBP
PN
40μm
CASP3+GFP
b
Wake
NREM
REM
Lights on
Lights off
VTA Vgat-GFP
VTA Vgat-CASP3
Percentage
Time (h)
c
Episode number
Episode duration (min)
d
VTA Vgat-GFP
77
WAKE
NREM
63
14
15
REM
VTA Vgat-CASP3
16
12
4
4
e
AAV-DIO-GCaMP6
Optical fiber
EEG
Vgat-Cre
Muscle EMG
GCaMP6
GFP
GABA
Merge
VTA
200μm
f
REM
Wake
NREM
EMG (μV)
Epoch
Frequency (Hz)
Photometry (μV)
30 s
g
Wake
NREM
REM
Photometry ΔF/F (%)
h
Wake to NREM
NREM to Wake
NREM to REM
REM to Wake
EMG (μV)
Epoch
Frequency (Hz)
Delta (μV²)
Photometry ΔF/F (%)
Time (s)

Figure 7

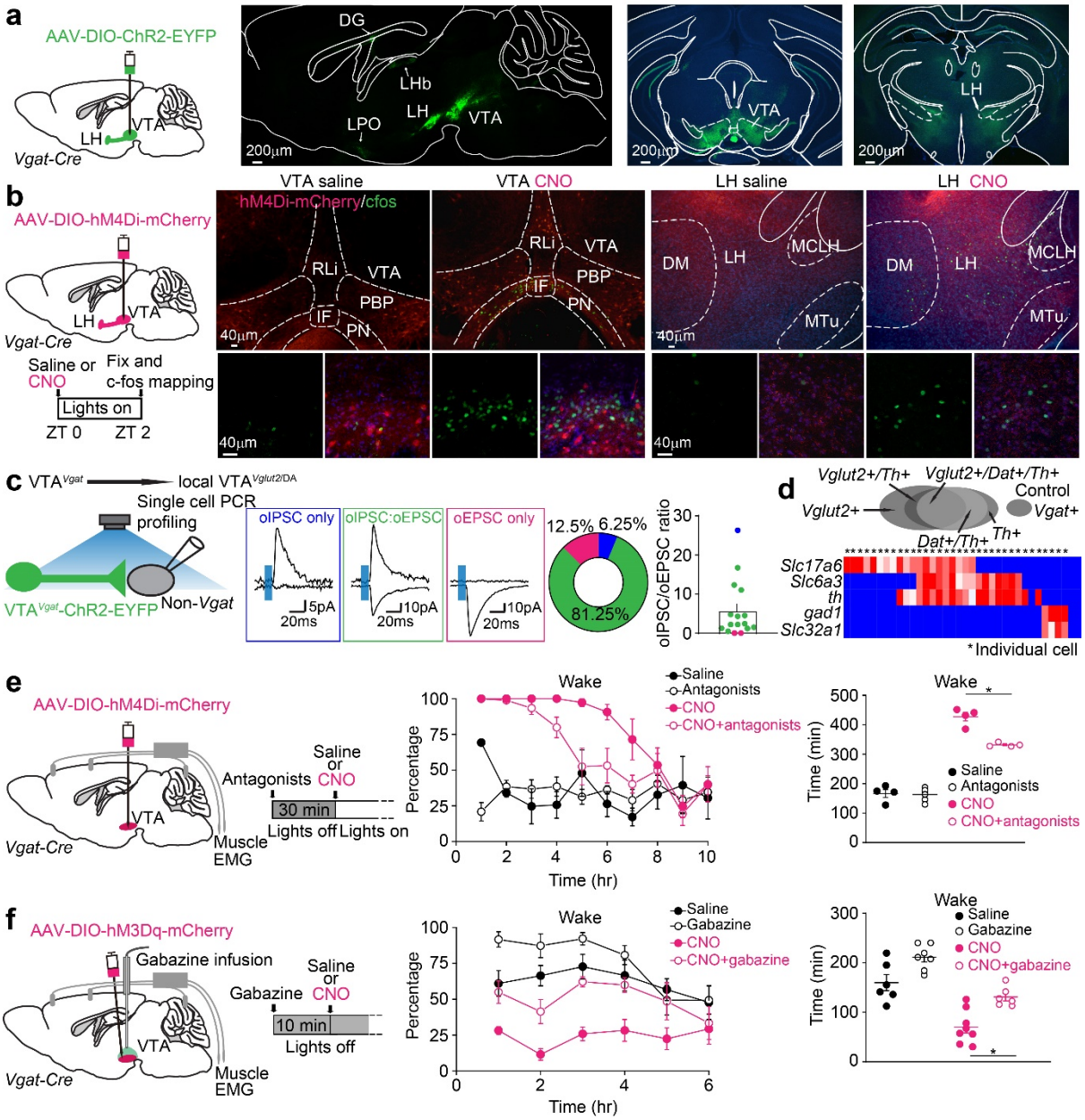
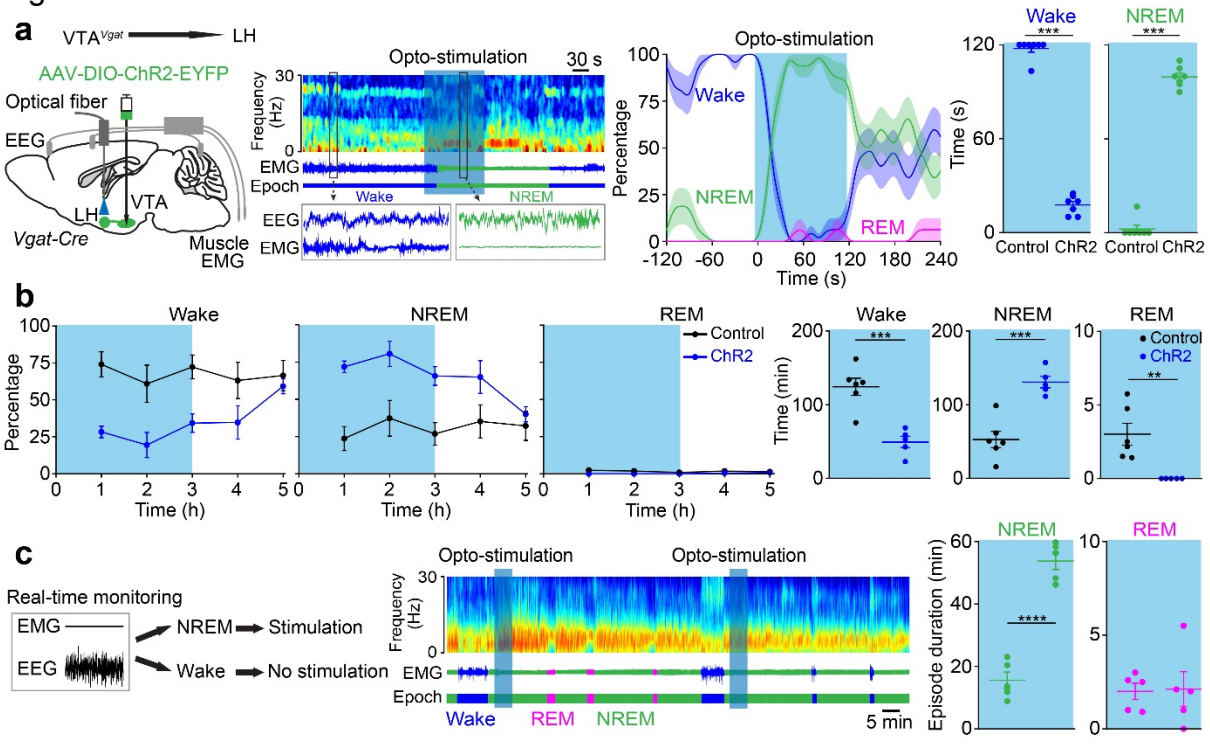
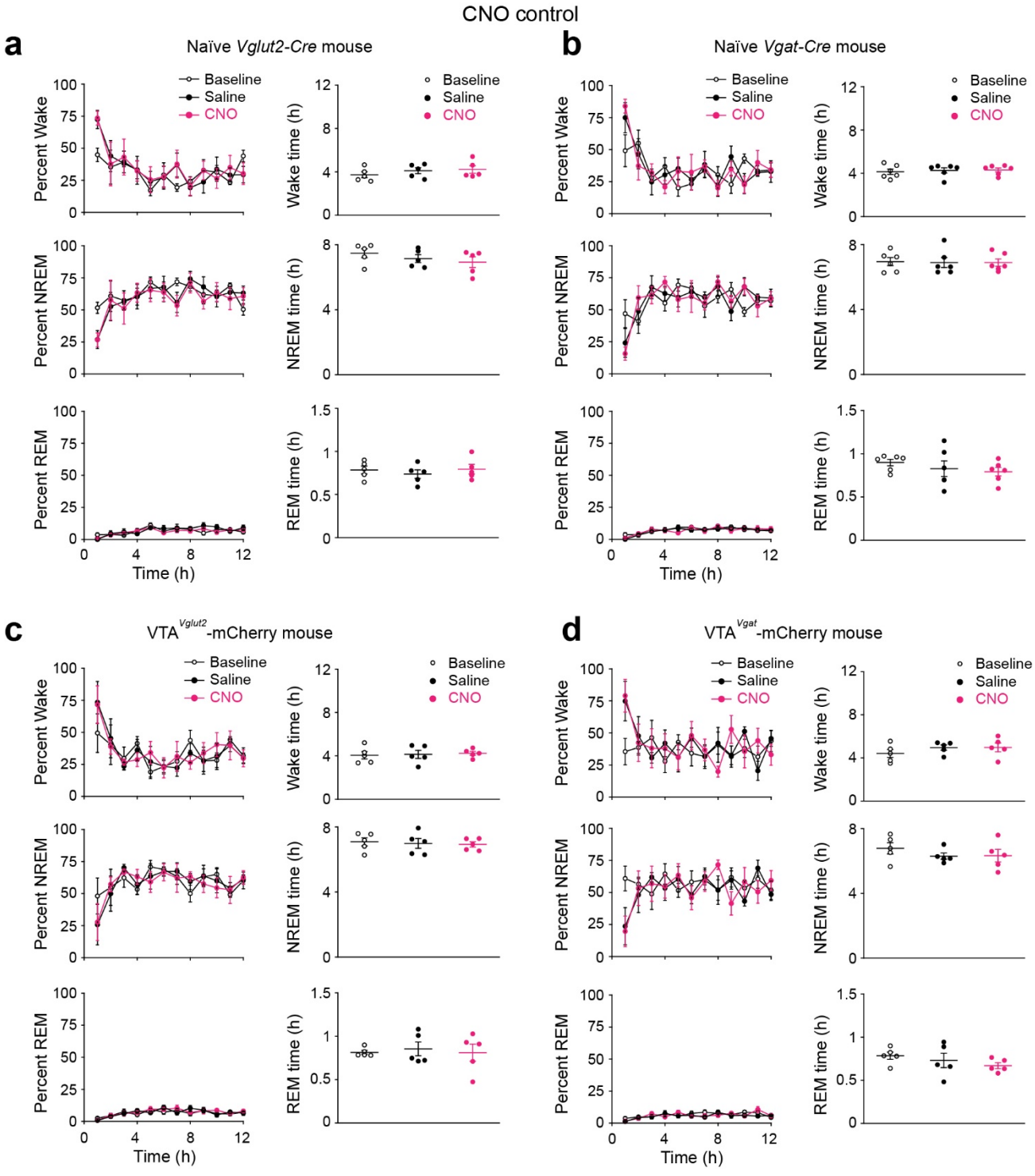

a
AAV-DIO-ChR2-EYFP
VTA
LH
Vgat-Cre
DG
LHb
LH
LPO
VTA
200μm
VTA
200μm
LH
200μm
b
AAV-DIO-hM4Di-mCherry
VTA
LH
Vgat-Cre
Saline or CNO
Fix and c-fos mapping
Lights on
ZT 0
ZT 2
VTA saline
VTA CNO
LH saline
LH CNO
hM4Di-mCherry/cfos
RLi
VTA
PBP
IF
PN
40μm
DM
LH
MCLH
MTu
c
VTA Vgat
local VTA Vglut2/DA
Single cell PCR profiling
VTA Vgat-ChR2-EYFP
Non-Vgat
oIPSC only
oIPSC:oEPSC
oEPSC only
5pA
20ms
10pA
20ms
12.5%
6.25%
81.25%
oIPSC/oEPSC ratio
d
Vglut2+/Th+
Vglut2+/Dat+/Th+
Control
Vglut2+
Vgat+
Dat+/Th+
Th+
Slc17a6
Slc6a3
th
gad1
Slc32a1
*Individual cell
e
AAV-DIO-hM4Di-mCherry
VTA
Vgat-Cre
Muscle EMG
Saline or CNO
Antagonists
30 min
Lights off
Lights on
Wake
Saline
Antagonists
CNO
CNO+antagonists
Percentage
Time (hr)
Time (min)
f
AAV-DIO-hM3Dq-mCherry
Gabazine infusion
VTA
Vgat-Cre
Muscle EMG
Saline or CNO
Gabazine
10 min
Lights off
Wake
Saline
Gabazine
CNO
CNO+gabazine
Percentage
Time (hr)
Time (min)

Figure 8


a
VTA Vgat
LH
AAV-DIO-ChR2-EYFP
Optical fiber
EEG
VTA
LH
Vgat-Cre
Muscle EMG
Opto-stimulation
30 s
Frequency (Hz)
EMG
Epoch
Wake
NREM
EEG
EMG
Opto-stimulation
Percentage
Wake
NREM
REM
Time (s)
Wake
NREM
***
***
Time (s)
Control ChR2 Control ChR2
b
Wake
NREM
REM
Control
ChR2
Percentage
Time (h)
Time (h)
Time (h)
Wake
NREM
REM
Time (min)
***
***
**
c
Real-time monitoring
EMG
EEG
NREM
Stimulation
Wake
No stimulation
Opto-stimulation
Opto-stimulation
Frequency (Hz)
EMG
Epoch
Wake
REM
NREM
5 min
NREM
REM
Episode duration (min)
****

Supplementary Information

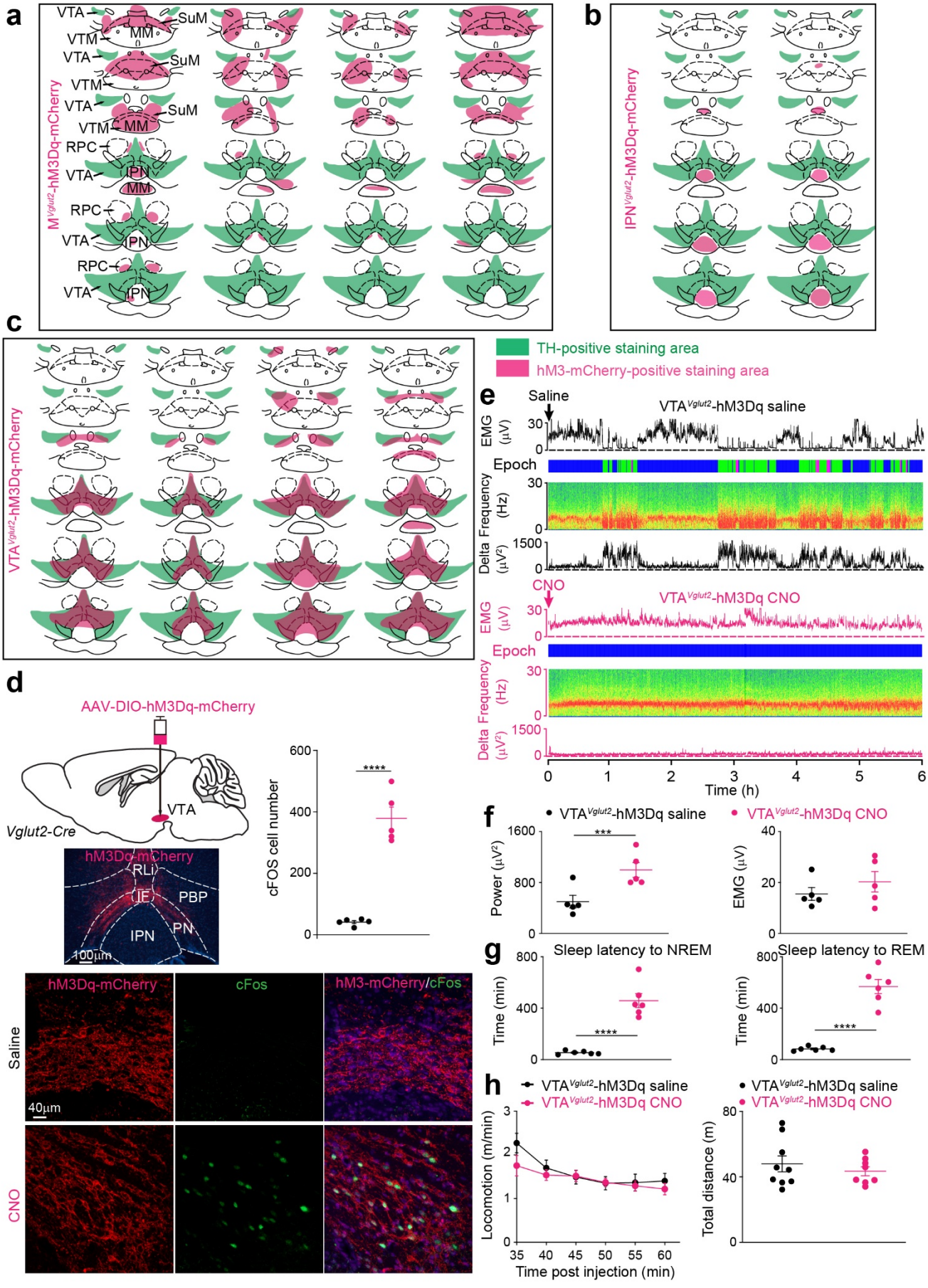


Supplementary Fig. 1 (Associated with Fig. 1, 3, 5, 7) CNO (1 mg/kg) controls for *Vglut2-ires-Cre* and *Vgat-ires-Cre* mice. CNO does not alter the amount of sleep or wake in the background strains of mice used in the study.

(a, b) Saline or CNO (1 mg/kg) was injected *i.p.* into *Vglut2-ires-Cre* mice (n=5 mice) (a) or *Vgat-ires-Cre* mice (n=6 mice) (b) which had not received any AAV injections. Percentage and time of wake, NREM and REM sleep were scored during the baseline sleep-wake cycle or after saline or CNO injection.

(c, d) AAV-DIO-mCherry was injected into the VTA of *Vglut2-ires-Cre* mice (n=5 mice) (c) or *Vgat-ires-Cre* mice (n=5 mice) (d). Percentage and time of wake, NREM and REM sleep were scored during the baseline sleep-wake cycle or after saline or CNO *i.p.* injection.

$p>0.05$, repeated measures one-way ANOVA and Bonferroni-Holm *post hoc* test. All error bars represent the SEM. For detailed statistics information, see Supplementary Table1.


a
VTA
SuM
MM
VTM
RPC
IPN
M Vglut2-hM3Dq-mCherry
b
IPN Vglut2-hM3Dq-mCherry
c
VTA Vglut2-hM3Dq-mCherry
TH-positive staining area
hM3-mCherry-positive staining area
d
AAV-DIO-hM3Dq-mCherry
VTA
Vglut2-Cre
hM3Dq-mCherry
RLi
IF
PBP
PN
IPN
100μm
cFOS cell number
****
hM3Dq-mCherry
cFos
hM3-mCherry/cFos
Saline
CNO
40μm
e
Saline
VTA Vglut2-hM3Dq saline
EMG (μV)
Epoch
Delta Frequency (μV²)
CNO
VTA Vglut2-hM3Dq CNO
Time (h)
f
VTA Vglut2-hM3Dq saline
VTA Vglut2-hM3Dq CNO
Power (μV²)
EMG (μV)
***
g
Sleep latency to NREM
Sleep latency to REM
Time (min)
****
h
VTA Vglut2-hM3Dq saline
VTA Vglut2-hM3Dq CNO
Locomotion (m/min)
Time post injection (min)
Total distance (m)

Supplementary Fig. 2 (Associated with Fig. 1)

Examples of expression of hM3Dq-mCherry expression in individual *Vglut2-Cre* mice

(a, b, c) hM3Dq-mCherry expression in individual *Vglut2-Cre* mice. Coronal brain sections shown as line diagrams from individual mice, from anterior to posterior, with areas of hM3Dq-mCherry receptor expression, shown schematically in magenta, in M^{Vglut2}-hM3Dq, IPN^{Vglut2}-hM3Dq and VTA^{Vglut2}-hM3Dq mice. Green indicates tyrosine hydroxylase (TH) staining. IPN, interpeduncular nucleus; MM, medial mammillary area; RPC, red nucleus, parvocellular part. SuM, supramammillary area. VTM, ventral tuberomammillary nucleus.

Chemogenetic activation of VTA^{Vglut2} neurons in *VTA^{Vglut2}-hM3Dq* mice promotes wakefulness but without hyperlocomotion

(d) One hour after CNO *i.p.* injection into VTA^{Vglut2}-hM3Dq mice, cFOS protein was elevated in hM3Dq-expressing VTA^{Vglut2} neurons (saline, n=5 mice; CNO, n=5 mice). Immunohistochemistry for hM3Dq-mCherry expression and cFOS in VTA^{Vglut2} neurons of VTA^{Vglut2}-hM3Dq mice 1 hour after CNO or saline *i.p.* injections. IF, interfasicular nucleus; RLi, rostral linear nucleus; PBP, parabrachial pigmented nucleus; PN, paranigral nucleus; IPN, interpeduncular nucleus.

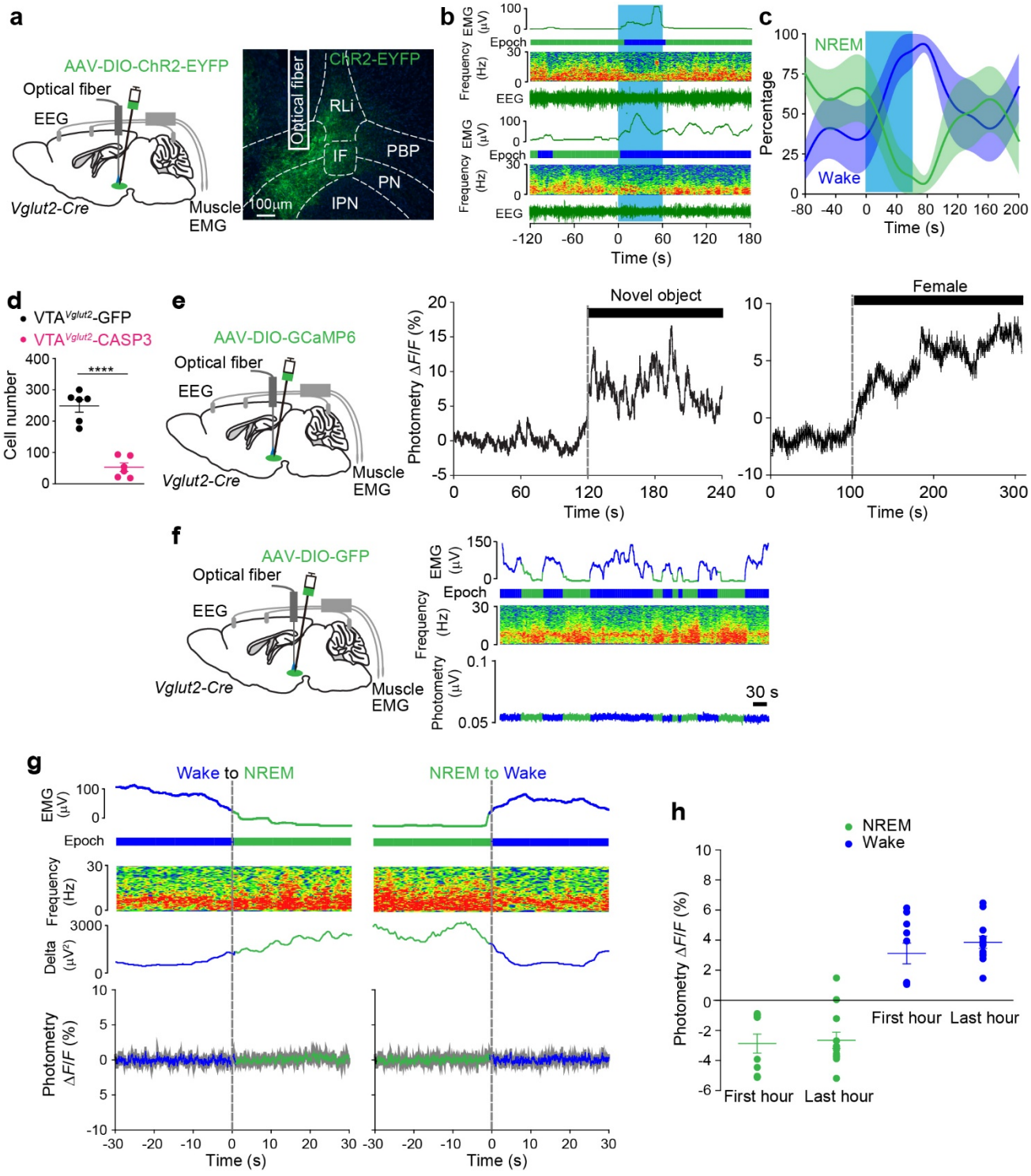
(e) Example of EMG, EEG and δ power spectra of VTA^{Vglut2}-hM3Dq mice that had received saline or CNO *i.p.* injection. “Epoch” indicates the vigilance state: blue, wake; green, NREM sleep; magenta, REM sleep.

(f) Theta power and EMG amplitude of VTA^{Vglut2}-hM3Dq mice that had received saline (n=5 mice) or CNO (n=5 mice) *i.p.* injections.

(g) Latency to NREM and REM sleep for VTA^{Vglut2}-hM3Dq mice that had received saline (n=6 mice) or CNO (n=6 mice) *i.p.* injections.

(h) Locomotor speed and distance travelled of VTA^{Vglut2}-hM3Dq mice that had received saline (n=9 mice) or CNO (n=8 mice) *i.p.* injections.

***p<0.001, ****p<0.0001; two-sided unpaired t-test. Error bars represent the SEM. For detailed statistics information, see Supplementary Table1.


a
AAV-DIO-ChR2-EYFP
Optical fiber
EEG
Vglut2-Cre
Muscle EMG
ChR2-EYFP
Optical fiber
RLi
IF
PBP
PN
IPN
100μm
b
EMG (μV)
Epoch
Frequency (Hz)
EEG
Time (s)
c
NREM
Wake
Percentage
Time (s)
d
VTA Vglut2-GFP
VTA Vglut2-CASP3
Cell number
****
e
AAV-DIO-GCaMP6
Optical fiber
EEG
Vglut2-Cre
Muscle EMG
Photometry ΔF/F (%)
Novel object
Female
Time (s)
f
AAV-DIO-GFP
Optical fiber
EEG
Vglut2-Cre
Muscle EMG
EMG (μV)
Epoch
Frequency (Hz)
Photometry (μV)
30 s
g
Wake to NREM
NREM to Wake
EMG (μV)
Epoch
Frequency (Hz)
Delta (μV²)
Photometry ΔF/F (%)
Time (s)
h
NREM
Wake
Photometry ΔF/F (%)
First hour
Last hour
First hour
Last hour

Supplementary Fig. 3 (Associated with Fig 1, 2, 3)

Optogenetic activation of VTA^{Vglut2} neurons promotes wakefulness

(a) Immunohistochemistry for ChR2-EYFP expression in VTA^{Vglut2} neurons of VTA^{Vglut2}-ChR2-EYFP mice and the track of optical fiber placement. The experiment was repeated independently 3 times. IF, interfasicular nucleus; RLi, rostral linear nucleus; PBP, parabrachial pigmented nucleus; PN, paranigral nucleus; IPN, interpeduncular nucleus.

(b) Example of EMG, EEG, epoch and EEG spectra of two VTA^{Vglut2}-ChR2-EYFP mice that had opto-activation. “Epoch” indicates the vigilance state: blue, wake; green, NREM sleep; magenta, REM sleep.

(c) Percentage of wake and NREM sleep of VTA^{Vglut2}-ChR2-EYFP mice (n=6 mice) that had opto-activation. The envelopes indicate the sem.

(d) Quantitative assessment of VTA^{Vglut2} lesioning. GFP-positive cell numbers of VTA^{Vglut2}-GFP mice (n=6 mice) and VTA^{Vglut2}-CASP3 mice (n=6 mice).

Additional photometry data for VTA^{Vglut2}-GCaMP6 mice and control photometry data (VTA^{Vglut2}-GFP mice)

(e) Ca^{2+} photometry signal of VTA^{Vglut2} neurons in VTA^{Vglut2}-GCaMP6 mice in the presence of novel objects and female mice.

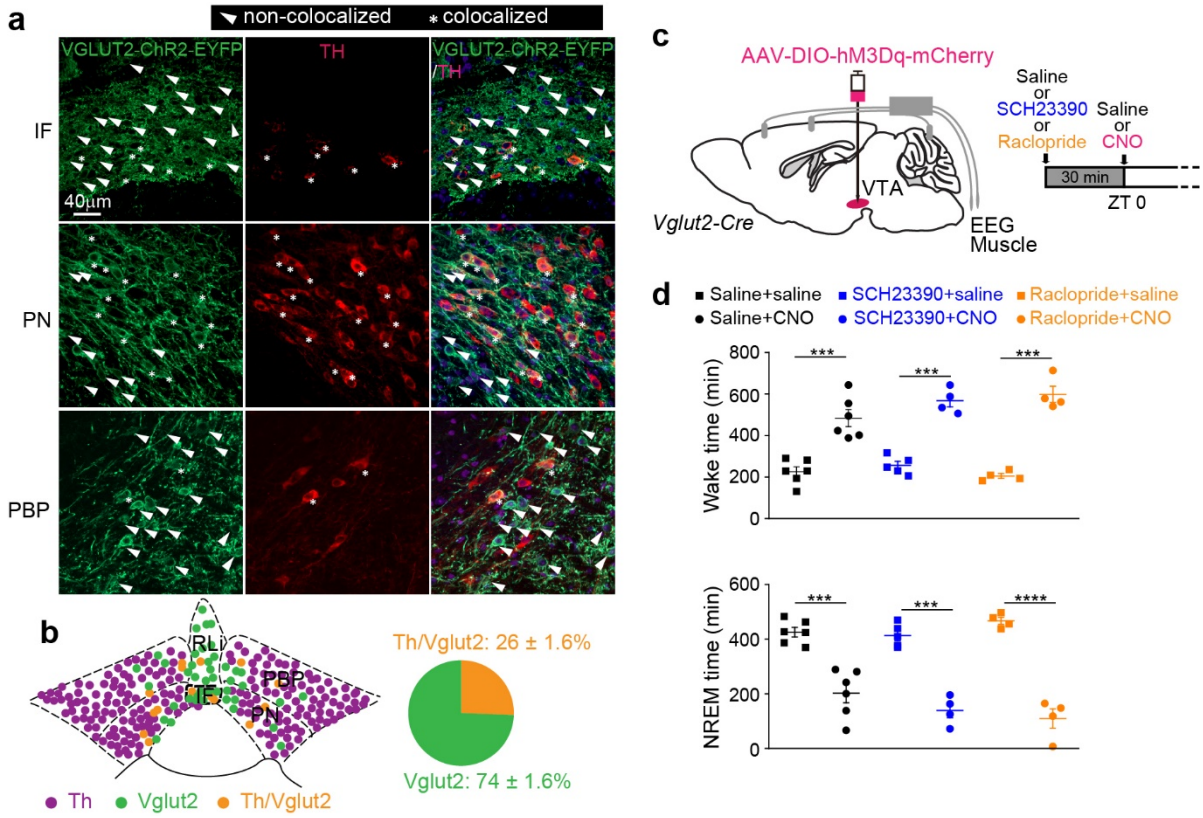
(f) Photometry control. Injection of AAV-DIO-GFP into the VTA of the *Vglut2-ires-Cre* mice. Ca^{2+} photometry spectra (bottom trace) recorded in the VTA of VTA^{Vglut2}-GFP mice aligned with the EEG (middle trace) and EMG (top trace) during wakefulness and NREM sleep. “Epoch” indicates the vigilance state: blue, wake; green, NREM sleep; magenta, REM sleep.

(g) Photometry control. Ca^{2+} signal in *Vglut2* neurons of VTA^{Vglut2}-GFP mice at the boundaries of the vigilance states. Ca^{2+} photometry $\Delta F/F$ ratio (bottom trace) in the VTA^{Vglut2}-GFP mice aligned with the extracted δ power in the EEG, the EEG spectra

and EMG during wakefulness and NREM sleep. “Epoch” indicates the vigilance state: blue, wake; green, NREM sleep; magenta, REM sleep.

(h) Photometry signal of VTA^{Vglut2} neurons in VTA^{Vglut2}-GCaMP6 mice during the first hour (1 hr) (n=4 mice; 10 sessions) and last hour (6 hr) (n= 4 mice; 12 sessions) of recording.

****p<0.0001; for d, two-sided unpaired t-test; for h, repeated measures two-way ANOVA and Bonferroni-Holm *post hoc* test. All error bars represent the SEM. For detailed statistics information, see Supplementary Table1.



Supplementary Fig. 4 (Associated with Fig 1, 2, 3)

***Vglut2* and *Th* neurons in the VTA are mostly distinct**

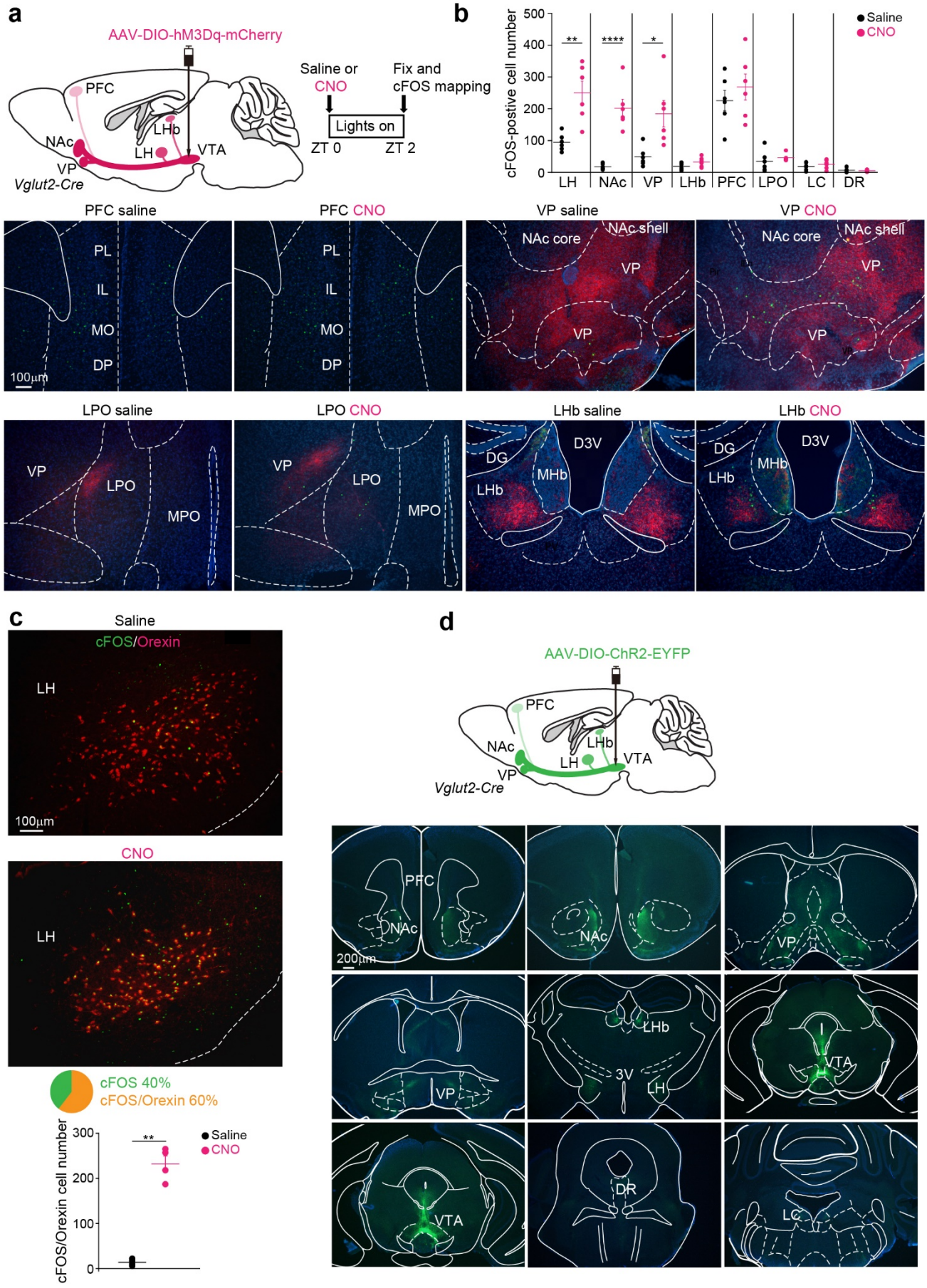
(a) Expression of ChR2-EYFP in tyrosine hydroxylase (TH)-positive neurons in the VTA of VTA^{Vglut2}-ChR2-EYFP mice**. The** experiment was repeated independently 4 times. IF, interfasicular nucleus; PN, paranigral nucleus; PBP, parabrachial pigment nucleus.

(b) Schematic of distribution of TH and *Vglut2* neurons and any colocalization in the VTA area (n=4 mice). RLi, rostral linear nucleus; PBP, parabrachial pigmented nucleus; PN, paranigral nucleus; IPN, interpeduncular nucleus. Data for pie chart represent as mean ± SEM.

VTA^{Vglut2} neuron-induced wakefulness does not depend on dopamine receptor activation

(c) Dopamine receptor D1 and D2/3 receptor antagonists (SCH23390 and raclopride respectively) were injected *i.p.* into VTA^{Vglut2}-hM3Dq mice 30 min before CNO injection, which took place at ZT0, the start of the “lights on” period.

(d) Wake and NREM time scored for 12 hours after saline or CNO injection into VTA^{Vglut2}-hM3Dq mice in the presence of dopamine receptor antagonists or control saline. *** $p<0.001$, ****$p<0.0001$, repeated measures two-way ANOVA and Bonferroni-Holm *post hoc* test. All error bars represent the SEM. For detailed statistics information, see Supplementary Table1.


a
AAV-DIO-hM3Dq-mCherry
PFC
LHb
NAc
LH
VTA
VP
Vglut2-Cre
Saline or CNO
Fix and cFOS mapping
Lights on
ZT 0
ZT 2
b
cFOS-postive cell number
Saline
CNO
LH
NAc
VP
LHb
PFC
LPO
LC
DR
PFC saline
PFC CNO
VP saline
VP CNO
PL
IL
MO
DP
100μm
NAc core
NAc shell
LPO saline
LPO CNO
LHb saline
LHb CNO
LPO
MPO
DG
D3V
MHb
c
Saline
cFOS/Orexin
CNO
cFOS 40%
cFOS/Orexin 60%
cFOS/Orexin cell number
d
AAV-DIO-ChR2-EYFP
200μm
3V

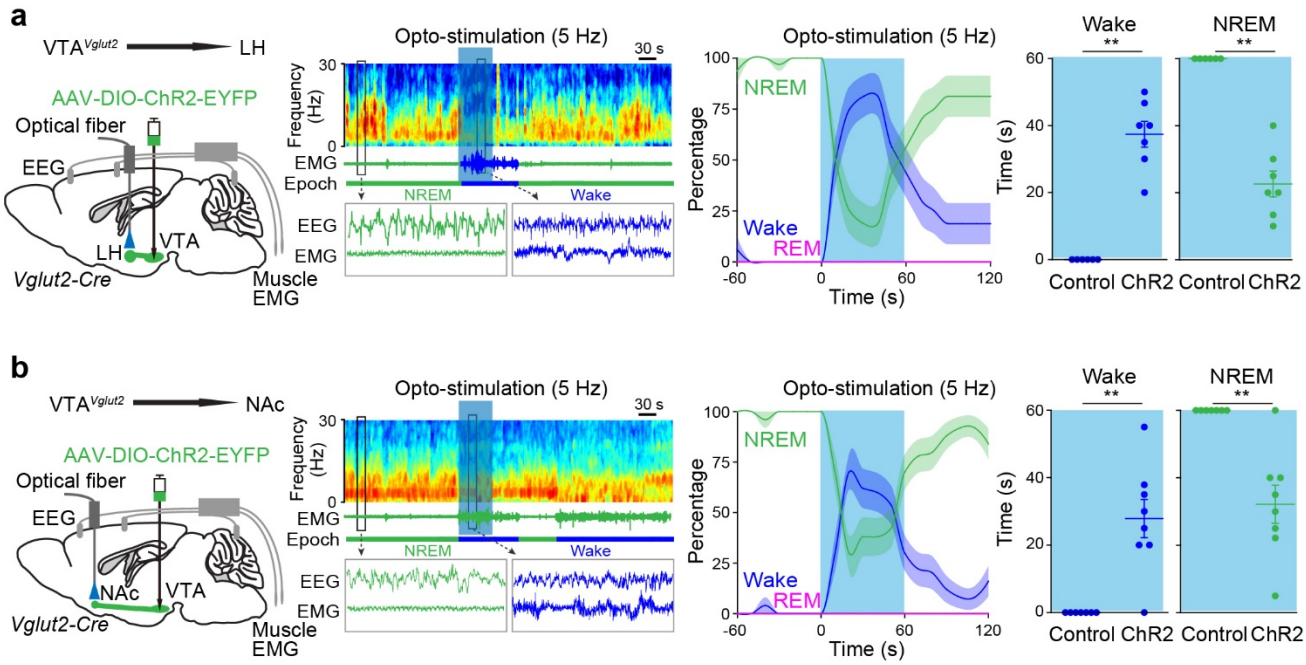
Supplementary Fig. 5 (Associated with Fig. 3) Chemogenetic and optogenetic circuit mapping of VTA^{Vglut2} neurons

(a, b) Chemogenetic mapping with cFOS expression following activation of VTA^{Vglut2} neurons. The number of cFOS neurons identified immunohistochemically (green dots) were counted (see graph in B) throughout the brain two hours after CNO (n=6 mice) or saline (n=6 mice) *i.p.* injection at ZT0 (start of "lights on") in VTA^{Vglut2}-hM3Dq mice. The magenta staining is the primary florescence of VTA^{Vglut2} axons containing hM3Dq-mCherry protein.

(c) Double-labelling and quantification of cFOS and orexin expression by immunocytochemistry in the LH area of VTA^{Vglut2}-hM3Dq mice 2 hours after saline (n = 4 mice) or CNO *i.p.* injection (n = 4 mice).

(d) Circuit mapping for VTA^{Vglut2}-ChR2-EYFP mice in whole brain. PFC, prefrontal cortex. PL, prelimbic cortex; IL, infralimbic cortex; MO, medial orbitocortex; DP, dorsal peduncular cortex; VP, ventral pallidum; NAc, nucleus accumbens; LPO, lateral preoptic area; MPO, medial preoptic area; LH, lateral hypothalamus; DM, dorsomedial hypothalamus; PeF, perifornical region; MCLH, magnocellular nucleus, lateral hypothalamus; MTu, medial tuberomammillary nucleus; LHb, lateral habenula; MHb, medial habenula; DG, dentate granule cells; D3V, dorsal third ventricle; LC, locus ceruleus, LDT, lateral dorsal tegmental area; VTA ventral tegmental area; DR, dorsal raphe.

*p<0.05, **p<0.01, ****p<0.0001; two-sided unpaired t-test. Error bars represent the SEM. For detailed statistics information, see Supplementary Table1.

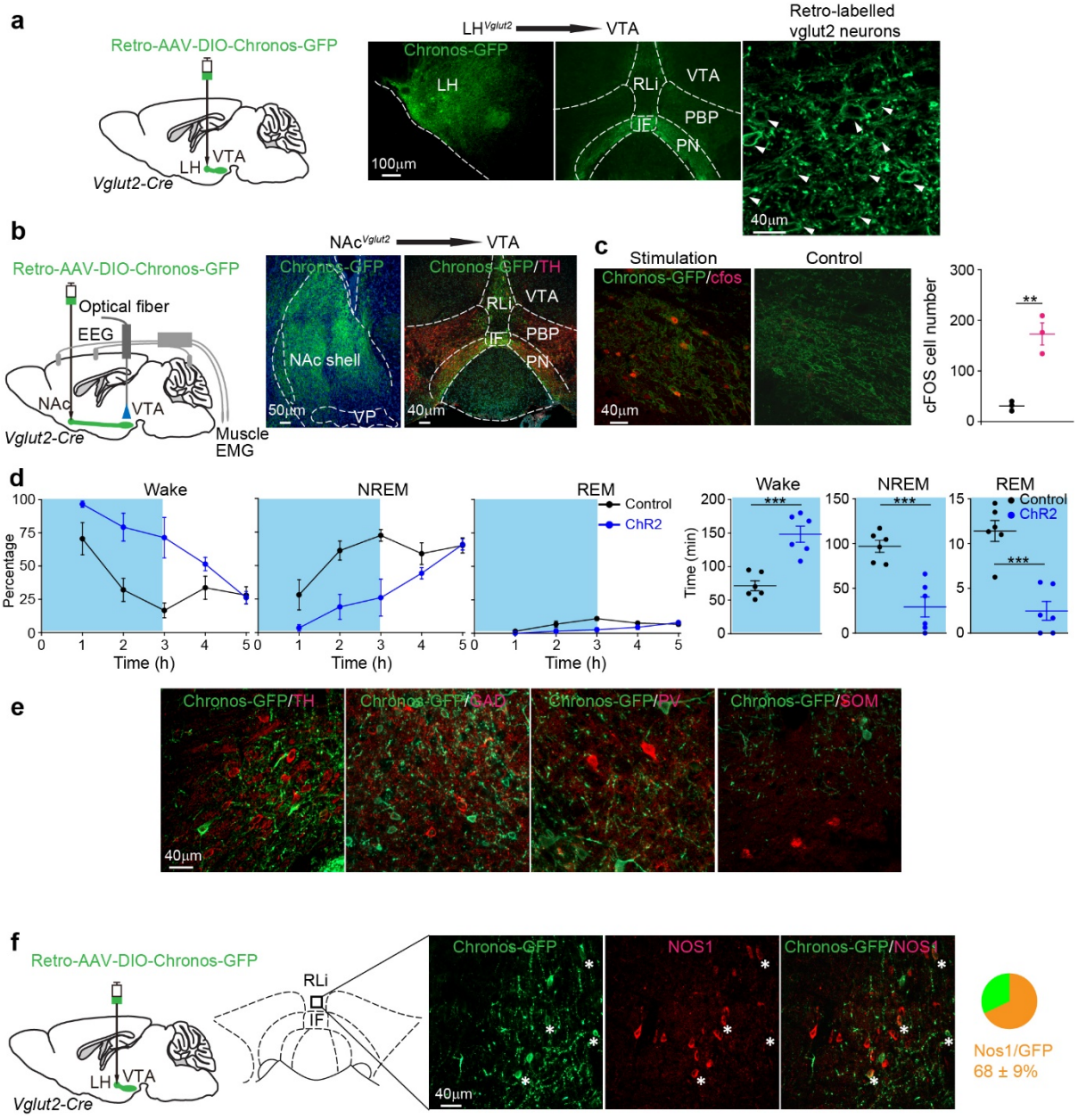


Supplementary Fig. 6 (Associated with Fig. 3) Optogenetic activation of VTA^{Vglut2}→LH or VTA^{Vglut2}→NAc projections

(a) For stimulating the VTA^{Vglut2}→LH projections, mice were given 60 s of opto-stimulation (5 Hz) during NREM sleep (‘‘lights on’’ period) and the percentage and time of wake and NREM sleep were scored (control: n=6 mice; 13 trials; ChR2: n=7 mice; 30 trials).

(b) For stimulating the VTA^{Vglut2}→NAc projections, mice were given 60 s of opto-stimulation (5 Hz) during NREM sleep (‘‘lights on’’ period) and the percentage and time of wake and NREM sleep were scored (control: n=7 mice; 18 trials; ChR2: n=8 mice; 25 trials).

**p<0.01, two-sided mann-whitney u test. All error bars represent the SEM. Shaded regions represent SEM. For detailed statistics information, see Supplementary Table1.


a
Retro-AAV-DIO-Chronos-GFP
LH
VTA
Vglut2-Cre
LH Vglut2 → VTA
Chronos-GFP
RLi
IF
PBP
PN
100µm
Retro-labelled vglut2 neurons
40µm
b
Retro-AAV-DIO-Chronos-GFP
Optical fiber
EEG
NAc
VTA
Vglut2-Cre
Muscle EMG
NAc Vglut2 → VTA
Chronos-GFP
NAc shell
VP
50µm
Chronos-GFP/TH
40µm
c
Stimulation
Control
Chronos-GFP/cfos
40µm
cFOS cell number
d
Wake
NREM
REM
Percentage
Time (h)
Control
ChR2
Time (min)
e
Chronos-GFP/TH
Chronos-GFP/GAD
Chronos-GFP/PV
Chronos-GFP/SOM
40µm
f
Retro-AAV-DIO-Chronos-GFP
LH
VTA
Vglut2-Cre
RLi
IF
Chronos-GFP
NOS1
Chronos-GFP/NOS1
40µm
Nos1/GFP
68 ± 9%

Supplementary Fig. 7 (Associated with Fig. 3)

Retro-labeling of VTA^{Vglut2}→LH and VTA^{Vglut2}→NAc projections

(a) Retro-AAV-DIO-Chronos-GFP was injected into the LH area of *Vglut2-ires-Cre* mice. Images show GFP staining in the LH and VTA areas. White arrows indicate retro-labeled soma in the VTA. The experiment was repeated independently 3 times.

(b) Retro-AAV-DIO-Chronos-GFP was injected into the NAc area of *Vglut2-ires-Cre* mice. Images show GFP staining in the NAc and VTA areas. The experiment was repeated independently 3 times.

Opto-activation of retro-labeled VTA^{vglut2} neurons

(c) Chronos-GFP and cFOS expression in Chronos (n=3 mice) or control mice (n=3 mice) after 2 hours of opto-stimulation (20 Hz for 2 seconds with 58 seconds interval).

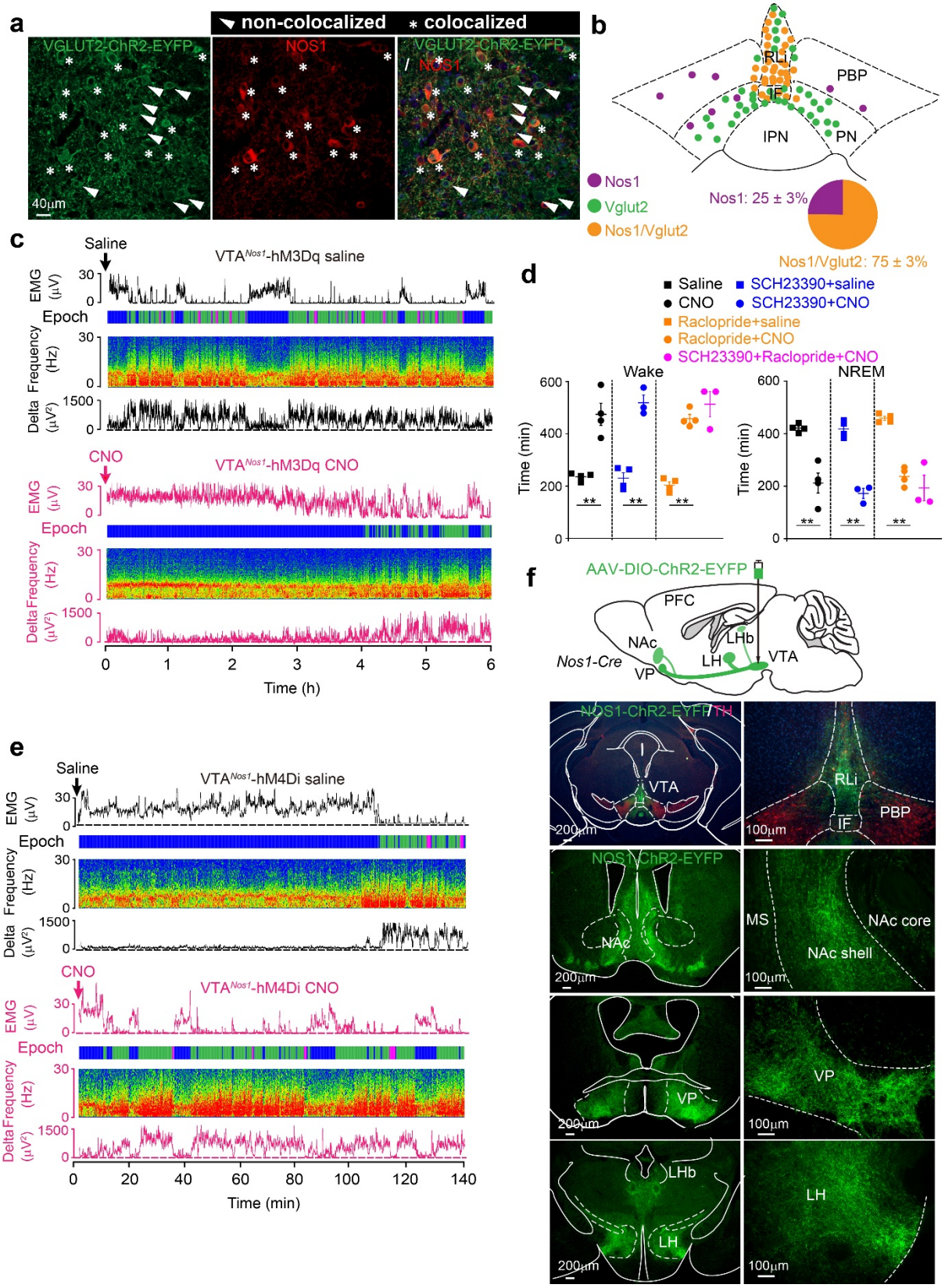
(d) An optical fiber was placed into the VTA area of Retro NAc^{Vglut2}-Chronos-GFP mice (n=6 mice) or control mice (n=6 mice), and mice were given 3 hours of opto-stimulation (20 Hz for 2 seconds with 58 seconds interval) and the percentage and time of wake, NREM and REM sleep were scored.

Identification of neuronal makers of retro-labeled VTA^{vglut2} neurons

(e) Double labeling of retro-labeled VTA^{vglut2} neurons with TH, GAD, PV or SOM. The experiment was repeated independently 3 times.

(f) Retro-AAV-DIO-Chronos-GFP was injected into the LH area of *Vglut2-ires-Cre* mice. Chronos-GFP expression was detected in cells of the VTA, and Chronos-GFP retro-labeled VTA midline soma (from LH injection) were doubled labelled with NOS1 (n= 4 mice). Data for pie chart represent as mean ± SEM.

**p<0.01, ***p<0.001; two-sided unpaired t-test. Error bars represent the SEM. For detailed statistics information, see Supplementary Table1.


a
non-colocalized
colocalized
VGLUT2-ChR2-EYFP
NOS1
VGLUT2-ChR2-EYFP / NOS1
40μm
b
RLi
PBP
IF
IPN
PN
Nos1
Vglut2
Nos1/Vglut2
Nos1: 25 ± 3%
Nos1/Vglut2: 75 ± 3%
c
Saline
VTA^Nos1-hM3Dq saline
EMG (μV)
Epoch
Frequency (Hz)
Delta (μV²)
CNO
VTA^Nos1-hM3Dq CNO
Time (h)
d
Saline
SCH23390+saline
CNO
SCH23390+CNO
Raclopride+saline
Raclopride+CNO
SCH23390+Raclopride+CNO
Wake
NREM
Time (min)
e
Saline
VTA^Nos1-hM4Di saline
CNO
VTA^Nos1-hM4Di CNO
Time (min)
f
AAV-DIO-ChR2-EYFP
PFC
NAc
LHb
LH
VTA
VP
Nos1-Cre
NOS1-ChR2-EYFP/TH
NOS1-ChR2-EYFP
MS
NAc core
NAc shell
200μm
100μm

Supplementary Fig. 8 (Associated with Fig. 3)

The majority of midline VTA^{Vglut2} neurons express NOS1

(a, b) Immunohistochemistry staining of midline VTA neurons in VTA^{Vglut2}-ChR2-EYFP mice with GFP and NOS1 (n = 3 mice). Data for pie chart represent mean ± SEM. The majority of *Nos1*/*Vglut2* neurons are in the midline VTA area (see schematic). IF, interfasicular nucleus; RLi, rostral linear nucleus; PBP, parabrachial pigmented nucleus; PN, paranigral nucleus; IPN, interpeduncular nucleus.

VTA^{Nos1} induced wakefulness is independent of dopamine activation

(c) Examples of EEG, EMG and delta power spectra from CNO or saline-injected *VTA^{Nos1}-hM3Dq* mice. “Epoch” indicates the vigilance state: blue, wake; green, NREM sleep; magenta, REM sleep.

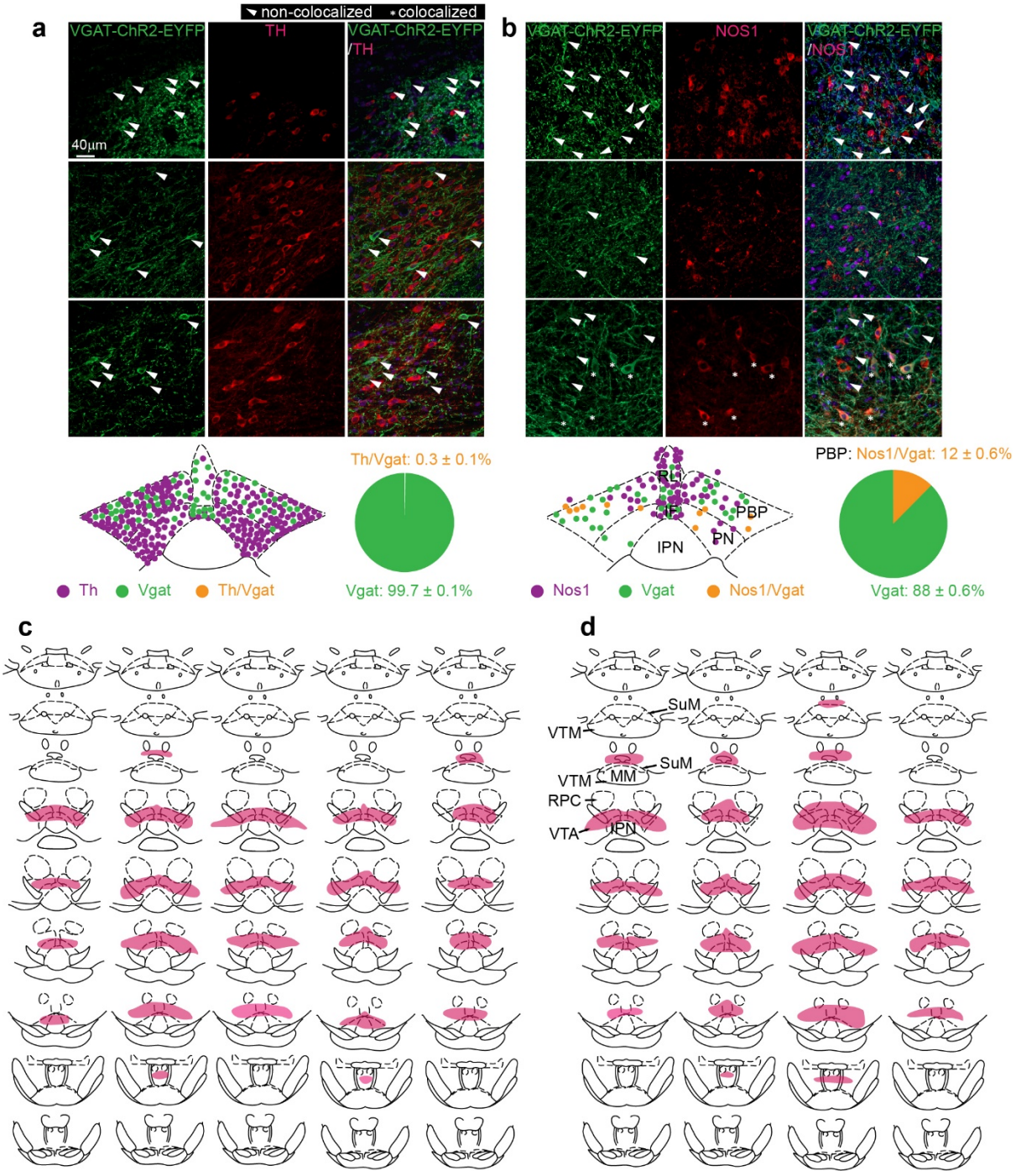
(d) Time of wake and NREM sleep from CNO or saline-injected *VTA^{Nos1}-hM3Dq* mice after dopamine receptor antagonist injections.

(e) Examples of EEG, EMG and delta power spectra from CNO or saline-injected VTA^{Nos1}-hM4Di mice. “Epoch” indicates the vigilance state: blue, wake; green, NREM sleep; magenta, REM sleep.

Optogenetic circuit mapping of VTA^{Nos1} neurons

(f) Injection of AAV-DIO-ChR2-EYFP into the VTA of the *Nos1-ires-Cre* mice. Circuit mapping for VTA^{Nos1}-ChR2-EYFP mice. The experiment was repeated independently 3 times. IF, interfasicular nucleus; PBP, parabrachial pigment nucleus. RLi, rostral linear nucleus; VP, ventral pallidum; NAc, nucleus accumbens; LH, lateral hypothalamus; LHb, lateral habenula;

**p<0.01, repeated measures two-way ANOVA and Bonferroni-Holm *post hoc* test. Error bars represent the SEM. For detailed statistics information, see Supplementary Table1.


a
non-colocalized
colocalized
VGAT-ChR2-EYFP
TH
VGAT-ChR2-EYFP /TH
40μm
b
VGAT-ChR2-EYFP
NOS1
VGAT-ChR2-EYFP /NOS1
Th/Vgat: 0.3 ± 0.1%
Vgat: 99.7 ± 0.1%
Th
Vgat
Th/Vgat
RL
IF
PBP
PN
IPN
PBP: Nos1/Vgat: 12 ± 0.6%
Vgat: 88 ± 0.6%
Nos1
Vgat
Nos1/Vgat
c
d
SuM
VTM
MM
RPC
VTA
IPN

Supplementary Fig. 9 (Associated with Fig. 5)

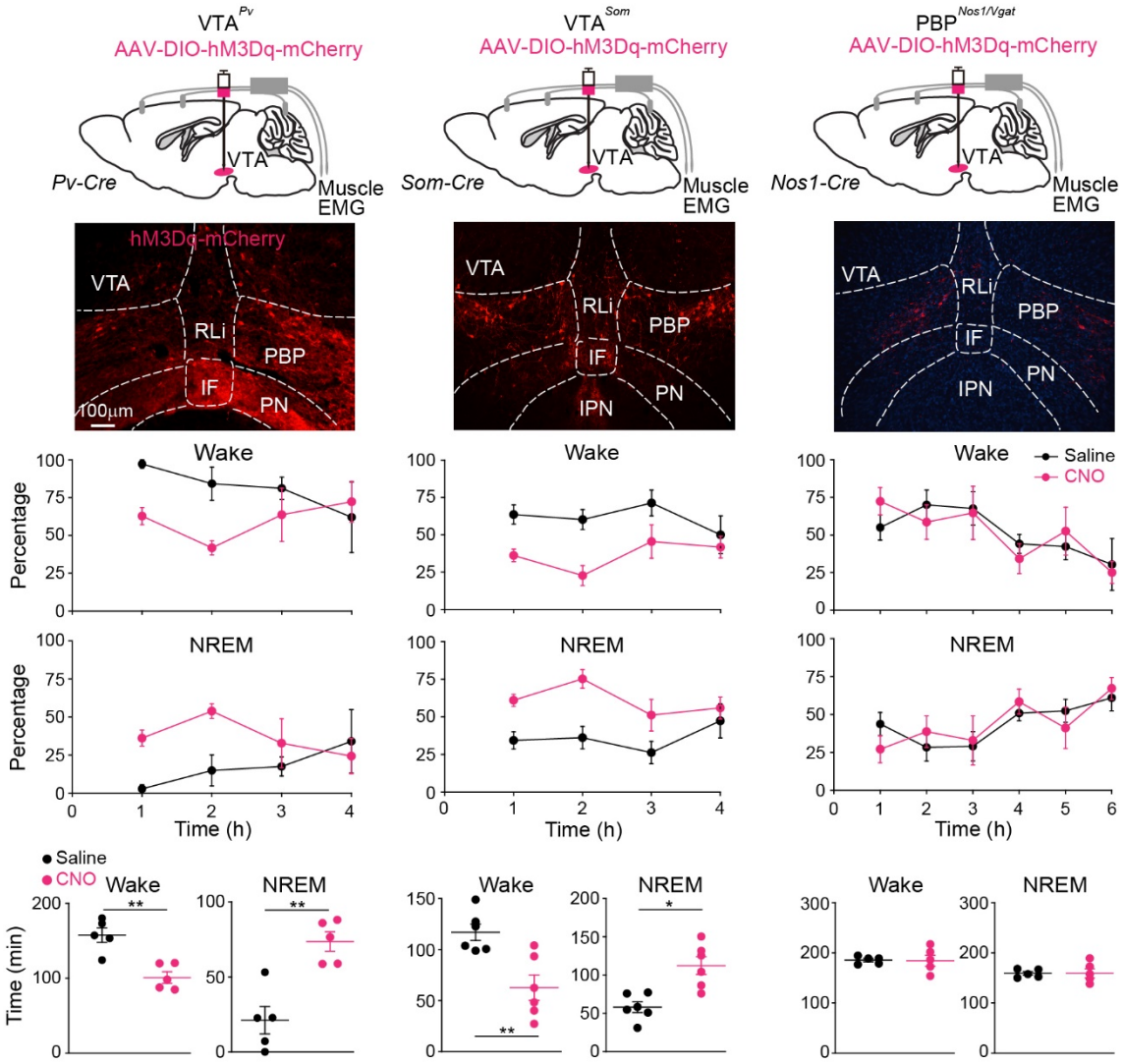
Immunocytochemical characterization of VTA^{Vgat} neurons

(a) In the VTA of VTA^{Vgat}-ChR2-EYFP mice, *Vgat*-expressing neurons are distinct from those expressing tyrosine hydroxylase (TH) (n=4 mice). Co-expression of EYFP and TH was rare. Data for pie chart represent mean ± SEM.

(b) In the midline VTA of VTA^{Vgat}-ChR2-EYFP mice, *Vgat*-expressing neurons are distinct from those expressing NOS1 (n=4 mice). Some VTA^{Vgat} cells in the PBP co-express NOS1 (12±0.6%). IF, interfasicular nucleus; RLi, rostral linear nucleus; PBP, parabrachial pigmented nucleus; PN, paranigral nucleus; IPN, interpeduncular nucleus. Data for pie chart represent as mean ± SEM.

Examples of expression of hM3Dq-mCherry and hM4Di-mCherry expression in individual *Vgat-ires-Cre* mice

(c, d) Sections shown as line diagrams from individual mice, from anterior to posterior, with areas of hM3Dq-mCherry (c) or hM4Di-mCherry (d) receptor expression, shown schematically in magenta, in VTA^{Vgat}-hM3Dq or VTA^{Vgat}-hM4Di mice. IPN, interpeduncular nucleus; MM, medial mammillary area; RPC, red nucleus, parvocellular part. SuM, supramammillary area. VTM, ventral tuberomammillary nucleus.

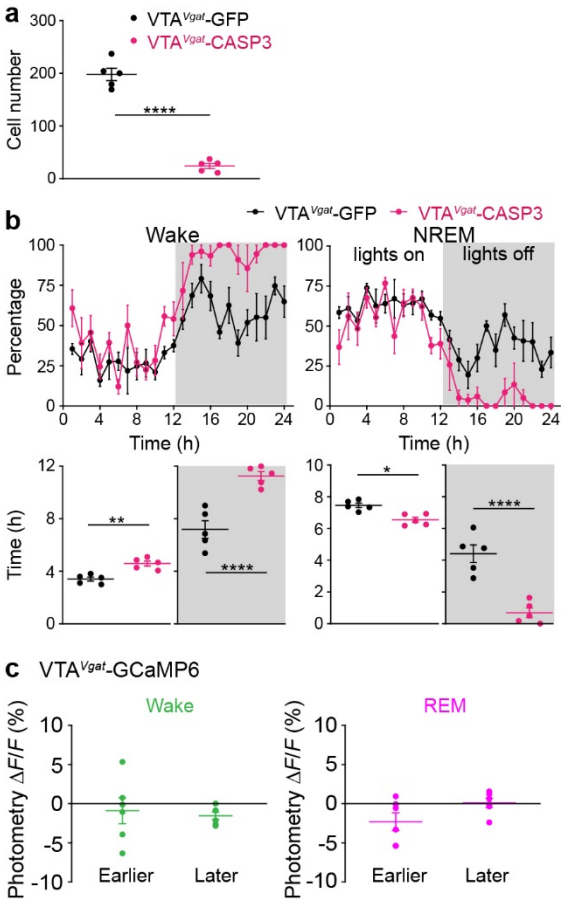


Supplementary Fig. 10 (Associated with Fig. 5)

Chemogenetic activation of subtypes of GABA neurons in the VTA

AAV-DIO-hM3Dq-mCherry was injected into the VTA area of *Pv-Cre* and *Som-ires-Cre* mice. AAV-DIO-hM3Dq-mCherry was also injected into the PBP area of *Nos1-ires-Cre* mice to cover NOS1/VGAT neurons (Supplementary Fig. 9b). Percentage and time of wake and NREM sleep were scored after saline or CNO injection (VTA^{Pv}-hM3Dq: saline n=5 mice; CNO n=5 mice; VTA^{Som}-hM3Dq: saline n=6 mice; CNO n=6 mice; PBP$^{Nos1/Vgat}$-hM3Dq: saline n=5 mice; CNO n=5 mice). IF, interfasicular nucleus; PBP, parabrachial pigmented nucleus; PN, paranigral nucleus; IPN, interpeduncular nucleus; RLi, rostral linear nucleus;

*p<0.05, **p<0.01; two-sided unpaired t-test. Error bars represent the SEM. For detailed statistics information, see Supplementary Table1.



Supplementary Fig. 11 (Associated with Fig. 6)

Sleep-wake patterns of VTA^{Vgat}-CASP3 mice

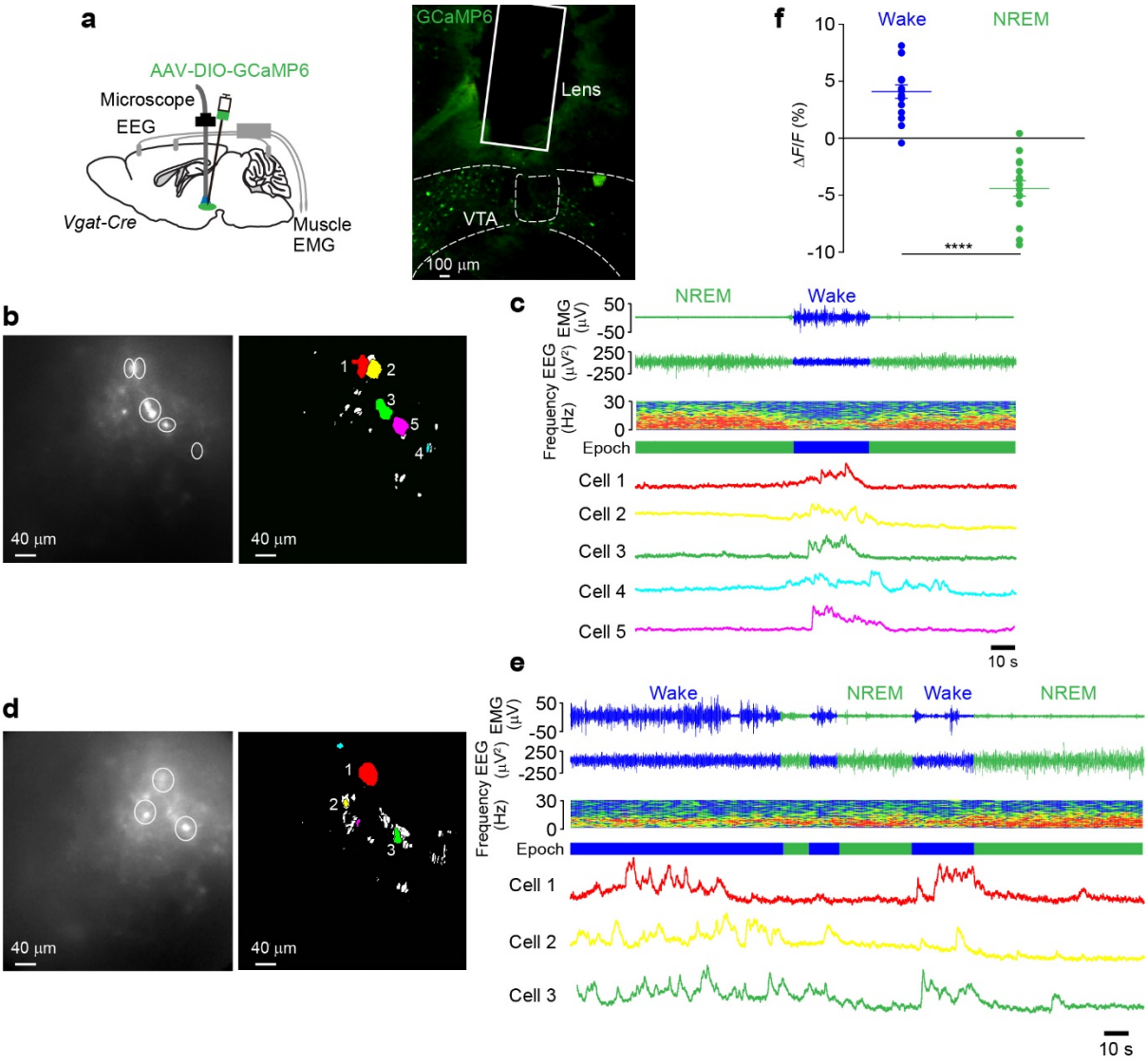
(a) GFP-positive cell numbers of VTA^{Vgat}-GFP mice (n=5 mice) and VTA^{Vgat}-CASP3 mice (n=5 mice).

(b) Percentage and time of wake, NERM or REM sleep of VTA^{Vgat}-GFP mice (n=5 mice) and VTA^{Vgat}-CASP3 mice (n=5 mice) 4 months after virus injection.

Ca^{2+} signals of VTA^{Vgat} neurons during individual bouts of REM sleep and wake

(c) Within an individual bout of wake or REM sleep, the Ca^{2+} signal of the VTA^{Vgat} cells during the earlier and later parts of the bout did not change significantly (n=6 mice; 95 sessions for wake and 131 sessions for REM sleep).

*p<0.05, **p<0.01, ****p<0.0001; two-sided for a and b, unpaired t-tests; for c, two-sided paired t-test. Error bars represent the SEM. For detailed statistics information, see Supplementary Table1.



Supplementary Fig. 12 (Associated with Fig. 6)

***In vivo* Ca^{2+} imaging of VTA^{Vgat} neurons and correlating their activity with vigilance state shows that VTA^{Vgat} neurons are wake-active**

(a) AAV-DIO-GCaMP6f was injected into the VTA area of *Vgat-ires-Cre* mice and a GRIN lens was implanted into the VTA. GCaMP6 expression can be detected in the VTA area. The trace of where the lens was placed is illustrated. The experiment was repeated independently 4 times.

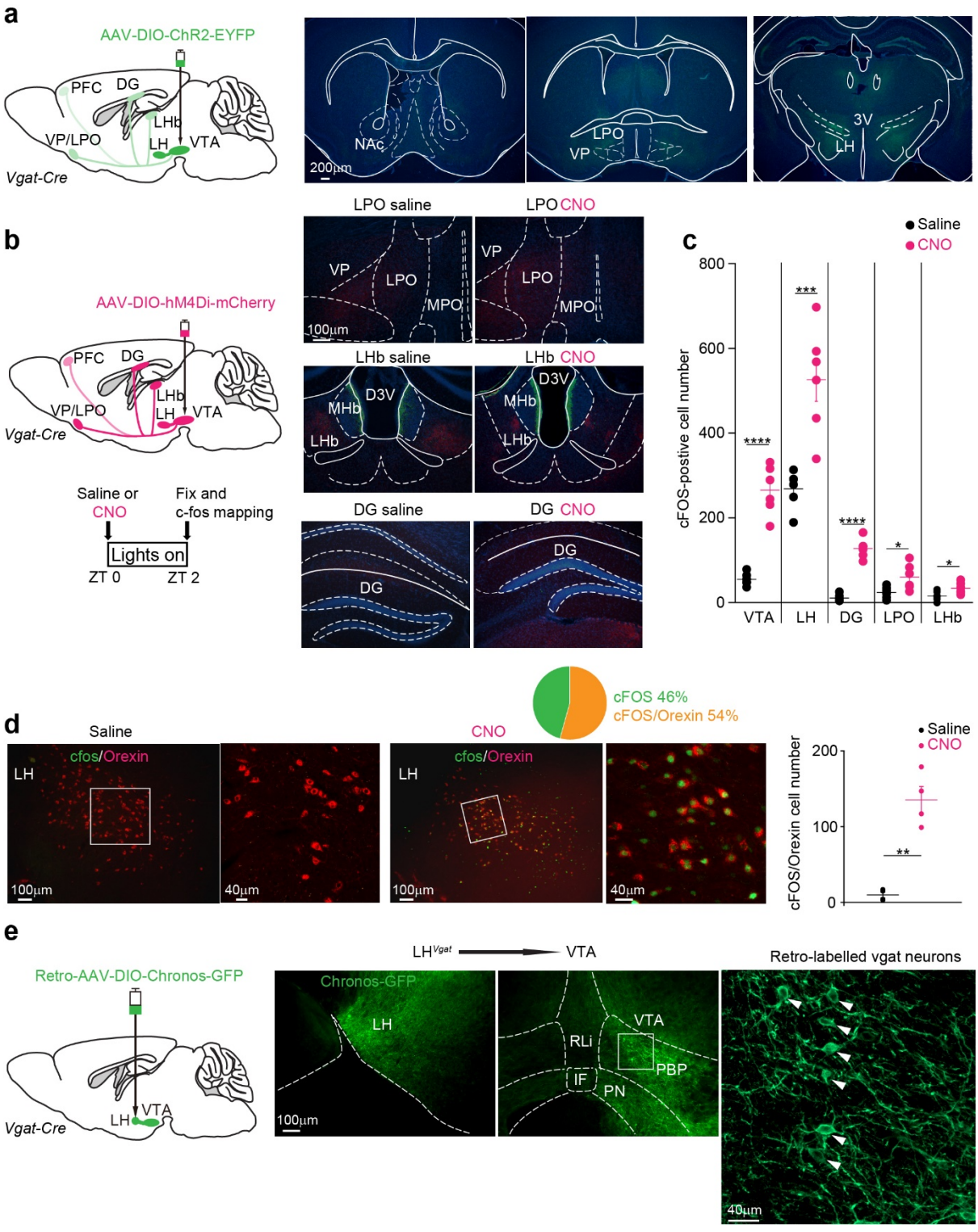
(b) An example of Ca^{2+} imaging and activity map indicating individual cells (colour-coded) that have been recorded.

(c) Ca^{2+} traces recorded in the imaging during NREM sleep or wakefulness for the cells shown in panel b. Examples of EEG, EMG and delta power spectra. “Epoch” indicates the vigilance state: blue, wake; green, NREM sleep.

(d) Another example of Ca^{2+} imaging and activity map indicating individual cells (colour-coded) that have been recorded.

(e) Ca^{2+} traces recorded in the imaging during NREM sleep or wakefulness for the cells shown in panel d. Examples of EEG, EMG and delta power spectra. “Epoch” indicates the vigilance state: blue, wake; green, NREM sleep.

(f) $\Delta F/F$ ratio of the Ca^{2+} photometry signal in VTA^{Vgat}-GCaMP6f mice during wakefulness and NREM sleep (16 cells of 4 mice). ****p<0.0001; two-sided paired t-test. Error bars represent the SEM. For detailed statistics information, see Supplementary Table1.


a
AAV-DIO-ChR2-EYFP
PFC
DG
LHb
VP/LPO
LH
VTA
Vgat-Cre
NAc
200μm
LPO
VP
3V
LH
b
AAV-DIO-hM4Di-mCherry
PFC
DG
LHb
VP/LPO
LH
VTA
Vgat-Cre
Saline or CNO
Fix and c-fos mapping
Lights on
ZT 0
ZT 2
LPO saline
LPO CNO
VP
LPO
MPO
100μm
LHb saline
LHb CNO
D3V
MHb
LHb
DG saline
DG CNO
DG
c
Saline
CNO
cFOS-postive cell number
800
600
400
200
0
****
***
****
*
*
VTA
LH
DG
LPO
LHb
d
Saline
CNO
cfos/Orexin
LH
100μm
40μm
cFOS 46%
cFOS/Orexin 54%
cFOS/Orexin cell number
200
100
0
**
e
Retro-AAV-DIO-Chronos-GFP
LH
VTA
Vgat-Cre
LHVgat
VTA
Retro-labelled vgat neurons
Chronos-GFP
LH
100μm
VTA
RLi
PBP
IF
PN
40μm

Supplementary Fig. 13 (Associated with Fig. 7, 8)

Chemogenetic and optogenetic circuit mapping of VTA^{Vgat} neurons

(a) Circuit mapping for VTA^{Vgat}-ChR2-EYFP mice in whole brain.

(b) Chemogenetic mapping with cFOS expression following inhibition of VTA^{Vgat} neurons. The number of cFOS neurons identified immunohistochemically (green dots) were counted (see graph in c) throughout the brain two hours after CNO or saline injection at ZT0 (start of "lights on") in VTA^{Vgat}-hM4D$_i$ mice. The magenta/pink staining is the primary florescence of VTA^{Vgat} axons containing hM4D$_i$-mCherry protein.

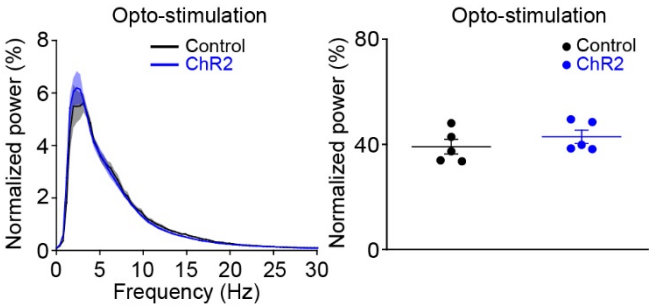
(c) cFOS induction in different brain areas of VTA^{Vgat}-hM4D$_i$ mice after saline (n=6 mice) or CNO (n=6 mice) *i.p.* injection.

(d) Double-labelling and quantification of cFOS and orexin immunocytochemistry in the LH area of VTA^{Vgat}-hM4Di mice 2 hours after saline (n=4 mice) or CNO *i.p.* injection (n=4 mice).

(e) Retro-AAV-DIO-Chronos-GFP was injected into the LH area of *Vgat-ires-Cre* mice. Images show GFP staining in the LH and VTA areas. White arrows indicate retro-labelled soma in the VTA.

VP, ventral pallidum; NAc, nucleus accumbens; LPO, lateral preoptic area; MPO, medial preoptic area; LH, lateral hypothalamus; LHb, lateral habenula; MHb, medial habenula; DG, dentate granule cells; D3V, dorsal 3rd ventricle; 3V, 3rd ventricle; IF, interfasicular nucleus; RLi, rostral linear nucleus; PBP, parabrachial pigmented nucleus; PN, paranigral nucleus; IPN, interpeduncular nucleus.

*p<0.05, **p<0.01, ***p<0.001, ****p<0.0001; two-sided unpaired t-test. Error bars represent the SEM. For detailed statistics information, see Supplementary Table1.

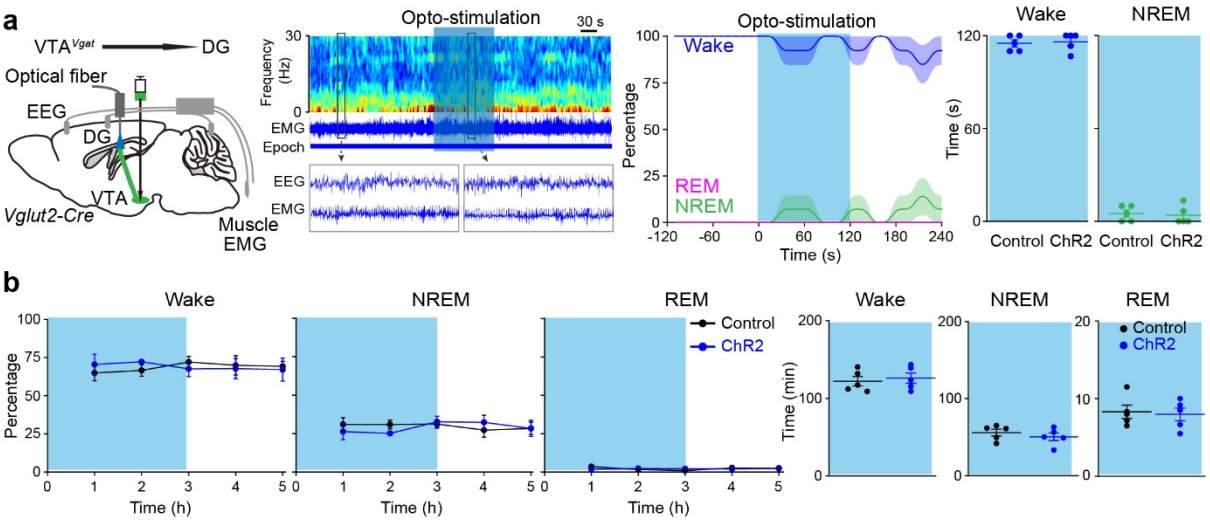


Supplementary Fig. 14 (Associated with Fig. 8)

EEG power spectrum during optogenetic activation of the VTA^{Vgat}→LH projection

EEG power spectrum and delta power (0.5-4 Hz) for NREM sleep during 5 min of opto-stimulation.

p>0.05, two-sided unpaired t-test. Shaded regions represent SEM. All error bars represent the SEM. For detailed statistics information, see Supplementary Table1.

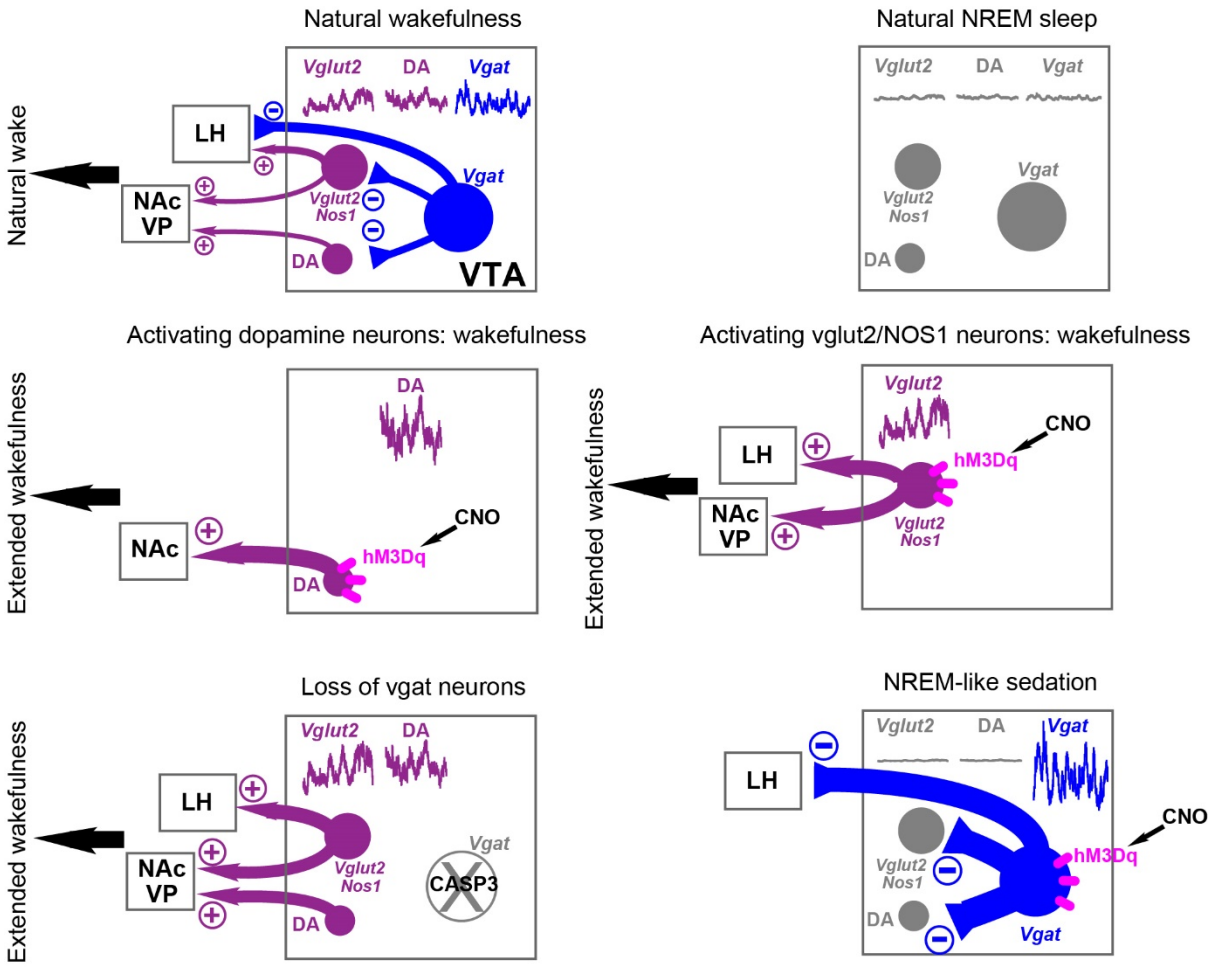


Supplementary Fig. 15 (Associated with Figs. 7 & 8)

Optogenetic activation of the VTA^{Vgat}→DG projection

(a, b) For activating the VTA^{Vgat}→DG projection, an optical fiber was placed into the DG area of VTA^{Vgat}-ChR2-EYFP mice. (a) Mice were given 120 s of opto-stimulation (20 Hz) during wakefulness and the percentage and time of wake and NREM were scored (control: n=5 mice; 10 trials; ChR2: n=6 mice; 13 trials). (b) mice (control: n=5 mice; ChR2: n=5 mice) were given 3 hours of opto-stimulation during wake period and the percentage and time of wake, NREM and REM sleep were scored.

p>0.05, for a and b, two-sided unpaired t-test. Shaded regions represent SEM. All error bars represent the SEM. For detailed statistics information, see Supplementary Table1.



Supplementary Fig. 16 (Associated with Figs. 1-8)

Conceptual circuit diagrams illustrating a hypothesis of how VTA^{Vgat}, VTA^{Vglut2} and VTA^{DA} neurons contribute to the regulation of vigilance states

The top left-hand box shows the situation in wakefulness. In the VTA, VTA$^{Vglut2/Nos1}$, VTA^{Vgat} and VTA^{DA} neurons are all selectively wake (and REM-sleep) active[5]. The top right-hand box illustrates that during natural NREM sleep, all types of neurons in the VTA are silent or less active (as indicated by grey shading). The traces are schematics of the Ca^{2+} photometry signals for the different sorts of neurons in the VTA. The photometry signal for DA neurons is inferred from ref[5]. During wakefulness, the hypothesis is that the VTA$^{Vglut2/Nos1}$ and VTA^{DA} neurons are contributing to the generation of wakefulness by exciting the nucleus accumbens shell (NAc)/ventral

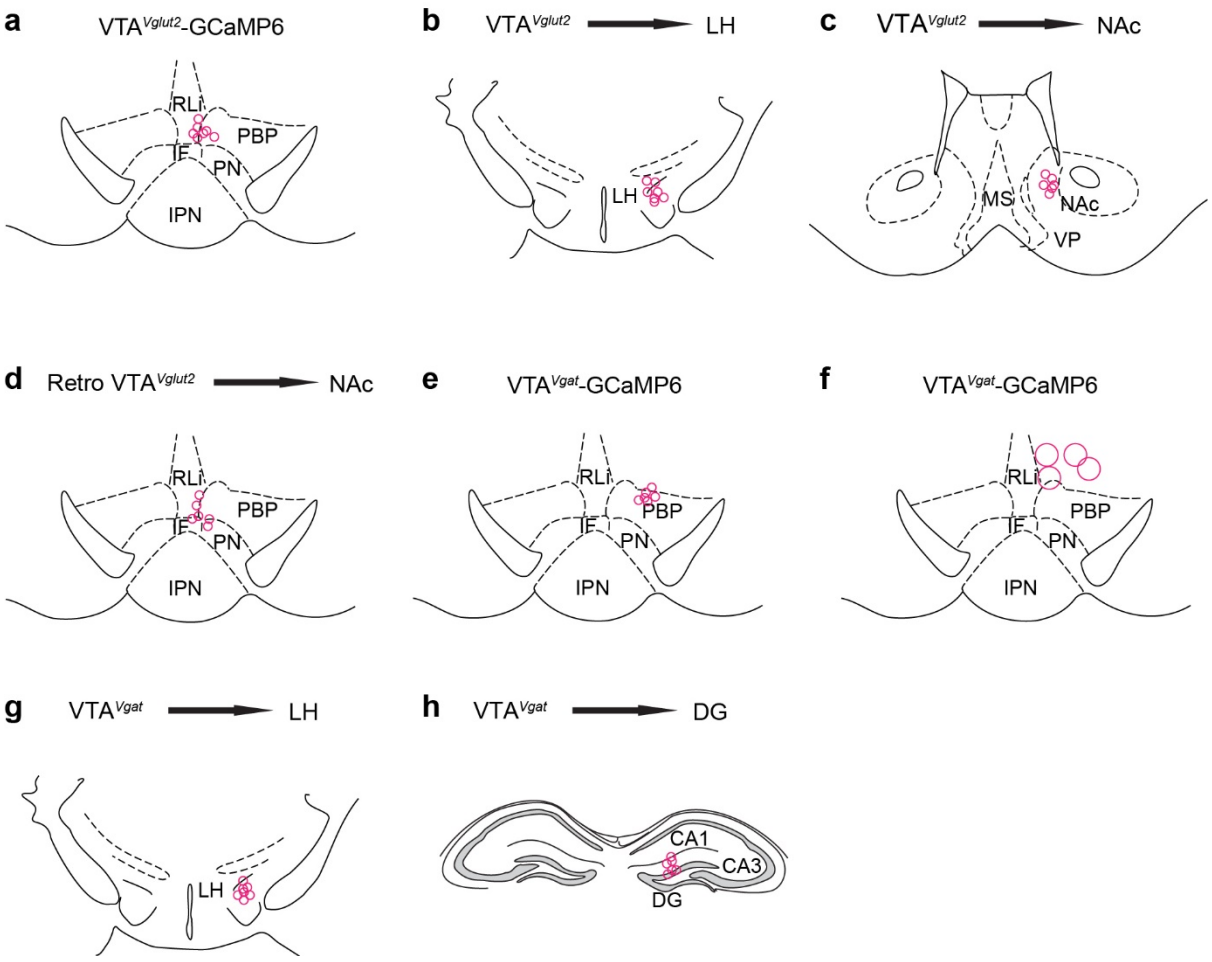
pallidum (VP) and orexin neurons in the lateral hypothalamus (LH). VTA^{Vgat} neurons would be providing an ongoing inhibitory tone onto the VTA$^{Vglut2/Nos1}$and VTA^{DA} neurons, as well as to the lateral hypothalamus. The consequence of this wake-on inhibitory tone is that the extent of wakefulness is limited.

The middle left-hand box summarizes data that selective chemogenetic activation of VTA^{DA} neurons produces wake[8], as does their selective optogenetic activation[5].

The middle right-hand box shows that chemogentically activating VTA$^{Vglut2/Nos1}$ neurons alone also induces wakefulness (our study).

The bottom left-hand box illustrates that pathological loss of the VTA^{Vgat} neurons (using caspase) produces extended wakefulness. The loss of sleep lasts for many months. A hypothesis is that this is because of loss of inhibition onto the VTA$^{Vglut2/Nos1}$, VTA^{DA} neurons and the LH.

The bottom right-hand box shows the converse from lesioning the VTA^{Vgat} neurons. The selective activation of VTA^{Vgat} neurons, in this case chemogenetically with CNO, produces a profound NREM-like sedation. Our results suggest that this is because of inhibition of the LH and VTA$^{Vglut2/Nos1}$ and VTA^{DA} neurons.



Supplementary Fig. 17 (Associated with Figs. 1-8)

Fiber placements for the optogenetic and photometry experiments

(a) Fiber placement in the VTA for the VTA^{Vglut2}-GCaMP6 mice.

(b) Fiber placement in the LH for the activation of the VTA^{Vglut2}→LH projections.

(c) Fiber placement in the NAc for the activation of the VTA^{Vglut2}→NAc projections.

(d) Fiber placement in the VTA for the activation of the retro NAc^{Vglut2}→VTA projections.

(e) Fiber placement in the VTA for the VTA^{Vgat}-GCaMP6 mice.

(f) GRIN lens placement in the VTA for the VTA^{Vgat}-GCaMP6 mice.

(g) Fiber placement in the LH for the activation of the VTA^{Vgat}→LH projections.

(h) Fiber placement in the DG for the activation of the VTA^{Vgat}→DG projections.

DG, dentate granule cells; IF, interfasicular nucleus; IPN, interpeduncular nucleus; LH, lateral hypothalamus; NAc, nucleus accumbens; PBP, parabrachial pigmented nucleus; PN, paranigral nucleus; RLi, rostral linear nucleus; VP, ventral pallidum.